Master's thesis

Gene silencing of cystatin B (*CSTB*) by RNAi: Implications for the altered JAK/STAT signaling pathway in Unverricht-Lundborg disease (EPM1)

Katarin Sandell

2013

University of Helsinki
Faculty of Medicine
Master's program of Translational medicine

CONTENTS:

LIST OF ABBREVIATIONS

AD	Alzheimer's disease
AGO	argonaute
AIRE	autoimmune regulator
BBB	blood brain barrier
BLAST	Basic Local Alignment Search Tool
bp	base pair
BSA	bovine serum albumin
cDNA	complementary DNA
CLN4B	Parry's disease
CNS	central nervous system
Cstb/CSTB	cystatin B
Cstb$^{-/-}$	cystatin B knockout
Ct	cycle threshold
CTSB	cathepsin B
DBD	DNA binding domain
ddsH_2O	double distilled sterile H_2O
del	deletion
DIV	days *in vitro*
DNase	deoxyribonuclease
dsRNA	double stranded RNA
E	efficiency
EEG	electroencephalography
EM	electron microscope
EPM1/ULD	Unverricht-Lundborg disease
EtOH	ethanol
exo-siRNA	exogenously introduced small interfering RNA
FBS	fetal bovine serum
FRET	fluorescence resonance energy transfer
GABA	γ-aminobutyric acid
GAPDH	glyceraldehyde 3-phosphate dehydrogenase
GAS	interferon-γ activation sequence
GC	guanine-cytosine
gDNA	genomic DNA
GFAP	glial fibrillary acidic protein
GFP	green fluorescent protein
GTPase	guanosine triphosphate hydrolase
HRP	horseradish peroxidase
IF	immunofluorescence
IFN	interferon
IFNAR	type I interferon receptor
IRF	interferon regulatory factor
IRF9/ISGF3γ/ P48	interferon regulatory factor 9
ISG	interferon stimulated gene
ISGF3	interferon stimulated gene factor 3
ISRE	interferon stimulated response element
JAK	Janus kinase
LD/EPM2	Lafora disease
LPS	lipopolysaccharide
MAPK1/ERK2	mitogen-activated protein kinase 1
MeOH	methanol
MERRF	Myoclonic epilepsy with ragged red fibers
MHC	major histocompatibility complex
miRNA	microRNA
mRNA	messenger RNA

MS	Multiple sclerosis
NCL	neuronal ceroid lipofuscinose
NF- κB	nuclear factor of kappa light polypeptide gene enhancer in B cells
NLS	nuclear localization signal
NO	nitric oxide
NO_2^-	nitrite
NOS	nitric oxide synthase
NOS1/nNOS	neuronal nitric oxide synthase
NOS2/iNOS	inducible nitric oxide synthase
NOS3/eNOS	endothelial nitric oxide synthase
NPC	nuclear pore complex
OMIM	Online Mendelian Inheritance in Man
P5	postnatal day 5
P14	postnatal day 14
PBS	phosphate buffered saline
PBST	phosphate buffered saline + Tween-20
PCR	polymerase chain reaction
PD	Parkinson's disease
PFA	paraformaldehyde
PIAS	protein inhibitor of activated STAT
PME	progressive myoclonus epilepsy
Pol III	RNA polymerase III
PTPase	protein tyrosine phosphatase
PVDF	polyvinylidene difluoride
qRT-PCR	quantitative real time polymerase chain reaction
R^2	correlation coefficient
RA	Rheumatoid arthritis
RISC	RNA induced silencing complex
Rn	detected fluorescence
RNAi	RNA interference
RNase	ribonuclease
RT	real time/reverse transcriptase
SDS	sodium dodecyl sulphate
SDS-PAGE	sodium dodecyl sulphate polyacrylamide gel electrophoresis
SH2	SRC homology 2
shRNA	short hairpin RNA
siRNA	small interfering RNA
SOCS	suppressor of cytokine signaling
STAT	signal transducer and activator of transcription
TBE	Tris/borate/EDTA
TBP	TATA-box binding protein
TYK	tyrosine kinase
UTR	untranslated region
VGAT/ SLC32A1	vesicular GABA transporter
WB	Western blot
wt	wild type

1. REVIEW OF THE LITERATURE

1.1. Progressive myoclonus epilepsies

Progressive myoclonus epilepsies (PMEs) are a group of clinically and etiologically heterogeneous diseases, comprehending symptoms such as epileptic seizures, myoclonus, and progressive neurological degeneration with cognitive impairment (Marseille Consensus Group, 1990). The PMEs are rare, and most of them are autosomal recessively inherited. There are, however, also autosomal dominant and mitochondrially inherited forms, such as the Parry's disease (CLN4B) and myoclonic epilepsy with ragged red fibers (MERRF). The disease onset of PMEs is often in childhood or in early adolescence, most giving a poor diagnose and usually leading to death of the patient within the first decades after onset (de Siqueira, 2010). The five most common PME disease types are Unverricht-Lundborg disease (EPM1/ULD), Lafora disease (LD/EPM2), neuronal ceroid lipofuscinoses (NCLs), MERRF, and sialidoses (Lehesjoki, 2003).

The PME diagnoses have traditionally been based on clinical features, electroencephalography (EEG), and electron microscopy (EM) findings (Berkovic et al, 1986), but nowadays they rely mainly on molecular genetic testing (Shahwan et al, 2005). There is no cure for any of the PMEs (de Siqueira, 2010), but symptoms such as the epileptic seizures can be controlled by medication, even if progression of the diseases is inevitable.

Up to 1% of all epileptic syndromes worldwide concerning children and adolescents belong to a PME disorder (de Siqueira, 2010), but the geographical distribution of the individual diseases is unequal. EPM1 is for example the most prominent PME disorder in Northern Europe, USA and Canada, whereas Lafora disease is the most common in Mediterranean countries, India, and in countries where consanguineous marriages are common (Delgado-Escueta et al, 2001).

Many of the PMEs are mis- or underdiagnosed in several countries due to the similarity of the clinical symptoms to more common epilepsy types (de Siqueira, 2010; Shahwan et al, 2005).

1.1.1 Unverricht-Lundborg disease (EPM1/ULD)

EPM1 (OMIM 254800) was initially described by Unverricht in 1891 (Unverricht, 1891) and by Lundborg in 1903 (Lundborg, 1903), and it is the most common PME type (Lehesjoki, 2003). The disease occurs with low frequency in all populations, but it is geographically more common in places with founder effect or in regions where consanguineous marriages are common (Genton, 2010), i.e. in Finland and in certain countries of the Western Mediterranean region (Magaudda et al, 2006). The incidence of EPM1 in Finland is 1:20 000 births per year (Norio & Koskiniemi, 1979), and there are about 200 diagnosed cases (Kälviäinen et al, 2008). Statistics are not available from other countries, and it seems like EPM1 is underdiagnosed in many of them due to the clinical heterogeneity of the symptoms and the similarity of its initial stages to other epilepsy types (De Haan et al, 2004). Until 1989, EPM1 was divided into two separate conditions, the Baltic and the Mediterranean epilepsies, of which the Baltic was considered to be more severe. However, in the Marseille meeting in 1989 both conditions were defined as the same (Marseille Consensus Group, 1990), and it was later discovered that possible differences in symptomatology are most likely due to environmental factors, such as the rehabilitative medication (Kälviäinen et al, 2008).

1.1.1.1 Clinical features of EPM1

EPM1 is autosomal recessively inherited and the age of disease onset is between 6 and 16 years (Kälviäinen et al, 2008). Stimulus sensitive myoclonus has been reported as the first symptom in over 50% of EPM1 cases (Shahwan et al, 2005) and it has been described, together with generalized tonic-clonic epileptic seizures and a characteristic EEG, as the initial symptoms for EPM1 (Koskiniemi, 1986; Koskiniemi, 1987; Norio & Koskiniemi, 1979).

The stimulus-sensitive myoclonus is often triggered by light, sound, touch, and/or physical exertion and the jerks are disabling and resistant to therapy. The myoclonic jerks progress in severity during the initial years after disease onset, but they stabilize over time both in amount and severity, resulting in an increased tolerance in most patients (Genton, 2010; Kälviäinen et al, 2008). The epileptic seizures are infrequent in the beginning and vary in manifestation being focal, multifocal, or generalized, developing into a series of myoclonic seizures. Like the myoclonic jerks, the epileptic seizures increase both in amount and severity during the first 3-7 years after disease onset, but since the seizures can be treated with anti-epileptic drugs, they may in some patients be completely excluded (Koskiniemi, 1986; Koskiniemi, 1987; Norio & Koskiniemi, 1979).

EPM1 progresses within a few years into ataxia, incoordination, dysarthria, and a constant intention tremor. About one third of the patients become severely disabled and wheelchair bound, being unable to eat or drink without assistance (Kälviäinen et al, 2008). Most of the patients have, however, fluctuations with both good and bad days (Genton, 2010; Kälviäinen et al, 2008), and it may take up to years or even decades before these patients lose their ability to walk (Kälviäinen et al, 2008). The cognition of EPM1 patients remains rather intact for a long time after disease onset, but over time a mild decline in intellectual performance starts to manifest. Depression and other psychiatric symptoms are very common amongst EPM1 patients, due to which, psychosocial rehabilitation is one of the most important supporting therapies (Kälviäinen et al, 2008).

The clinical picture and progression rate of EPM1 varies both between and inside families (Kälviäinen et al, 2008). Some mild forms of EPM1 do not follow the full symptomatology, sometimes leading to a delayed diagnosis or the disease to be misdiagnosed. EPM1 itself is not fatal and due to effective therapies, the life expectancy of today's patients is only slightly shorter than the general populations (Lehesjoki, 2002).

1.1.1.2 Pathogenesis

Neuropathological studies of EPM1 patients are limited, but post-mortem analyses have revealed both atrophy and gliosis in the brain, especially in the cerebellum, thalamus, frontotemporal cortex, and hippocampus (Cohen et al, 2011; Haltia et al, 1969; Koskiniemi et al, 1974). Voxel-based morphometry and cortical thickness analyses have shown regional thinning in the sensorimotor, visual, and auditory cortical areas of EPM1 patients (Koskenkorva et al, 2009; Koskenkorva et al, 2012). The thinning increases with the disease, and it is correlated with the degree of the motoric symptoms that the patients present (Koskenkorva et al, 2009; Koskenkorva et al, 2012), i.e. ataxia and dysarthria. The loss of γ-aminobutyric acid (GABA) -ergic Purkinje cells and non-specific degenerative changes in the cerebellar cortex that have been observed in histopathological examinations (Eldridge et al, 1983) translates into functional disabilities in motoric tasks of the patients. Neuronal cytoplasmic inclusions, positive for stainings with the lysosomal marker CD68 and the lysosomal protein cathepsin B, have also been detected (Cohen et al, 2011).

The skeletal characteristics are also altered in EPM1 patients. The first report of increased scull thickness, scoliosis, and osteoporosis was published by Koskiniemi et al. (1974), but a more detailed report of progressive thickening of the cranial bones, thoracic and lumbar scoliosis, ossicles in feet, and arachnodactyly has not been reported until recently (Korja et al, 2007; Suoranta et al, 2012).

1.1.2 The cystatin B gene

The gene underlying EPM1, cystatin B (*CSTB*, OMIM 601145) (**Figure 1**), on chromosome 21q22.3 (Lehesjoki et al, 1991) encodes for an intracellular cysteine proteinase inhibitor, cystatin B (CSTB) (Pennacchio et al, 1996). The gene has five putative transcripts of which one is known to be protein coding (Joensuu et al, 2007). The main transcript has three exons which are translated into 98 amino acids.

1.1.2.1 Mutations in CSTB

Fourteen loss-of-function mutations in the *CSTB* gene underlying EPM1 have been described (Bespalova et al, 1997a; Canafoglia et al, 2012; De Haan et al, 2004; Erdinc et al, 2010; Joensuu et al, 2007; Kagitani-Shimono et al, 2002; Lafreniere et al, 1997; Lalioti et al, 1997a; Lalioti et al, 1997b; Pennacchio et al, 1996; Pinto et al, 2012; Virtaneva et al, 1997). The most common mutation is a 12-nucleotide long dodecamer expansion repeat (5'-CCCC GCCC CGCG-3') in the promoter area of the gene (Lalioti et al, 1997b), leading to unstable initiation of transcription and a significantly reduced gene expression with less than 10% of *CSTB* mRNA produced (Joensuu et al, 2007). The dodecamer repeat is polymorphic and exists in the healthy population in 2-3 copies, while EPM1-associated alleles contain at least 30 copies. The number of expansion repeats is in general not correlated with the severity of the disease symptoms (Lalioti et al, 1998), but patients with more than 68 repeats on one allele have both an earlier onset of the symptoms and higher myoclonus rating scores in comparison to patients with 68 repeats or less (Hyppönen et al, unpublished).

The remaining 13 EPM1-associated mutations affect splice sites, change amino acids, or are predicted to express a truncated protein (Joensuu et al, 2008). The identified *CSTB* mutations are summarized in **Table 1** and their positions are illustrated in **Figure 1**.

Table 1. The identified mutations in the *CSTB* gene underlying EPM1. Modified from Joensuu et al, 2008

Mutation	Position of mutation/ mutation type	Predicted consequence on protein level	Reference
Dodecamer repeat expansion	5' UTR/expansion	Reduced *CSTB* expression	Lafreniere et al, 1997; Lalioti et al, 1997b; Virtaneva et al, 1997
c.10G>C	Exon 1/missense	p.Gly4Arg	Lalioti et al, 1997a
c.66G>A	Exon 1/splice site?	p.Gln22Gln	Pinto et al, 2012
c.67-1G>C	Intron 1/splice site	p.delVal23_Lys56	Bespalova et al, 1997a; Lafreniere et al, 1997; Lalioti et al, 1997a; Pennacchio et al, 1996
c.125C>A	Exon 2/nonsense	p.Ser42Ter	Erdinc et al, 2010
c.136C>T	Exon 2/nonsense	p.Gln46Ter	Canafoglia et al, 2012*
c.149G>A	Exon 2/missense	p.Gly50Glu	Joensuu et al, 2007
c.168T>A	Exon 2/splice site	Aberrant splicing?	Kagitani-Shimono et al, 2002
c.168 + 1_18del	Intron 2/deletion	p.delVal23_Lys56 p.Val57GlufsTer28	Joensuu et al, 2007
c.168+2_168+21delinsAA	Intron 2/deletion + insertion	?	Canafoglia et al, 2012*
c.169–2A>G	Intron 2/splice site	Aberrant splicing?	De Haan et al, 2004; Lafreniere et al, 1997; Pennacchio et al, 1996
c.202C>T	Exon 3/nonsense	p.Arg68Ter	De Haan et al, 2004; Lafreniere et al, 1997; Pennacchio et al, 1996
c.212A>C	Exon 3/missense	p.Gln71Pro	De Haan et al, 2004
c.218_219delTC	Exon 3/deletion	p.Leu73fsTer3	Bespalova et al, 1997b; Lafreniere et al, 1997; Lalioti et al, 1997a

*Discrepancy in position of mutations in article. Positions confirmed by Elena Gennaro, personal communication (22.4.2013)

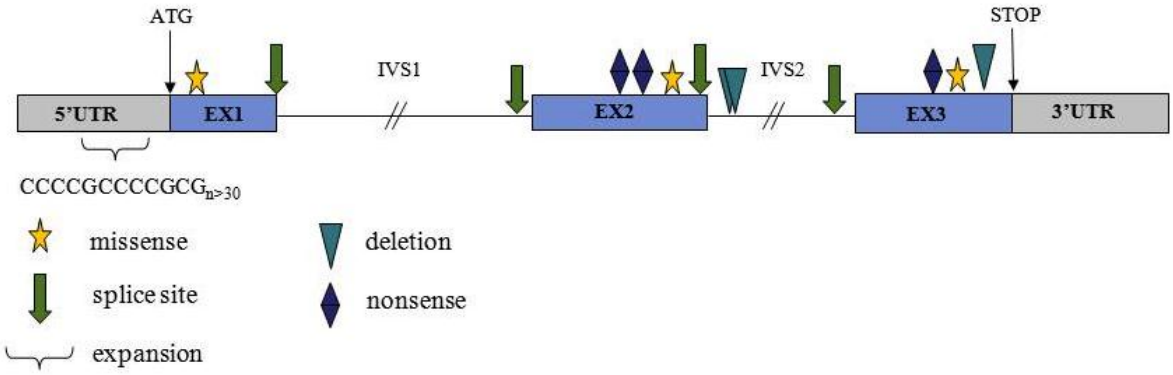

Figure 1. The identified *CSTB* mutations presented according to their position and mutation type. UTR = untranslated region, IVS = intervening sequence, EX = exon. Modified from Joensuu et al, 2008

About 90% of all EPM1 patients and 99% of the Finnish patients carry the expansion repeat allele (Kälviäinen et al, 2008), to which most patients are homozygous. The remaining reported patients are compound heterozygous for the expansion and one of the other mutations, with the exception of two cases (Lalioti et al, 1997a; Pinto et al, 2012), who are homozygous for a missense (c.10G>C) or a splice site mutation (c.66G>A). Compound heterozygous patients with the expansion and the c.202C>T mutation have been reported to have more severe symptoms than patients homozygous for the expansion mutation (Koskenkorva et al, 2011). The nonsense mutation c.202C>T causes an early termination codon and lack of functional CSTB protein, and therefore there is even less functional CSTB protein produced in comparison to <10% from the repeat expansion allele (Koskenkorva et al, 2011).

1.1.3 The cystatin B protein

The CSTB protein belongs to the type 1 cystatin family, which, together with type 2 cystatins and kininogens, belongs to the cystatin superfamily. The superfamily contains proteins rich in cystatin-like sequences and many of its members, such as CSTB, function as cysteine protease inhibitors (Rawlings & Barrett, 1990).

CSTB is ubiquitously expressed, and its cellular localization is dependent on the developmental stage of the cell. CSTB is located mainly in the nucleus in proliferating cells, whereas in mature cells it is mainly found in the cytoplasm and associated with lysosomes (Alakurtti et al, 2005; Čeru et al, 2010b). Higher expression levels of CSTB have been observed in cerebellar Purkinje cells and in Bergmann glia in the human adult central nervous system (CNS) (Brännvall et al, 2003), and also in cerebellar oligodendrocyte progenitor cells in the rat CNS (Riccio et al, 2005).

The full-length CSTB protein consists of a single polypeptide chain without disulphide bonds or carbohydrate side chains, and it folds into a neutral protein with a molecular weight of 11 kDa (Järvinen & Rinne, 1982; Ritonja et al, 1985). The schematic structure of the CSTB protein is presented in **Figure 2**.

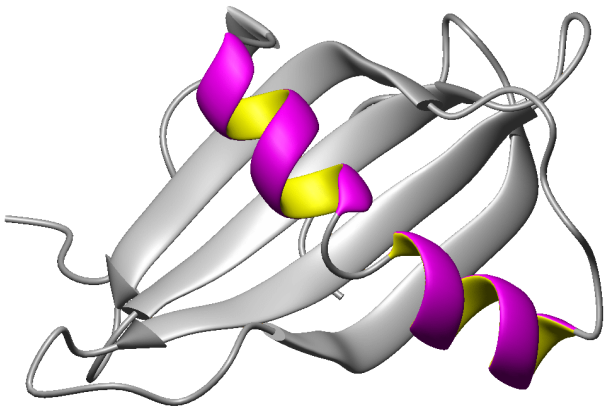

Figure 2. The schematic structure of the human cystatin B protein consists of a five-stranded beta-sheet (silver) wrapped around a five-turn alpha-helix (purple). The human CSTB contains also a carboxy-terminal strand, which runs in parallel with the convex side of the beta-sheet Stubbs et al, 1990.
Modified from: http://bioch.szote.u-szeged.hu/astrojan/protein/pictures/cystat3.gif

CSTB counteracts lysosomal protease activity, i.e. papains and certain cathepsins, both *in vitro* (cathepsins B, H, S, L and K) (Brömme et al, 1991; Green et al, 1984; Laitala-Leinonen et al, 2006), and *in vivo* in lymphoblastoid cells (cathepsins B, S, and L) (Rinne et al, 2002). Cathepsins reside mainly in the lysosomes, but they are hypothesized to leak out to the cytosol, where they are inhibited by CSTB (Rinne et al, 2002). The

association between CSTB and cathepsins is tight, but reversible, and it is mediated by non-covalent forces via the highly conserved QVVAG (Gln-Val-Val-Ala-Gly) sequence in CSTB, forming the first hairpin loop at its N-terminus (Stubbs et al, 1990). The cathepsins possess several intra- and pericellular catalytic roles, in which the inhibitory function of CSTB has particular importance. As an example, in proliferating cells *in vitro*, the loss of CSTB-mediated inhibition of cathepsin L in the nucleus makes cells enter the S phase earlier, thereby speeding up the cell cycle (Čeru et al, 2010a). CSTB participates also in inhibiting bone resorption *in vitro* by downregulating the activity of cathepsin K in osteoclasts (Laitala-Leinonen et al, 2006).

1.1.4 The cystatin B deficient *(Cstb*$^{-/-}$*)* mouse

A mouse model for EPM1 was created by targeted disruption of the *Cstb* exon 1 (Pennacchio et al, 1998) leading to loss-of-function of the gene, thereby mimicking the *CSTB* mutations in EPM1 patients.

The *Cstb*$^{-/-}$ mice are born with no visible difference to wild type (wt) mice, and after weaning, at 1-3 months of age, they have the same body size, grooming behavior, coordination and strength as the control mice (Pennacchio et al, 1998). The *Cstb*$^{-/-}$ mice, however, develop myoclonic seizures during sleep at one month of age, consisting of twitches in the whiskers, ears, and the tail, leading to facial spasms and shaking of the torso and the limbs. The attacks last from a few seconds up to several minutes, and they usually end with a large myoclonic outburst (Pennacchio et al, 1998). Worsening of the myoclonus is paralleled with decreased stainings with the γ-aminobutyric acid (GABA) terminal density marker, vesicular GABA transporter (VGAT) in the cortex, indicating a reduction in GABA terminals, as it has been reported in 8 months old *Cstb*$^{-/-}$ mice (Buzzi et al, 2012). The reduced amount of GABA interneurons leads to loss of inhibition and hyperexcitability in the cortex, which might contribute to the myoclonic seizures (Buzzi et al, 2012).

At six months of age the *Cstb*$^{-/-}$ mice develop a mild ataxia which gets progressively worse (Pennacchio et al, 1998). The ataxia phenotype has been associated with loss of cerebellar granule cells, supported by both histopathological findings (Pennacchio et

al, 1998) and stereological analyses (Tegelberg et al, 2012). Atrophy of the cortex and the cerebellum in *Cstb*$^{-/-}$ mice is observed from two months of age, reaching an almost 50% volume loss by the age of six months (Tegelberg et al, 2012). Positive terminal deoxynucleotidyl transferase dUTP nick end labeling (TUNEL) stainings have also indicated that the cerebellar granule neurons of *Cstb*$^{-/-}$ mice are in an apoptotic state (Pennacchio et al, 1998; Shannon et al, 2002). Double knockout mice for *Cstb* and cathepsin B (*Ctsb*) (*Cstb*$^{-/-}$/*Ctsb*$^{-/-}$) present with less TUNEL positive cerebellar granule neurons and milder neurological symptoms, suggesting that the described EPM1 symptoms in mouse are at least partly mediated through CTSB (Houseweart et al, 2003).

Widespread gliosis has been observed in the brains of older (16-18 months) *Cstb*$^{-/-}$ mice (Shannon et al, 2002), but also in other animal models with epilepsy as phenotype (Avignone et al, 2008; Taniwaki et al, 1996). Microglial activation has been reported to occur after epileptic seizures (Taniwaki et al, 1996), but Tegelberg et al. showed increased F4/80 positive cells in *Cstb*$^{-/-}$ mice indicating activation of microglia already at postnatal day 14 (P14). This was followed by increased GFAP positive cells at one month of age, indicating activation of astroglia and suggesting an inflammation phenotype already before any of the previously described symptoms of EPM1 start to manifest (Tegelberg et al, 2012). The progression of the symptoms and the histopathological changes in the *Cstb*$^{-/-}$ mouse are shown in **Figure 3**.

The genetic background of the mice affects the severity of the symptoms, i.e. the strain 129Sv (seizure prone) is more affected than the cross C57BLx129Sv (seizure resistant). Only *Cstb*$^{-/-}$ mice in the 129Sv background develop myoclonic seizures, while ataxia and abnormalities in brain, such as neural loss and gliosis, are seen in both backgrounds (Pennacchio et al, 1998; Shannon et al, 2002). Photosensitivity, tonic-clonic epileptic seizures, myoclonic jerks while being awake, or an abnormal EEG have not been detected in *Cstb*$^{-/-}$ mice in neither background (Pennacchio et al, 1998).

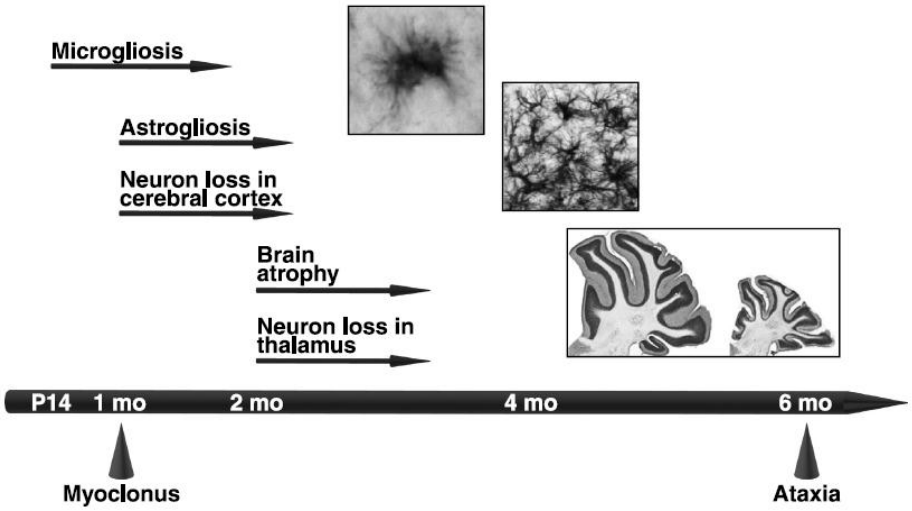

Figure 3. The symptomatic and histopathological findings in the *Cstb*$^{-/-}$ mouse. Adapted from Tegelberg et al, 2012 with permission of Wolters Kluwer Health

1.1.4.1 Exon array analysis from primary microglia of P5 Cstb$^{-/-}$ *mice*

Histopathological data from the brain of *Cstb*$^{-/-}$ mice revealed early and progressive activation of microglia (Tegelberg et al, 2012). Therefore, an exon array analysis (Exon array 1.0 ST) was conducted from the cultured primary microglia of postnatal day 5 (P5+14DIV) *Cstb*$^{-/-}$ mice, in order to study gene expression profiles (Körber et al, unpublished). Downregulation of several interferon stimulated genes (ISGs) was detected, and the downregulation of the genes signal transducer and activator of transcription 1 and 2 (*Stat1* and *Stat2*), and interferon regulatory factor 9 (*Irf9*) suggested an altered Janus kinase (JAK)/STAT signaling pathway in the *Cstb*$^{-/-}$ mice microglia (Körber et al, unpublished). **Table 2** summarizes selected genes and their expression levels from the exon array analysis.

Table 2. The relative gene expression profile from P5 *Cstb*$^{-/-}$ mice microglia. Modified from Körber et al, unpublished.

Fold change	Gene symbol	Gene description
-9,3	*Cstb*	cystatin B
-2,7	*Stat1*	signal transducer and activator of transcription 1
-2,5	*Stat2*	signal transducer and activator of transcription 2
-1,6	*Irf9*	interferon regulatory factor 9

1.2. Microglia

Microglia are resident macrophages and the predominant immune cells of the CNS. They regulate the immunological response to physiological and pathological conditions in the brain, which is shielded by the blood brain barrier (BBB). During conditions such as inflammation, lesions, and neurological disorders, the BBB becomes leaky and other immune cells, such as leukocytes, invade the CNS (Brown & Neher, 2010; Liu & Hong, 2003).

Microglia can be in a resting, an activated, or a phagocytic state, depending on the present microenvironment. The states differ from each other both structurally and functionally, and **Figure 4** presents the main structural differences.

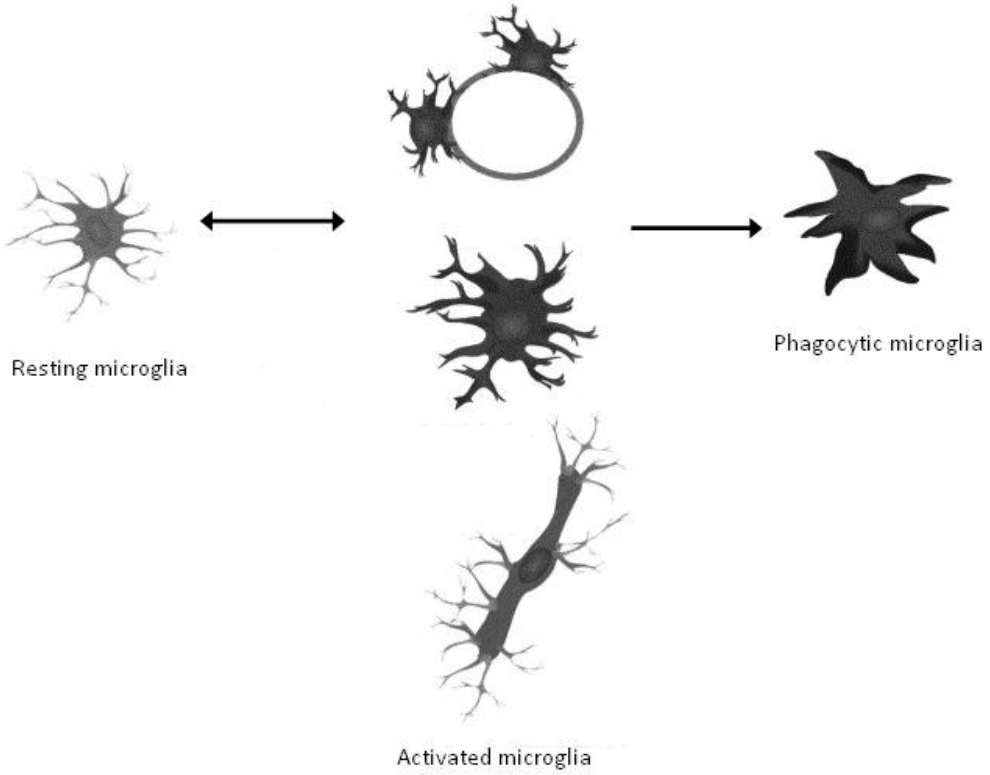

Figure 4. The microglial morphology is a hallmark for their activation state. Modified from Orr et al, 2002

The resting microglia has a highly branched and ramified morphology, and it is the predominant form of microglia in the healthy CNS. The resting microglia does not have phagocytic activity, but it is highly motile, surveying its microenvironment with its processes (Kreutzberg, 1996; Nimmerjahn et al, 2005). When triggered by an environmental signal, the resting microglia becomes activated and starts expressing an amoeboid phenotype. The activated form of microglia has phagocytic activity, and it scavenges dead cells in the brain and releases immunoeffector molecules (Kreutzberg, 1996; Nakajima & Kohsaka, 2001). If the environmental signal persists, the microglia transform to the third, the most active, phagocytic form, which is large and has a round cell shape. Both the activated and the phagocytic form express major histocompatibility complex (MHC) class II molecules and present antigens, triggering additional immune related responses (Brown & Neher, 2010; Czeh et al, 2011; Nakajima & Kohsaka, 2001). This activation of the adaptive immune system is an

important function of the acquired immune system (Orr et al, 2002), which is crucial for healing, but can be neurotoxic when prolonged (Czeh et al, 2011; Liu & Hong, 2003).

Epileptic seizures and ageing lead to higher microglial activity and sensitivity, causing microglial reactivity (Avignone et al, 2008; Beach et al, 1995; Czeh et al, 2011). Hyperactive microglia has been observed in certain neurodegenerative disorders, such as Alzheimer´s disease (AD), Parkinson´s disease (PD) (Liu & Hong, 2003; McGeer et al, 1988), and multiple sclerosis (MS) (Jack et al, 2005).

1.3. Janus kinase (JAK)/Signal transducer and activator of transcription (STAT) signaling pathway

Viruses, bacteria and some tumors activate the innate immune system, leading to cytokine secretion from lymphocytes. These cytokines, in particular interferon alpha (IFN-α), - beta (IFN-β), and - gamma (IFN-γ), mediate the activation of the subsequent type I and type II interferon signaling cascades via the JAK/STAT signaling pathway, leading to transcriptional activation of gene expression (Darnell et al, 1994; Liu et al, 1998b).

1.3.1. Signal transducer and activator of transcription (STAT) 1 and 2

The signal transducer and activator of transcription (*STAT*) –genes form a family, which in mammals comprises seven members, *STAT1, STAT2, STAT3, STAT4, STAT5A, STAT5B,* and *STAT6.* STATs activate the transcription of genes involved in cell growth, differentiation, apoptosis, and immune responses (Lim & Cao, 2006). All STAT proteins share similar structural motifs, including a central DNA-binding domain (DBD), a Src homology 2 (SH2) -domain, and a tyrosine residue (Y701) at the carboxy-terminal (Lim & Cao, 2006). The *STAT1* (OMIM 600555) and *STAT2* (OMIM 600556) genomic loci are at 2q32.2 and 12q13.3, respectively. STAT1 has two isoforms, STAT1α (84 kDa), and

STAT1β (91 kDa) (Baran-Marszak et al, 2004), whereas STAT2 has only one known isoform (113 kDa) (Fu et al, 1990).

STAT1 and STAT2 are regulated on phosphorylation level by the activity of the kinases JAK1, TYK2, and several dephosphorylating protein tyrosine phosphatases (PTPases). STAT1 is directly inhibited *in vitro* by protein inhibitor of activated STAT1 (PIAS1) in the nucleus, which blocks the DNA binding region of STAT1 (Liu et al, 1998a). PIAS1 has also been observed to upregulate the *CSTB* promoter activity in the African green monkey kidney cell line, COS-1 (Ilmarinen et al, 2008). However, similar experiments in the murine macrophage cell line, RAW264.7, have revealed an opposite effect of PIAS1 by downregulating the *CSTB* promoter activity (Körber et al, unpublished). PIAS1 interacts also *in vitro* with the transcriptional regulator autoimmune regulator (AIRE), which has been shown to strongly repress the *CSTB* promoter in COS-1 cells (Ilmarinen et al, 2008).

All STATs are also indirectly regulated by suppressor of cytokine signaling (SOCS) proteins, which inhibit the kinase activity of JAKs (Krebs & Hilton, 2001).

1.3.2. Interferon regulatory factor 9 (IRF9)

The interferon regulatory factor 9 (IRF9), also known as interferon (IFN) stimulated gene factor 3γ (ISGF3γ) or p48, is encoded by the *IRF9* gene (OMIM 147574) on locus 14q11.2, and it belongs to the family of interferon regulatory factors (IRFs) (Reich, 2002). The ten members of the IRF family (IRF1-10) activate transcription of interferon stimulated genes inducing cell growth, proliferation, differentiation, apoptosis, and immune responses (Ousman et al, 2005).

Gene expression of IRFs may be constitutive, induced, and tissue-specific, and it is often associated with viral infections or tumorigenesis. Interferons induce the expression of most IRFs, which in the nucleus regulate gene expression. The expression of IRF3 and IRF9 is, however, relatively constant in most cells and their activity is solely regulated by redistribution between the nucleus and the cytoplasm (Reich, 2002; Savitsky et al, 2010). IRF3 and IRF9 do not regulate the activity of ISGs

per se, but function only when in complex with other, non-IRF proteins, such as the STATs (Reich, 2002).

1.3.3. The Interferon-stimulated gene factor 3 (ISGF3) -complex

The interferon-stimulated gene factor 3 (ISGF3) –complex is an activator of transcription of type I (IFN-α, IFN-β) ISGs during viral activation and drives the cell to an antiviral state with reduced cellular proliferation and protein synthesis (Schindler et al, 1992). STAT1, STAT2, and IRF9 build the ISGF3 –complex.

Interferon secretion from lymphocytes and their binding to their specific receptor units initiate an intracellular signaling cascade, the JAK/STAT signaling pathway (**Figure 5**). The receptor unit of type I IFN receptor (IFNAR) is facing to the extracellular space and it consists of two distinct transmembrane subunits, Interferon receptor 1 (IFNAR1) and Interferon receptor 2 (IFNAR2) (de Weerd et al, 2007). The receptor subunits do not have a phosphorylation activity *per se*, therefore they are pre-associated with the JAK1 and TYK2 kinases (de Weerd et al, 2007; Reich, 2007), which phosphorylate the carboxy-terminal tyrosine residues (Y701) of free cytoplasmic STAT1 and STAT2. Upon phosphorylation, the STATs undergo a conformation change and form heterodimers at their phosphotyrosine and SH2 domains (Reich, 2007). Unphosphorylated IRF9 binds to the phosphorylated STAT1-STAT2 heterodimer at the amino terminal coiled-coil region of STAT2, and forms the ISGF3 complex. Dimerization of STATs reveals a nuclear localization signal (NLS), which binds to importin-α receptors in the cytoplasm. Importin-α mediates the translocation of the ISGF3 complex to the nucleus via importin-β receptors through the nuclear pore complex (NPC), which spans across the nuclear membrane. The translocation is an active process mediated by the small guanosine triphosphate hydrolase (GTPase) Ran (Fagerlund et al, 2002; Liu et al, 1998b; Sekimoto et al, 1996). The NLS is unrevealed in monomeric STAT proteins keeping their localization mainly cytoplasmic when in a latent, unphosphorylated state (Reich, 2007).

In the nucleus, the ISGF3 complex binds to DNA at interferon stimulated response elements (ISREs) (Gutch et al, 1992) in the promoter area of ISGs, and activates

transcription of these genes via the carboxy-terminal transactivation domain of STAT2 (Fu et al, 1992; Gutch et al, 1992). STAT2 requires a sequence-specific part of ISRE for transcriptional activation, and is unable to form stable interactions with DNA without STAT1 (Frahm et al, 2006).

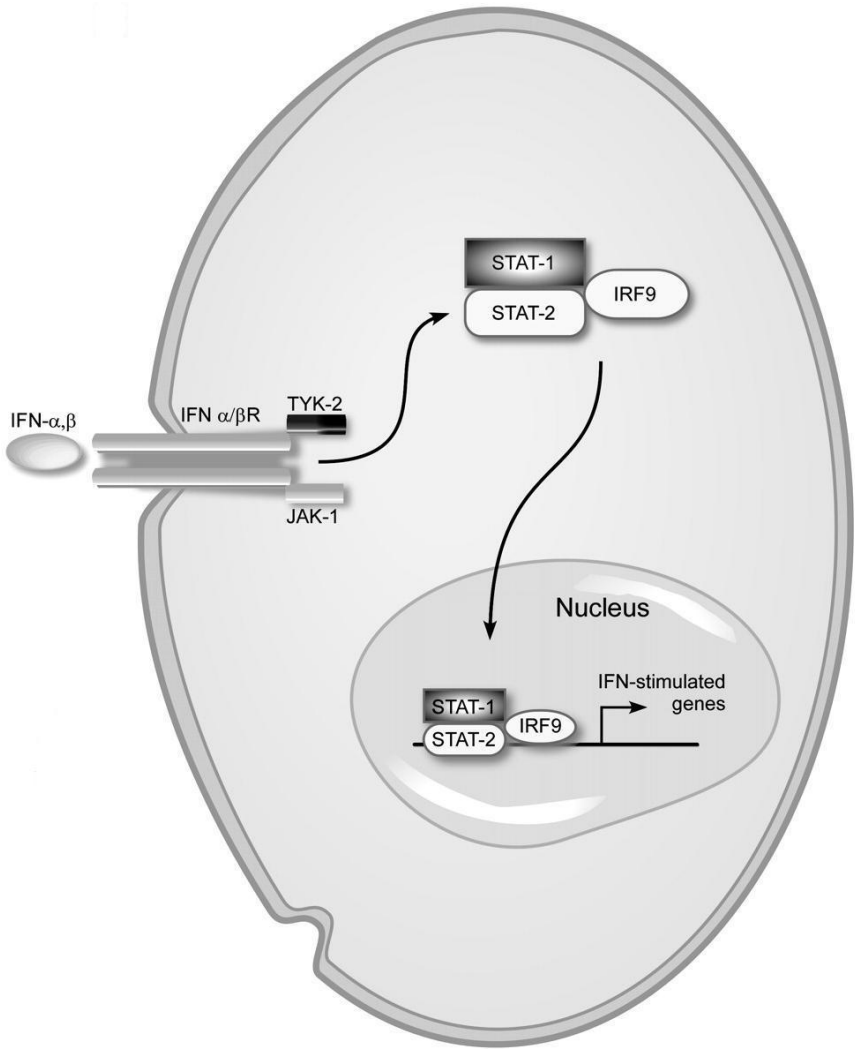

Figure 5. The type I interferon mediated signaling cascade leads to transcription of antiviral genes in the cell. Modified from Dropulic & Cohen, 2011

1.4. Inducible nitric oxide synthase (iNOS) and nitric oxide (NO)

The chemical compound nitric oxide (NO) is an important signaling molecule in the body, participating in i.e. vasodilatation, neurotransmission, inflammatory responses, and apoptosis (Chan & Riches, 2001; Gao et al, 1997; Kröncke et al, 1997; Martin et al, 1994). Microglia produce and release NO during inflammation, triggering subsequent immune related responses.

NO is produced by nitric oxide synthase (NOS) as a by-product in the arginine-citrulline pathway (**Figure 6**), where L-arginine is converted to citrulline (Martin et al, 1994). Neurons are highly susceptible to the effects of NO (Aquilano et al, 2011; Kröncke et al, 1998), and therefore it is one of the most strictly regulated molecules, being spatiotemporally regulated by several mediator proteins (Gao et al, 1997; Kröncke et al, 1998). The cerebella of *Cstb*$^{-/-}$ mice were shown to be sensitized to oxidative stress (Lehtinen et al, 2009), suggesting that *Cstb* is associated with regulation of the redox-homeostasis.

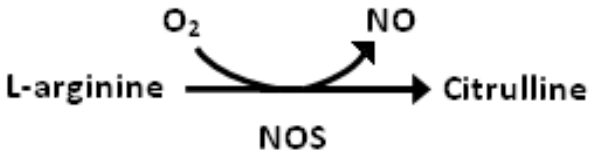

Figure 6. The arginine-citrulline pathway produces nitric oxide as a by-product

The *NOS* gene has three isoforms, neuronal *NOS (NOS1, nNOS),* inducible *NOS (NOS2, iNOS)*, and endothelial *NOS (NOS3, eNOS)*. The inducible form, *iNOS*, is activated in response to i.e. pathogenic attacks, resulting in long-term innate immunological responses (Brosnan et al, 1997). The human *iNOS* gene is located on chromosome 17q11.2, and it has 27 exons (Xu et al, 1996). The promoter area of *iNOS* is one of the longest and most complex known, indicating a tight control of gene expression

(Kröncke et al, 1998). In the human brain, *iNOS* is expressed in astrocytes and in microglia, but also in neurons during their early developmental stages (Heneka & Feinstein, 2001).

The two other NOS isoforms, nNOS and eNOS, participate in short-term events such as neurotransmission and vasodilatation. The balance between the short-term and the long-term NO production gives the basis for the physiological vs. pathophysiological actions of NO, which is thought to play an important role in human neurodegenerative diseases (Brosnan et al, 1997). This is supported by the observation that neuronal iNOS is not expressed in the healthy adult brain, but re-expression with increasing age and age-related neurological disorders has been observed (Heneka & Feinstein, 2001). The activation signals for induction of *iNOS* are cell- and species specific, and the expression starts late, hours after the initial stimuli (Brosnan et al, 1997; Koprowski et al, 1993; Kröncke et al, 1998). In order to produce massive amounts of NO, iNOS requires interferon induced activation of the cell.

The two main pathways which are involved in the transcriptional control of *iNOS* are the IFN-γ induced JAK/STAT signaling pathway and the nuclear factor of kappa light polypeptide gene enhancer in B cells (NF-κB) pathway. Homodimerized phosphorylated STAT1α complexes translocate to the nucleus and bind to the interferon-γ activation sequence (GAS) in the promoter of the *iNOS* gene and activates its expression (Gao et al, 1997). The *iNOS* gene expression can also be induced without transcription activators binding to the GAS site, but the amount of iNOS and the subsequent NO produced is significantly lower (Gao et al, 1997).

Both lipopolysaccharide (LPS) and IFN-γ induce *iNOS* expression in the murine macrophage cell line RAW264.7, of which the IFN-γ induced JAK/STAT signaling pathway is of particular importance, since the macrophages start mediating inflammatory signals when activated (Guo et al, 2007). NO production has been largely studied in rodent macrophages and it has been discovered to play an important role as a cytotoxic effector molecule (Kröncke et al, 1998). These results have, however, not been observed in human macrophages even if they express *iNOS*. Human diseases with chronic inflammation, i.e. rheumatoid arthritis (RA) and multiple sclerosis (MS)

have been associated with elevated *iNOS* expression (Kröncke et al, 1998) and the iNOS protein has also been found in post-mortem brain samples from patients with Alzheimer´s and Parkinson´s disease. Whether elevated iNOS expression is a primary or a secondary cause for the diseases has, however, not been elucidated (Kröncke et al, 1998).

1.5. RNA interference as a technique for *in vitro* models

In vitro disease models are beneficial and convenient tools in medical science if patient samples are not available. They are of particular importance if biochemical mechanisms are not understood (Gartler et al, 1962) or the disease is of multigenic origin, i.e. many cancer types. Simplification of the macroenvironment, enabling the studies to be conducted in a controlled fashion, is the key for *in vitro* studies, but they do, however, never completely substitute *in vivo* models, thus can assumptions of disease mechanisms not be made solely based on them (Black, 1976).

1.5.1. RNA interference

RNA interference (RNAi) is a powerful and specific post-transcriptional gene regulation mechanism, which utilizes double-stranded RNA (dsRNA) in silencing the expression of a specific gene by inhibiting protein translation (Pecot et al, 2011). RNAi pathways are conserved in nearly all animals and plants, but the mechanism was, however, not discovered until the end of the 20th century. Andrew Fire and Craig C. Mello were rewarded the Nobel Prize in Physiology or Medicine in 2006 for their work on RNAi, which was published in 1998 (Fire et al, 1998).

RNAi is widely used in biochemical and clinical research for knocking down genes, and latest advances have enabled its use as a therapeutic tool for treating i.e. different cancers. Suppression of oncogenes is challenging by traditional methods (small molecular inhibitors and antibodies) because the oncogenes are difficult to target specifically. Synthetic small interfering RNAs (siRNAs) have successfully been introduced to patients *in vivo* in more than 15 clinical trials, but these trials are

ongoing and the results will show the effect on disease progression within the next few years (Burnett & Rossi, 2012).

1.5.2. RNA inhibitors

The interfering RNA molecules are either endogenously transcribed during nearly all essential processes of the cell, such as developmental stages and viral infections, or exogenously introduced to the cell by viruses or by transfection. There are several types of repressing RNA molecules, of which microRNA (miRNA) and short interfering RNA (siRNA) are the best characterized.

1.5.2.1. Endogenous RNA inhibitors

Both miRNA and siRNA sequences are endogenously transcribed as precursors, which are cleaved and modified in the cell. The same locus in the genome can code for two different miRNAs from opposite strands, as has been reported in *Drosophila melanogaster* (Stark et al, 2008), pointing out the massive diversity and quantity of endogenous miRNAs. The siRNAs can arise from intergenic sequences, gene coding sequences, introns, and from transposable elements, as observed in *Arabidopsis thaliana* (Llave et al, 2002).

The miRNA sequence is originally transcribed as a long stem-and-loop precursor (pri-miRNA), which is cleaved in the nucleus by the ribonuclease (RNase) Drosha to a pre-miRNA (**Figure 7**), and exported to the cytoplasm. In the cytoplasm, the pre-miRNA is cleaved by another RNase, Dicer, to its mature 21-23 base pair (bp) form (Burnett & Rossi, 2012). The siRNA sequences, which lack the stem-and-loop structure, are linear and are processed by Dicer only.

Both miRNA and siRNA sequences are double-stranded, consisting of a sense- and an antisense strand, also known as passenger- and guide strands. The antisense strand is complementary to the target mRNA sequence, and the sense strand is hypothesized to mediate the binding to members of the argonaute (AGO) protein family (**Figure 7**) in

the catalytic site of the RNA-induced silencing complex (RISC). The RISC cleaves and removes the sense strand, and guides the antisense strand to the 3' untranslated region (UTR) of the target mRNA sequence. If the siRNA is less than 100% complementary to the target sequence, the mRNA will be degraded, otherwise it gets cleaved (Burnett & Rossi, 2012).

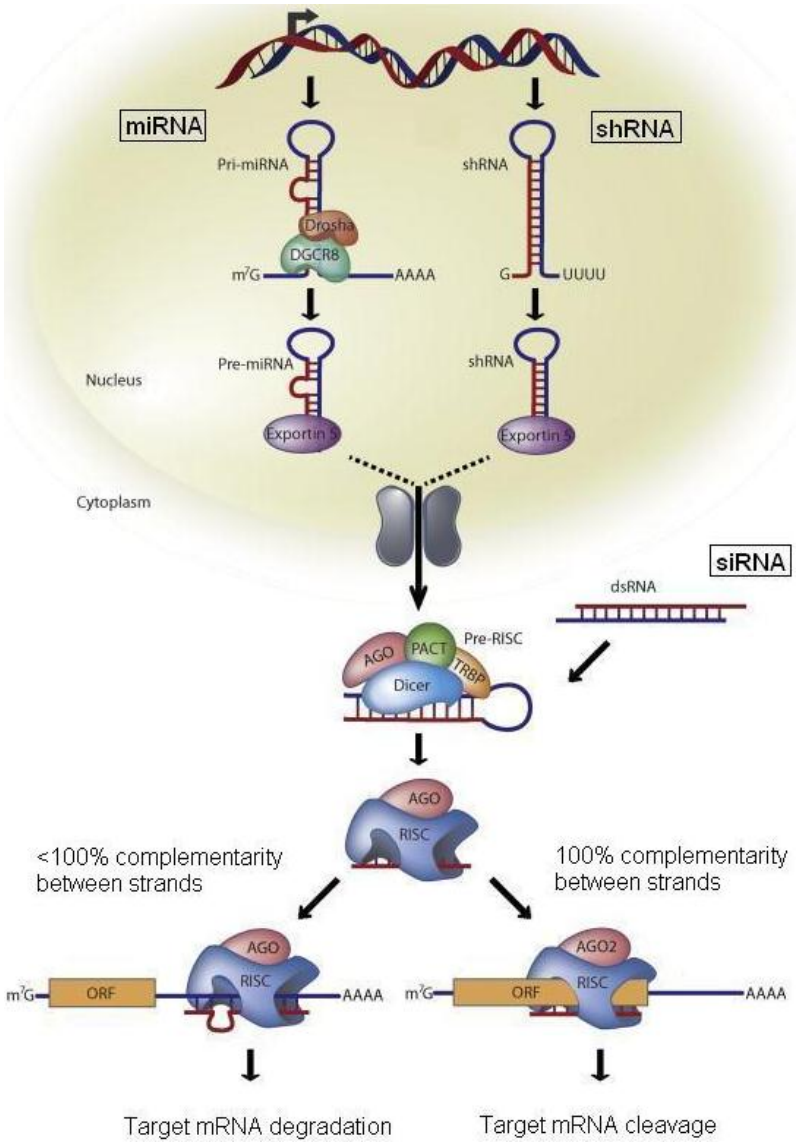

Figure 7. The best characterized RNAi pathways. The endogenously transcribed miRNA and shRNA sequences are exported as stem-and-loop precursors from the nucleus to the cytoplasm, where they become modified by the RNase Dicer. Dicer modifies also the exogenously introduced linear siRNA sequence. All three RNA inhibitors are further bound by the multimer protein unit RISC, which guides the antisense-strand (red) of the RNA inhibitor to the target mRNA-sequence (blue), and catalyzes its proteolytic processing. Modified from Burnett & Rossi, 2012

1.5.2.2. Exogenous RNA inhibitors

Exogenously introduced synthetic RNA inhibitors, such as exo-siRNAs and short hairpin RNAs (shRNAs), act similarly as the endogenously transcribed RNA inhibitors. Synthetic siRNA oligos are 21-26 nucleotide long double-stranded sequences with a two nucleotide overhang in both 3' ends. The synthetic siRNA antisense strand is, like the endogenous siRNA, complementary to the mRNA sequence of the target gene, and the siRNA is processed and targeted in a similar way as endogenous siRNAs by Dicer and RISC (Burnett & Rossi, 2012; Rao et al, 2009b). The efficiency of synthetic siRNA inhibition is, however, hard to predict, because target gene specific features, such as the guanine-cytosine (GC) content, point-specific nucleotides, and specific motif sequences have been reported to affect RNAi efficiency (Chan et al, 2009; Takasaki, 2010). Synthetic siRNAs have also been reported to be potential activators of the innate immune system in some mammalian cell lines, leading to the release of cytokines, such as interferons (Eberle et al, 2008; Jiang et al, 2004; Robbins et al, 2009; Sledz et al, 2003).

Cell proliferation and endogenous degradation of the exo-siRNA sequences result in siRNA dilution and loss of RNAi (Rao et al, 2009a; Sandy et al, 2005), limiting the applications the method can be used for. Long-term events due to target gene suppression are therefore not possible to study by this method as a result of the transient effect of the exo-siRNA mediated RNA inhibition.

ShRNAs are exogenously synthesized DNA-sequences, which are cloned into plasmid vectors and transfected into target cells (Burnett & Rossi, 2012; Rao et al, 2009b). If transfected as such, the shRNA is transcribed from the plasmid and creates a transient RNAi effect (Sandy et al, 2005). ShRNA-plasmids can, however, also be introduced to the genome of the target cell by transduction. Some viral methods enable the integration of the shRNA into the genome, thereby creating a permanent genomic siRNA producing sequence and a stable knockdown of the target gene. The site of incorporation of the shRNA sequence is, however, random, and can lead to unknown off-target effects (Sandy et al, 2005). Transcription of the shRNA sequence is mediated by the catalytic action of RNA Polymerase III (Pol III), and the transcribed sequence

folds into a stem-and-loop precursor, resembling the miRNA structure (**Figure 7**) (Burnett & Rossi, 2012). Long-term RNA interference, mediated by stably transduced shRNA, increases greatly the amount of applications that RNAi can be used for.

1.5.3. Transfection methods

Transfection is a molecular method used in the field of cell biology to introduce foreign nucleic acids, i.e. siRNAs or gene expression plasmids, into mammalian cells (Zhang et al, 2009). The method is used for both overexpressing and knocking down genes, making it an important tool for modern genetics and therapeutic research. It has rapidly evolved into one of the most important tools in loss-of-function mutation studies (Carralot et al, 2009), but it has also other important applications, i.e. in vaccine development. Joseph S. Pagano and Antti Vaheri described already in 1965 in detail the transfection of primary Rhesus monkey kidney (MK) cells with the poliovirus (Pagano & Vaheri, 1965), and many of these applications described are still in use. The transfection methods of today can roughly be divided in chemical and physical interference with the cell membrane, the most common being cationic lipid-based reagents and electroporation. The choice of method depends on the cell type and the nucleic acids to be transfected. All methods have off-target effects, i.e. activation of unwanted signaling pathways, cytotoxicity, and cell death (Jiang et al, 2004; Zhang et al, 2009).

In the cationic lipid-based transfection, the uptake of extracellular nucleic acids is mediated by endocytosis, making it a physically gentle method. The negatively charged nucleic acids are first incubated with neutral and cationic lipids in order to form nucleic acid/liposome complexes. The uptake of the complexes by the cell membrane takes place by endocytosis, after which their content is released inside the cell. The releasing mechanism is unknown, but it is thought to be mediated by the lipids in the nucleic acid/liposome–complex (Zhang et al, 2009). The major drawbacks of this method are its rather low efficiency in hard-to-transfect cell lines and the cytotoxicity that the cationic lipids might create (Carralot et al, 2009).

Electroporation is, on the other hand, a very effective transfection method, which is based on predisposing the cells to an electric current. The electric current creates a transmembrane potential across the cell membrane (Zhang et al, 2009), changing the structure of the membrane and reversibly opening hydrophilic pores. The nucleic acids enter the cell directly through these pores without i.e. interacting with lysosomal compartments, thereby reducing the possibility for enzymatic degradation. The pores, however, open irreversibly if the transmembrane potential exceeds the tolerable threshold of the cell, leading to loss of membrane integrity and cell death. Due to its effectiveness compared to other transfection methods, electroporation is often used when transfecting i.e. primary cells or hard-to-transfect cell lines (Kim et al, 2008). Electroporation is traditionally performed in electroporation cuvettes or in thin capillary electrodes.

1.5.4. Quantitative gene expression analysis by the TaqMan method

TaqMan is a polymerase chain reaction (PCR) based method, which was originally created in order to simultaneously be able to amplify and quantify DNA. The method is applied for quantifying gene expression and chromosomal DNA deletions, and for detecting genetic polymorphisms (Watson & Li, 2005). The template for TaqMan is DNA, usually complementary DNA (cDNA) transcribed from RNA.

Before amplifying the gene of interest, primers and probes, specific for the gene, are annealed with the template. The primers and probes are usually complementary to a cDNA region covering an exon-exon junction, which prevents the probe from binding to genomic DNA (gDNA) and thereby reduces the amount of false positive results (Proudnikov et al, 2003).

The probe has a quencher and a fluorochrome-labeled reporter covalently attached to it (**Figure 8**), utilizing fluorescence resonance energy transfer (FRET). When the probe is in an intact state the quencher is physically near to the reporter, reducing the fluorescence that the reporter emits, and no fluorescence signal is detected. When amplification proceeds to the locus where the probe is bound, the Taq-polymerase (from the marine Thermus *aquaticus*) cleaves the probe by its 5’ exonuclease activity,

causing the reporter and quencher to dissociate. The effect of FRET diminishes, and the fluorescence signal from the reporter becomes detectable in a thermal cycler.

The detected fluorescence is directly proportional to the amount of free reporter, and therefore to the amount of template in the logarithmic phase of the PCR cycle (Holland et al, 1991; Hoorfar et al, 2004; Proudnikov et al, 2003). The detected fluorescence signal from the gene of interest is normalized to an inner control, i.e. a housekeeping gene, by which bias, such as differences in template amount, is corrected (Holland et al, 1991).

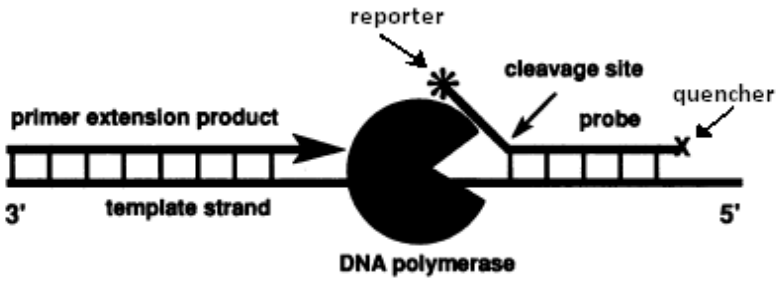

Figure 8. **The principle of the TaqMan method.** Modified from Holland et al, 1991

1.5.4.1. Computational methods for TaqMan analysis

There are different computational methods for determining the relative gene expression levels, of which the standard line method, the delta delta Ct (ΔΔCt) – method, and the Pfaffl –method are well known and commonly used (Heid et al, 1996; Livak & Schmittgen, 2001; Pfaffl, 2001).

The TaqMan software displays the results, with the cycle number of the PCR run on the X-axis and the detected fluorescence (Rn) exponentially as an arbitrary unit, on the Y-axis (**Figure 9**). The cycle, in which the detected fluorescence exceeds a linear baseline, is called the cycle threshold (Ct), and it is used to compute the gene

expression. The Ct value is dependent i.e. on DNA concentration, and therefore, is it not a measurement of gene expression *per se* (Heid et al, 1996).

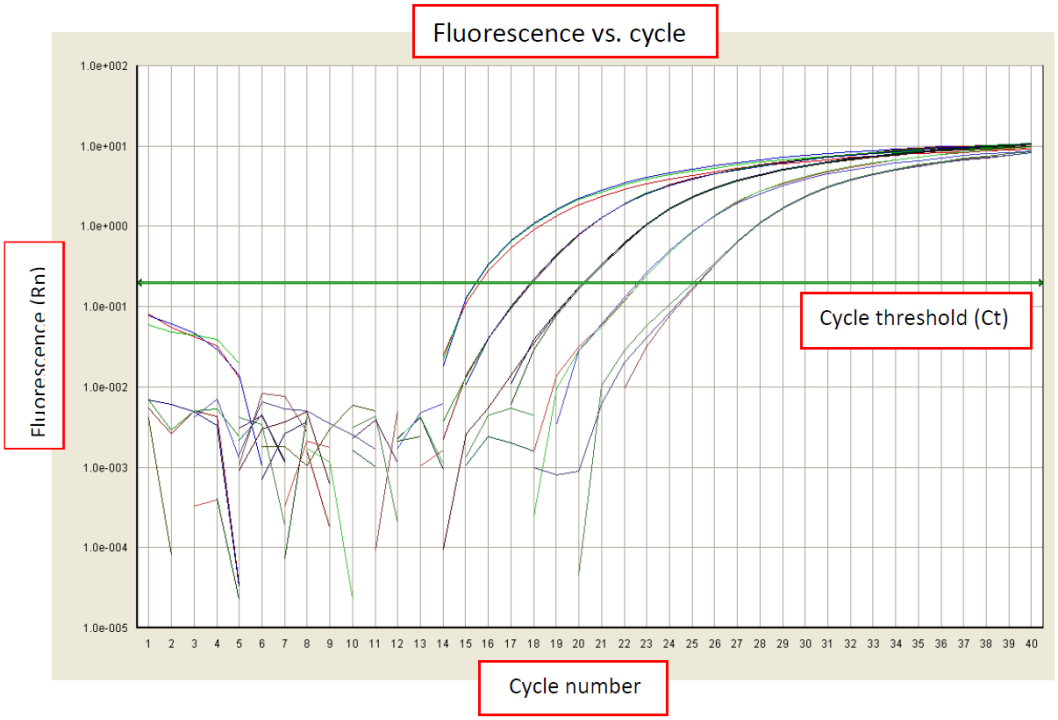

Figure 9. The amplification plot obtained from the Abi Prism 7000 software after running triplicates of 5-fold standard samples. The cycle number on the X-axis shows at which cycle the captured fluorescence (Rn) on the Y-axis exceeds the cycle threshold (Ct). A higher concentration of template decreases the Ct for the sample. The signals below the Ct are emitted from primer-dimers and other artifacts, which no dot affect the final results.

The standard curve – method

The standard curve method is a traditional method for determining both absolute and relative gene expressions. A serial dilution for the gene of interest and the reference gene is measured on the same PCR plate as the samples. Values for the standard dilutions, either absolute or relative, are set. The standard curve of the gene of interest and the reference gene is used to calculate the target gene expression based on the obtained Ct values. Normalization to the reference gene and comparison of the

treated samples to their controls gives the relative change in gene expression (Heid et al, 1996).

The standard curve method is easy to perform and it does not require complex mathematical formulas. However, in order to be able to analyze the results, the standard dilutions have to be accurately made, and the standard curve should have a correlation coefficient (R^2) of at least 0.98 (**Figure 10**) (Heid et al, 1996). The standard dilutions of the individual genes require much space (15 wells per gene if 5-fold dilutions are done in triplicates) on each PCR plate, restricting the amount of space for actual samples. Standard curves on each plate also increase the consumption of reagents, and thereby the costs for the already expensive TaqMan method. Therefore, computational methods without using the standard line have become popular during the past years.

The delta delta Ct (ΔΔCt) – method

In the ΔΔCt –method, no standard curve is used to determine the gene expression of a gene of interest. The method is based on several assumptions, such as equal template concentrations and primer-probe efficiencies, though differences in primer-probe efficiencies are one of the most bias-creating factors. The primer-probe efficiencies can, however, be validated in advance by creating a standard line (**Figure 10**) for all primer-probes. The slope of the linear standard line represents the PCR-efficiency of the primer-probe set, and in order to get valid results, it should be equal (difference <0.1) between genes that are compared to each other (Livak & Schmittgen, 2001).

The ΔCt value between the Ct of the gene of interest and the Ct of the reference gene is calculated separately for the treated and the control samples, after which the difference between them (ΔΔCt) is calculated, representing the change in relative gene expression.

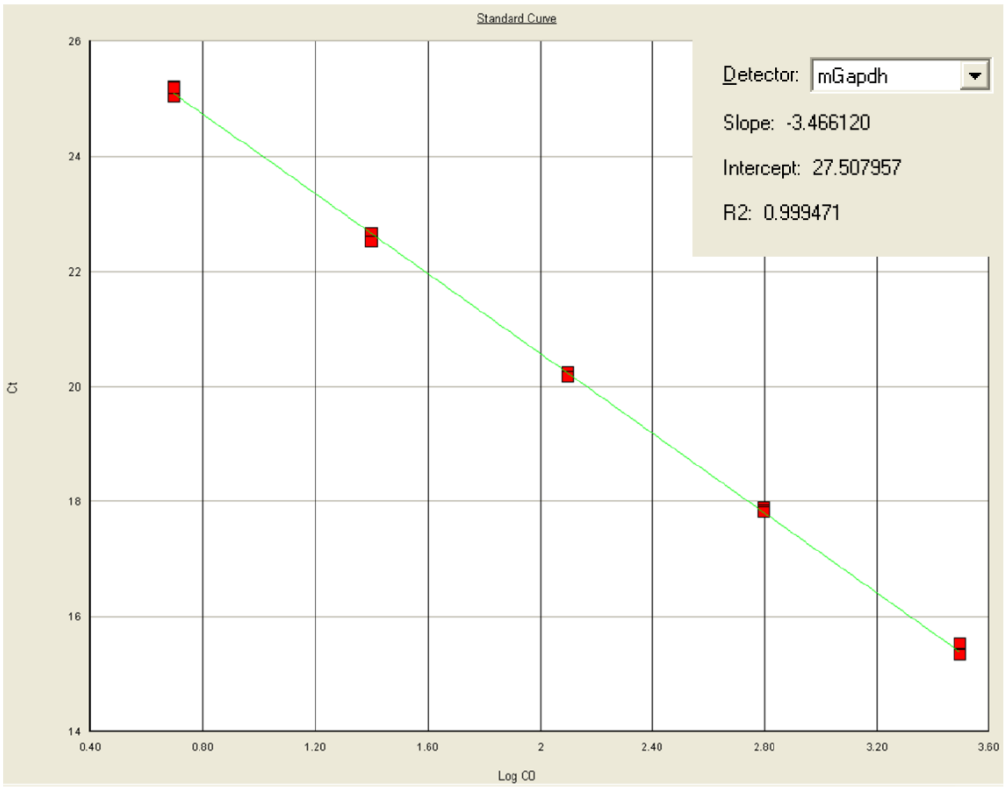

Figure 10. **The standard line for mGapdh.** In this standard line, five standard dilutions have been measured in triplicates, giving a correlation coefficient (R^2) of 0.999. The slope of the standard line describes the PCR-efficiency of the primer-probe, being optimal at -3.3. The accuracy of the standard line increases with increased amount of standard dilutions in the dilution series.

The Pfaffl – method

The Pfaffl –method is very similar to the ΔΔCt –method. The biases affecting the Ct values of the samples, such as differences in template amount and the efficiency of the primer-probe sets, are, however, corrected when using this method (Pfaffl, 2001).

Contrary to the ΔΔCt –method, the ΔCt values for each gene are calculated by subtracting the Ct value of the treated sample from the Ct value of the control sample. The sample specific efficiency, $E_{\text{target gene}}$, is achieved by calculating the primer-probe specific efficiency (E) to the power of the previously obtained ΔCt value. The primer-probe specific efficiency is determined based on the slope of its standard line. The

relative gene expression is finally obtained by normalizing the sample specific efficiency of the target gene to the sample specific efficiency of its reference gene.

The full formula for the Pfaffl –method is shown in **Equation 1**.

$$Relative\ gene\ expression = \frac{(E\ target\ gene)^{\Delta Ct\ target\ gene\ (control\ sample - treated\ sample)}}{(E\ reference\ gene)^{\Delta Ct\ reference\ gene\ (control\ sample - treated\ sample)}}$$

Equation 1. The Pfaffl – method takes into account the sample specific Ct and the efficiency of the primer-probes before normalization is done.

2. AIMS OF THE STUDY

There were two aims of this study:

- To create an *in vitro* disease model of EPM1 in two cell lines by knocking down cystatin B (*CSTB*) mRNA utilizing RNAi gene silencing technique. The models are exploited in the future when the physiological functions of CSTB and the pathophysiological consequences of CSTB deficiency are studied.
- To study the interferon regulated JAK/STAT signaling pathway in the cystatin B knockdown cells, which was downregulated in primary microglia of *Cstb*$^{-/-}$ mice, as revealed by a previously performed gene expression profiling.

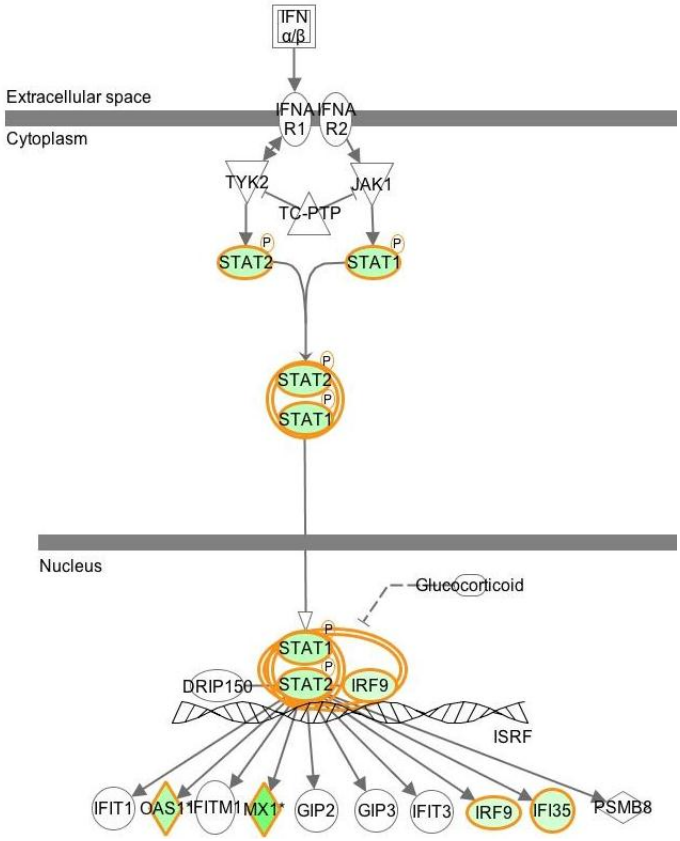

Figure 11. Type I interferon-regulated Janus kinase (JAK)/Signal transducer and activator of transcription (STAT) –signaling pathway. A previously performed gene expression profiling revealed a downregulation in several members (green) of the pathway. The original network was generated through the use of IPA (Ingenuity Systems, www.ingenuity.com) and modified accordingly.

3. MATERIALS AND METHODS

3.1. Cell lines

3.1.1. Cell origin and culturing conditions

The human cervical adenocarcinoma cell line HeLa was purchased from ATCC-LGC (Manassas, VA, USA) and cultured in 1x Dulbecco´s Modified Eagle Medium (DMEM) (Lonza, Basel, Switzerland) with 1x glutamine (GlutaMAX, GIBCO, Life Technologies, Carlsbad, CA, USA), 1x Penicillin Streptomycin (PenStrep) (Invitrogen, Life Technologies, Carlsbad, CA, USA), and 10% Fetal Bovine Serum (FBS) (Biowest, Nuaillé, France). HeLa cells were cultured on Ø10 cm cell dishes (Becton, Dickinson and Company, Franklin Lakes, NJ, USA).

The murine macrophage cell line RAW264.7 was a kind gift from professor Heikki Rauvala, University of Helsinki (Helsinki, Finland) and cultured in 1x Roswell Park Memorial Institute (RPMI) 1640 medium (GIBCO, Life Technologies, Carlsbad, CA, USA) with 1x glutamine, 1x PenStrep, and 10% FBS. RAW264.7 cells were cultured in T-75 cell flasks (Thermo Fisher Scientific, Waltham, MA, USA).

3.1.2. Passaging of cells

HeLa and RAW264.7 cells were washed twice with pre-warmed (37°C) 0.01 M (1x) phosphate buffered saline (PBS) (Liuoslaboratorio, Biomedicum, Helsinki, Finland) (see appendix), after which they were dissociated from the culture dish by trypsinization or scraping. One milliliter room temperature warm trypsin (TrypLE^{TM} Express, GIBCO, Life Technologies, Carlsbad, CA, USA) was added to the HeLa cells and they were incubated for 2 minutes in 37°C. Trypsinization was inhibited by adding 2 ml pre-warmed FBS containing growth media to the culture dish. The cells were collected in a 15 ml falcon tube (Thermo Fisher Scientific, Waltham, MA, USA) and pelleted by centrifugation at 1000 g (Megafuge 1.0, Heraeus Instruments GmbH, Hanau, Germany) for 5 min at

room temperature. The supernatant was discarded and the pellet was resuspended in growth media. The RAW264.7 cells were detached from the culture dish by scraping them into 1 ml 1x PBS, after which they were pelleted and resuspended in growth medium.

The HeLa and RAW264.7 cells were plated in a 1:2 – 1:6 ratio in a total volume of 5 and 12 ml growth media, respectively. The cells were cultured at 37°C, 5% CO_2 for one month or until fifteen passages had been exceeded. The cells were further passaged when they reached a confluency of 70-80%.

3.2. Transfection

Transfection of plasmid constructs and siRNAs into the HeLa and RAW264.7 cells was done by electroporation (Neon transfection system, Invitrogen, Life Technologies, Carlsbad, CA, USA) with provided transfection reagents. The transfections were done following the manufacturer's protocol described below.

HeLa cells were co-transfected with one out of four different siRNAs against human *CSTB* mRNA (**Table 3**) and a plasmid expressing the autofluorescent Green Fluorescent Protein (GFP) (pEGFP-F, Clontech, Mountain View, CA, USA). A mitogen activated protein kinase 1 (MAPK1) -siRNA was used as a positive control and a nonsense siRNA (Neg-siRNA), complementary to no known mRNA sequence, was used as a negative control for RNA inhibition in HeLa cells.

Table 3. siRNAs used for RNA inhibition in HeLa and RAW264.7 cells. The sense sequence is identical to the mRNA sequence transcribed from the gene.

siRNA	Sense-Sequence (5' – 3')	Manufacturer
Hs_CSTB_2 FlexiTube siRNA (SI00355936)	CAAGAAGTTCCCTGTGTTTAA	Qiagen, Venlo, Holland
Hs_CSTB_4 FlexiTube siRNA (SI00355950)	TCCAATCTCTCCCTCATGAAA	Qiagen, Venlo, Holland
Hs_CSTB_6 FlexiTube siRNA (SI03177377)	CAGGTGAGGTCCCAGCTTGAA	Qiagen, Venlo, Holland
Hs_CSTB_7 FlexiTube siRNA (SI04337375)	CAAGCCCTTGACCTTATCTAA	Qiagen, Venlo, Holland
Mm/Hs_MAPK1 control siRNA (1022564)	CAGAGCUUUGGAGUCAGCATTTT	Qiagen, Venlo, Holland
AllStars Negative Control siRNA (1027280)	Proprietary	Qiagen, Venlo, Holland
Mm_Cstb_1 FlexiTube siRNA (SI00961555)	CCCAGCTTGAATCGAAAGAAA	Qiagen, Venlo, Holland
Mm_Gapd_3 FlexiTube siRNA (SI01009393)	AAAUCCGUUCACACCGACCTT	Qiagen, Venlo, Holland

RAW264.7 cells were transfected with a mouse Cstb-siRNA, the negative control siRNA, and a siRNA against the mouse glyceraldehyde 3-phosphate dehydrogenase (*Gapdh*) mRNA sequence as positive control. The MAPK1-siRNA used in HeLa cells was not used in the RAW264.7 cells as positive control, since the *Mapk1* gene is involved in inflammatory pathways mediated by macrophages. All sense sequences of the siRNAs were aligned to known mRNA sequences by using the BLAST tool (http://blast.ncbi.nlm.nih.gov).

The siRNAs, used for RAW264.7 cell transfections, were labeled by the manufacturer with an AlexaFluor-647 fluorochrome in their 3' –end. The fluorochrome enabled the transfection efficiency to be monitored by immunofluorescence (IF) microscopy analysis, without performing immunofluorescence stainings of the mouse CSTB protein, against which a proper antibody does not exist. The transfected siRNAs and plasmids are shown in **Tables 4** and **5**.

Mock-transfected cells, which were electroporated without siRNA or plasmid transfection, were used as control to detect off-target effects of the transfection method.

Table 4. Plasmids and siRNAs transfected to HeLa cells

Plasmid + siRNA	Purpose
pEGFP + CSTB_2 siRNA	Knockdown of *CSTB*
pEGFP + CSTB_4 siRNA	Knockdown of *CSTB*
pEGFP + CSTB_6 siRNA	Knockdown of *CSTB*
pEGFP + CSTB_7 siRNA	Knockdown of *CSTB*
pEGFP + MAPK1 siRNA	Positive control, knockdown of *MAPK1*
pEGFP + Nonsense siRNA	Negative control

Table 5. siRNAs transfected to RAW264.7 cells

siRNA	Purpose
Cstb-siRNA	Knockdown of *Cstb*
Gapdh-siRNA	Positive control, knockdown of *Gapdh*
Neg-siRNA	Negative control
Mock-transfected cells	Electroporation control
Untreated cells	Control

For transfections, 7.7 x10^5 HeLa or 5.0 x10^6 RAW264.7 cells were used per reaction. The HeLa cells were dissociated by trypsinization and the RAW264.7 cells by scraping. The cell amount, mean size, and viability were determined (Cellometer Auto T4, Nexcelom Bioscience, Lawrence, MA, USA), and the cells were washed twice with pre-warmed 1x PBS and centrifuged at 850 g for 5 min at room temperature.

The HeLa cell pellets were carefully resuspended in 90 µl buffer R, provided in the transfection kit. The volumes were set to 100 µl by adding 5 µl pEGFP [1.35 µg/µl] and 5 µl siRNA [50 µM] in nuclease-free water to each tube. The cell suspensions were mixed before transfection by pipetting them up-and-down avoiding air bubbles. One hundred microliters of cell suspension were taken up in the transfection pipette tip and the tip was placed in the transfection pipette station with buffer E2.

The RAW264.7 cell pellets were resuspended into 90 µl buffer R, after which 10 µl siRNA [100 µM] in nuclease-free water was added into a final volume of 100 µl. Cell preparations were done in a similar way as with HeLa cells.

The electroporation parameters are shown in **Table 6**.

Table 6. Parameters used for electroporation of HeLa and RAW264.7 cells

Cell type	Voltage	Pulse width (ms)	Amount of pulses
RAW264.7	1680	20	1
HeLa	1005	35	2

Electroporated HeLa cells were resuspended in 5 ml pre-warmed transfection media (see appendix) and plated on Ø 6 cm cell dishes (7.7 $x10^5$ cells) and on UV-treated Ø 13 mm cover slips (VWR international, Radnor, PA, USA) (7.7 $x10^4$ cells) in 12-well cell dishes (Thermo Scientific, Waltham, MA, USA).

RAW264.7 cells were resuspended in 6 ml transfection media, and plated on Ø 6 cm cell dishes (3.3 $x10^6$ cells), in T-75 cell culture flasks (6.6 $x10^6$ cells) and on UV-treated Ø 13 mm cover slips (2.5 $x10^5$ cells) in 12-well cell dishes.

The transfected amounts plasmid and siRNA, and the number of cells per 100 µl reaction are shown in **Table 7**.

Table 7. The amount of cells, plasmid and siRNA per reaction

Cell type	Amount of cells	Plasmid (µg)	siRNA (µM)
HeLa	7.7 $x10^5$	5.7 (pEGFP)	2.5
RAW264.7	5.0 $x10^6$	-	10

All cells were incubated at 37°C in 5% CO_2.

HeLa cells were collected 48 hours post-transfection, and RAW264.7 cells were collected at time points 12, 24, 36, 48, 60, 72 and 96 hours post-transfection.

3.3. Total RNA preparation

Total RNA was extracted from transfected and control RAW264.7 cells from Ø 6 cm cell dishes, plated with 3.3 x10^6 cells, using an RNase Plus Mini Kit (Qiagen, Venlo, Holland) according to the manufacturer´s protocol described below. All steps of the extraction protocol were done at room temperature with reagents supplied by the kit.

The cells were washed twice with pre-warmed 1x PBS and lysed with 1 ml 0.01% 2-mercaptoethanol (Sigma Aldrich, St. Louis, MO, USA)/buffer RLT plus. The cells were harvested and homogenized by 30 strokes with an RNase-free 21 G needle (Yamaguchi Medical Instruments Co. Ltd, Osaka, Japan) attached to a 1 ml syringe (BD Plastipak, Becton, Dickinson and Company, Franklin Lakes, NJ, USA). The cell lysate was pipetted into a gDNA eliminator spin column and centrifuged (Microcentrifuge 5415D, Eppendorf, Hamburg, Germany) at 10 000 rpm for 30 seconds. The flow through was mixed with an equal amount of 70% ethanol (EtOH) (ETAX, Altia, Helsinki, Finland) and centrifuged in 700 µl aliquots through an RNase spin column at 10 000 rpm for 15 seconds. The RNA was washed with 700 µl buffer RW1, followed by centrifugation at 10 000 rpm for 15 seconds.

For RAW264.7 cells transfected with the Gapdh-siRNA, an additional DNase treatment was done by using a compatible RNase free DNase set (Qiagen, Venlo, Holland). After loading the RNA to the RNase spin column, the column was washed with 350 µl buffer RW1. DNase (1500 Kunitz units), diluted in nuclease-free water, was mixed 1:7 with buffer RDD, which was included in the RNase free DNase set, and loaded in the RNase spin column. An incubation period of 15 minutes at room temperature followed, after which an additional 350 µl of buffer RW1 was used for washing the column.

All columns were washed twice with 500 µl buffer RPE:EtOH (1:4), followed by centrifugations at 10 000 rpm for 15 seconds and two minutes. The spin columns were dried by centrifugation in 13 200 rpm for one minute. RNA was eluted from the spin columns with 30 µl RNase-free water by centrifugation at 10 000 rpm for 30 seconds.

The RNA concentrations and the purity of the samples were measured spectrophotometrically (Nanodrop 1000, Thermo Scientific, Waltham, MA, USA)

against nuclease-free water, and the samples were diluted in nuclease-free water to a final concentration of 1 µg/µl.

RNA samples were stored at -80°C.

3.4. Reverse transcription of RNA to cDNA and verification of reverse transcription by the S15 gene polymerase chain reaction

Total RNA was transcribed to cDNA using the iScript kit (Bio-Rad, Hercules, CA, USA). The reactions were prepared in 0.2 ml PCR-tubes (StarPCR tubes, Starlab Group, Merenschwand, Switzerland) on ice using 1 µl RNA [1 µg/µl] as template, after which 19 µl reverse transcriptase (RT) reaction mix (**Table 8**) was added. A reaction without template was used as a negative control.

RNA was transcribed to cDNA using the PCR program in **Table 9**.

Table 8. Reaction mix for cDNA synthesis

Reagent	Reverse transcription reaction (µl)	Negative control reaction (µl)
RNA template [1 µg/µl]	1	-
5x iScript reaction mix	4	4
Nuclease-free water	14	15
iScript reverse transcriptase enzyme	1	1
Total volume	**20**	**20**

Table 9. Reverse transcription PCR program

Temperature (°C)	Time (min.)
25	5
42	30
85	5
4	∞

Successful cDNA synthesis and the absence of genomic DNA were confirmed by amplification of the ribosomal subunit S15 gene from the cDNA and the RNA.

The protocol for the S15 gene PCR reaction and the amplification program are shown in Table 10 and 11, respectively, and the primer sequences for the S15 gene PCR are seen in the appendix.

Table 10. S15 PCR reaction mix

Reagent	**µl**
Template	1
10x Standard reaction buffer (Biotools, Jupiter, FL, USA)	2
dNTP [10 µM] (F-560, Finnzymes, Espoo, Finland)	0.4
S15 forward primer [20 µM] (Sigma Aldrich, St. Louis, MO, USA)	0.5
S15 reverse primer [20 µM] (Sigma Aldrich, St. Louis, MO, USA)	0.5
DNA-polymerase (1 U/µl) (Biotools, Jupiter, FL, USA)	0.6
Nuclease-free water	15
Total volume	**20**

Table 11. S15 amplification program

Temperature (°C)	**Time (min.)**	
94	5	
94	0.5	
55	0.5	30 cycles
72	0.5	
72	10	

After amplification, 4 µl of 6x loading buffer (Orange Dye, Fermentas, Thermo Scientific, Waltham, MA, USA) were added to the PCR products and they were electrophoresed in 0.5x Tris/borate/EDTA (TBE) (Thermo Scientific, Waltham, MA, USA) for 40 minutes in 120 V in a 1.5% agarose (BIO-41025, Biotop Oy, Turku,

Finland)/TBE gel containing the DNA binding fluorescent stain Midori Green (Nippon Genetics Europe, Dueren, Germany). Four microliters of DNA-ladder (100 bp+500 bp, 0.05 µg/µl) (O'RangeRuler, Fermentas, Thermo Scientific, Waltham, MA, USA) was used as a marker for DNA bands of different sizes and the PCR products were visualized by UV-light (AlphaImager, Protein Simple, Santa Clara, CA, USA).

3.5. Quantitative real-time PCR

Gene expression levels from the Cstb-siRNA, Neg-siRNA, and Gapdh-siRNA transfected cells, and the mock-transfected control cells, were measured by quantitative real-time PCR (qRT-PCR) using the TaqMan method, according to the protocol by Applied Biosystems (Foster City, CA, USA)
(https://tools.invitrogen.com/content/sfs/manuals/cms_041280.pdf).

The expression levels of target genes were compared to the expression level of the general transcription factor TATA-box binding protein gene (*Tbp*), which was used as an endogenous control. Two or three experimental runs were performed for all samples. Reactions were prepared in duplicates, and expression values having a standard deviation of ± 0.2 were excluded. The mRNA expression levels were calculated using the Pfaffl method (Pfaffl, 2001).

The TaqMan primer-probes (**Table 12**) were pre-designed by the manufacturer and they were intron-spanning, with the exception of the *Gapdh* primer-probe. Cstb-siRNA and Neg-siRNA transfected cells were measured for the gene expression levels of *Cstb*, *Stat1*, *Stat2*, *Irf9*, and *Tbp*, and Gapdh-siRNA transfected cells were measured for *Cstb*, *Stat1*, *Tbp*, and *Gapdh*. All genes listed in **Table 12** were measured for the expression levels of the mock-transfected cells.

Table 12. Primer-probes used in TaqMan-qRT-PCR

Probe	ID	Manufacturer
Cystatin B (*Cstb*)	Mm00432769_m1	Applied Biosystems, Foster City, CA, USA
Signal transducer and activator of transcription 1 (*Stat1*)	Mm00439531_m1	Applied Biosystems, Foster City, CA, USA
Signal transducer and activator of transcription 2 (*Stat2*)	Mm00490880_m1	Applied Biosystems, Foster City, CA, USA
Interferon regulatory factor 9 (*Irf9*)	Mm00492679_m1	Applied Biosystems, Foster City, CA, USA
TATA box binding protein (*Tbp*)	Mm00446973_m1	Applied Biosystems, Foster City, CA, USA
Glyceraldehyde 3-phosphate dehydrogenase (*Gapdh*)	Mm99999915_g1	Applied Biosystems, Foster City, CA, USA

The cDNA was diluted 1:2 with nuclease-free water, and 2 µl of the dilution was used per PCR-reaction of 20 µl containing reagents seen in **Table 13**.

Table 13. Reaction mix for TaqMan qRT-PCR

Reagent	µl
cDNA template	2
2x TaqMan Universal PCR Master Mix (Roche Applied Science, Penzberg, Germany)	10
TaqMan primer-probe (Table 12)	1
Nuclease-free water	7
Total volume	**20**

The reactions were performed in a 96-well plate (MicroAmp, Applied Biosystems, Foster City, CA, USA), and the qRT-PCR program was carried out with the ABI PRISM 7000 Sequence detection system (Applied Biosystems, Foster City, CA, USA). The program for TaqMan qRT-PCR is seen **Table 14**.

Table 14. PCR program for TaqMan qRT-PCR

Temperature (°C)	Time (min.)	
50	2	
95	10	
95	0:15	40 cycles
60	1	

The results were analyzed with the ABI PRISM 7000 system software (Applied Biosystems, Foster City, CA, USA), and MS Excel (Microsoft Corporation, Redmond, WA, USA).

3.6. Fixation of cells with phosphate-buffered 4% paraformaldehyde (PFA)

HeLa and RAW264.7 cells plated on coverslips, 7.7 x10^4 and 2.5 x10^5 respectively, were fixed with 4% paraformaldehyde (PFA) (PFA/PBS) (Liuoslaboratorio, Biomedicum, Helsinki, Finland). The coverslips were carefully moved to a sterile 12-well cell dish and the cells were washed twice with 1 ml pre-warmed 1x PBS. The cells were fixed for 15 minutes at room temperature with 1 ml 4% PFA. The PFA was removed, and the fixed cells were washed twice with 1x PBS, after which they were stored in 1x PBS at +4°C protected from light.

3.7. Antibodies and indirect immunofluorescence stainings

All steps comprising the indirect immunofluorescence (IF) stainings were performed with the samples protected from light in order to inhibit bleaching of the fluorochrome labeled siRNAs, which were transfected to RAW264.7 cells.

The fixed cells were rinsed three times with 1x PBS, and the cell membranes were permeabilized with 0.1% Triton X-100 (Sigma Aldrich, St. Louis, MO, USA)/1x PBS for 10 min at room temperature. RAW264.7 cells were incubated with 0.5% Bovine Serum

Albumin Fraction V (BSA) (Roche Applied Science, Penzberg, Germany)/1x PBS and HeLa cells with 10% FBS/1x PBS for one hour at room temperature in slow shaking (See-saw rocker SSL4, Bibby Scientific, Staffordshire, UK) to prevent unspecific binding of antibodies.

The primary antibodies were diluted (**Table 15**) in cold 0.5% BSA/1x PBS and 1% FBS/1x PBS for RAW264.7 and HeLa cells, respectively. Thirty microliter primary antibody solution was incubated with the cells for one hour at room temperature. The diluent without antibody was used as a negative primary antibody control. The cells were washed three times for 15 minutes with the diluent.

Table 15. Primary antibodies used in indirect immunofluorescence stainings

Antibody	Dilution	Host	Manufacturer
STAT1	1:200	rabbit	Santa Cruz Biotechnology, Dallas, TX, USA
NOS2 (iNOS)	1:200	rabbit	Santa Cruz Biotechnology, Dallas, TX, USA
GFP	1:100	rabbit	Sigma Aldrich, St. Louis, MO, USA

An Alexa Fluor-488 labeled secondary antibody (donkey anti-rabbit) (Invitrogen, Life Technologies, Carlsbad, CA, USA) was diluted in cold 0.5% BSA/1x PBS or in 1% FBS/1x PBS, and 30 µl of the dilution was incubated with the cells for 30 minutes at room temperature. The diluent without antibody was used as a negative secondary antibody control.

The cells were washed three times for 15 minutes, once with the diluent and twice with 1x PBS at room temperature.

The DNA of the cells was stained by incubating the cells for five minutes in Hoechst (Molecular Probes, Life Technologies, Carlsbad, CA, USA), diluted 1:5000 in 1x PBS, in slow shaking at room temperature. The excess stain was washed off by rinsing the cells three times with 1x PBS.

Excess salts were washed off the coverslips by soaking them in double distilled sterile water (ddsH_2O) for 30 seconds. A drop of mounting media (Fluoromount, Sigma

Aldrich, St. Louis, MO, USA) was placed on a sterile microscope slide (Thermo Scientific, Waltham, MA, USA) and the coverslips were placed cell-side down on the drop. The samples were dried overnight at room temperature protected from light, after which they were stored at 8°C.

Epifluorescence (Zeiss AxioImager Z1, Carl Zeiss AG, Oberkochen, Germany) and confocal (Zeiss LSM 710, Carl Zeiss AG, Oberkochen, Germany) microscopy was used for visualizing the bound antibodies.

3.8. Protein extraction

Total protein was extracted from transfected HeLa and RAW264.7 cells (7.7 $x10^5$ and 6.6 $x10^6$ cells, respectively) growing on Ø 6 cm cell dishes and in T-75 cell culture flasks. Upon harvesting protein lysates from RAW264.7 cells at various time points, 200 µl growth media was collected from the cell culture dishes and stored at -80°C for further analysis.

The cell culture dishes were placed on ice and cells were washed twice with ice cold 1x PBS. Five hundred microliters of cold cell lysis buffer (see appendix) was added to the HeLa cells, and they were scraped off with a pre-cooled cell scraper and pipetted into a cooled eppendorf tube and kept on ice. Two hundred microliters cell lysis buffer was used in a similar way for RAW264.7 cells.

The cell suspensions were mixed by vortexing (Vortex-Genie2, Scientific Industries, Bohemia, NY, USA) three times for two seconds, after which the tubes were slowly rotated (Labover, type 460251) for five minutes at 8°C. The cells were centrifuged (Microcentrifuge 5415D, Eppendorf, Hamburg, Germany) at 10 000 rpm for 10 min at 8°C. The supernatant containing the soluble proteins was separated from the pelleted cell debris and transferred into a new pre-cooled eppendorf tube and stored at -20°C.

3.9. Detection of nitrite by the Griess test

Organic nitrite compounds were detected from the growth media of transfected RAW264.7 cells. Frozen growth media was thawn on ice, and cell debris was pelleted at 10 000 rpm for 10 minutes at +8°C.

Fifty microliters of growth media, collected at each examined time point, was pipetted as duplicates into a 96-well dish (Midland Scientific, Omaha, NE, USA) on ice. Nitrite (NO_2^-) standards (0, 2.5, 5, 10, 15, 20, 40, 60, 80, 100 µM), diluted in fresh growth media, were pipetted as duplicates in the same 96-well dish.

Fifty microliter Griess reagent (Sigma Aldrich, St. Louis, MO, USA) was carefully mixed in each sample and after an incubation period of 15 minutes at room temperature, the absorbance at 510 nm was measured (VICTOR^{2}™, PerkinElmer, Waltham, MA, USA) against the NO_2^- standard dilutions.

3.10. Measurement of protein concentration by the Bradford method

The protein lysates were diluted 1:5 with pre-cooled ddsH_2O, and 10 µl of the dilutions were carefully pipetted as triplicates into a 96-well dish (Midland Scientific, Omaha, NE, USA) on ice. BSA standard dilutions (0, 125, 250, 500, 750, 1000 ng/µl) were pipetted as duplicates in the same 96-well dish.

Two hundred microliters of Bradford dye (Bio-Rad Protein Assay, Bio-Rad, Hercules, CA, USA), diluted 1:5 with water, was added into each sample, which were mixed carefully avoiding bubbles. Each sample was incubated for five minutes at room temperature and the protein concentrations were measured spectrophotometrically (Labsystems multiskan MS, Helsinki, Finland) against the BSA standard dilutions.

Replicates with variation more than 10% were excluded, and the mean value was determined based on the remaining replicates.

3.11. SDS-polyacrylamide gel electrophoresis (SDS-PAGE)

Protein samples for SDS-PAGE were prepared on ice by diluting the protein lysates in pre-cooled ddsH_2O to 7.5 or 10 µg proteins per sample of HeLa or RAW264.7 cells. A 5x Laemmli buffer (see appendix) containing the reducing agent 2-mercaptoethanol (Sigma Aldrich, St. Louis, MO, USA) (2:1) was added to the diluted samples. The samples were heated (ThermoCell CHB202, Hangzhou Bioer Technology Co, Hangzhou, China) at +95°C for 5 min, after which they were quickly centrifuged (Spectrafuge 24D, Labnet International Inc., Woodbridge, NJ, USA).

Proteins were separated in 1x SDS-PAGE running buffer (Liuoslaboratorio, Biomedicum, Helsinki, Finland) (see appendix) in pre-casted Tris-Glycine gels (Mini-PROTEAN TGX, 12% and any kD, Bio-Rad, Hercules, CA, USA) using a pre-stained protein marker (SM1811, Fermentas, Thermo Scientific, Waltham, MA, USA for HeLa cells, and 161-0373, Bio-Rad, Hercules, CA, USA for RAW264.7 cells) as size marker. The separation was conducted using the following conditions; 90 V for 30 min, 110 V for 10 min and 130 V for 30 min (Bio-Rad PowerPac 1000, Bio-Rad, Hercules, CA, USA).

3.12. Western blot analysis

Proteins separated in the SDS-PAGE gel were electroblotted to a polyvinylidene difluoride (PVDF) membrane (GE Healthcare, Little Chalfont, UK). The PVDF membrane was activated with 100% methanol (MeOH) (Thermo Fisher Scientific, Waltham, MA, USA), after which it was rinsed in ddsH_2O for five minutes and equilibrated in 1x Tris-glycine transfer buffer (Liuoslaboratorio, Biomedicum, Helsinki, Finland) (see appendix) containing 20% MeOH.

The blotting system (Bio-Rad, Hercules, CA, USA) was assembled by placing the SDS-PAGE gel and the membrane against each other and placing two chromatography papers (Whatman, Grade 3MM Chr, GE Healthcare, Little Chalfont, UK) and a foam pad on each side. Air bubbles were eliminated and the assembled system was placed in a gel holder cassette. Proteins were transferred in ice cold 1x transfer buffer containing

20% MeOH under moderate stirring for 35 minutes in 0.35 A (Bio-Rad PowerPac 200, Bio-Rad, Hercules, CA, USA) at +8°C.

Successful transfer was confirmed by staining the membrane with Ponceau S (see appendix) for one minute, followed by rinsing it with ultrapure Milli-Q water (MQ-H_2O) and activation of the membrane with 100% MeOH, which revealed the transferred protein bands. The SDS-PAGE gel was stained after transfer with Bio-safe Coomassie stain (Bio-Rad, Hercules, CA, USA) to detect remaining proteins.

The PVDF membrane was rinsed in PBST (PBS/0.1% Tween-20 (Thermo Fisher Scientific, Waltham, MA, USA)) for five minutes in moderate shaking and blocked for unspecific binding of antibodies with 5% BSA/PBST for one hour at room temperature. Primary antibodies were diluted (**Table 16**) in 5% BSA/PBST and the solution was added to the membrane and incubated overnight at 8°C.

Table 16. Primary antibodies used in Western Blot analysis

Antibody	Dilution	Host	Manufacturer
CSTB (mouse)	1:1000	rabbit	Biogenesis, AbD Serotec, Kidlington, UK
STAT1	1:500	rabbit	Santa Cruz Biotechnology, Dallas, TX, USA
STAT2	1:1000	rabbit	Merck Millipore, Billerica, MA, USA
NOS2 (iNOS)	1:2000	rabbit	Santa Cruz Biotechnology, Dallas, TX, USA
ERK2 (MAPK1)	1:400	mouse	Santa Cruz Biotechnology, Dallas, TX, USA
Beta-tubulin	1:5000	mouse	Sigma Aldrich, St. Louis, MO, USA
2E7 (human CSTB)	1:1000	mouse	Kind gift from Eckehard Weber, Germany

The membrane was washed six times for 10 minutes with PBST at room temperature. For HeLa cells, a horseradish peroxidase (HRP)-conjugated secondary antibody (**Table 17**) was diluted in 5% BSA/PBST, and for RAW264.7 cells, a fluorochrome conjugated secondary antibody (**Table 18**) was diluted in 1% milk powder (Valio Oy, Helsinki, Finland)/PBST + 0.01 % SDS (Sigma Aldrich, St. Louis, MO, USA). Secondary antibodies

were incubated with the membrane for one hour at room temperature in moderate shaking, protected from light.

Table 17. Secondary antibodies used for HeLa cells in Western Blot analysis

Antibody	Dilution	Manufacturer
Goat Anti-mouse/HRP	1:5000	DAKO, Glostrup, Denmark
Swine Anti-rabbit/HRP	1:5000	DAKO, Glostrup, Denmark

Table 18. Secondary antibodies used for RAW264.7 cells in Western Blot analysis

Antibody	Dilution	Host	Manufacturer	Fluorochrome
Anti-mouse	1:10000	Goat	LI-COR Biosciences, Lincoln, NE, USA	IRDye® 800CW
Anti-rabbit	1:10000	Goat	LI-COR Biosciences, Lincoln, NE, USA	IRDye® 800CW

The membrane, to which the HeLa cell proteins had been transferred to, was washed three times with PBST, 15 minutes each. The membrane was incubated for five minutes protected from light with a chemiluminescent substrate (Thermo Fisher Scientific, Waltham, MA, USA) consisting of luminol and peroxide solutions diluted in 1x PBS (1:1:2). After the incubation period, the membrane was placed in a cassette (Trimax T16, 3M, St. Paul, MN, USA) between two plastic covers and air bubbles were removed. Proteins were detected by exposing the chemiluminescent membrane to an X-ray film (Kodak BioMax, Sigma Aldrich, St. Louis, MO, USA), and quantified with the software ImageJ (National Institutes of Health, Bethesda, MD, USA) (http://rsbweb.nih.gov/ij/).

The membrane, with proteins from RAW264.7 cells, was washed six times with PBST, 10 minutes each, after which it was quickly rinsed with 1x PBS. Bound antibodies were detected by scanning the membrane with the Odyssey Infrared Imaging system (LI-COR Biosciences, Lincoln, NE, USA), and quantified with the Odyssey Software (LI-COR Biosciences, Lincoln, NE, USA).

3.13. Statistical analyses

All results obtained from qRT-PCR, Western blot, and immunofluorescence analyses were normalized against mock-transfected cells, unless otherwise mentioned. Probability (p) was calculated using Student's two-tailed heteroscedastic t-test with values obtained from the Neg-siRNA transfected cells as the control data set. P-values < 0.05 were considered statistically significant.

4. RESULTS

4.1. Cystatin B knockdown in HeLa cells

4.1.1. Co-transfection of pEGFP and CSTB-siRNA to HeLa cells

RNA-inhibition was optimized in the human cervical carcinoma cell line, HeLa. Electroporation was chosen as transfection method, and in order to verify its success, a plasmid encoding the autofluorescent green fluorescent protein (pEGFP) was co-transfected with the CSTB-siRNA.

Immunofluorescence stainings with an anti-GFP antibody were carried out on cells, which had been fixed at 48 hours post-transfection. The expression of GFP showed which HeLa cells had been transfected (**Figure 12**). Morphological changes of HeLa cells due to transfection were not observed.

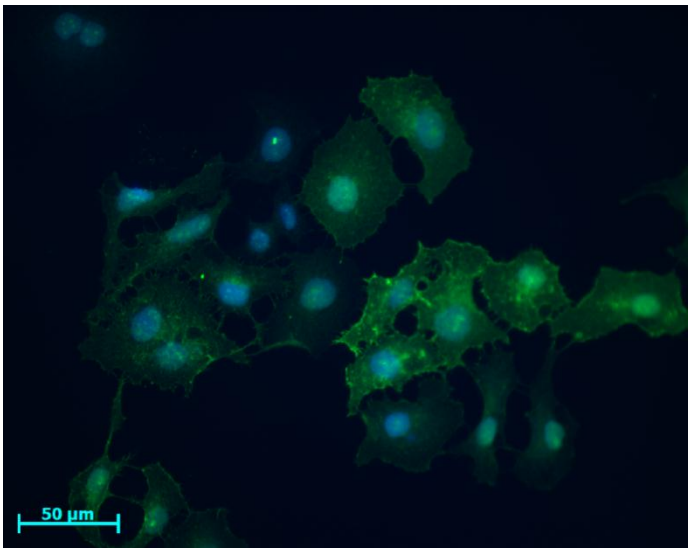

Figure 12. Anti-green fluorescent protein (GFP) (green) stained HeLa cells. Expression of GFP, proportional to the visualized fluorescence, shows which cells have been transfected with pEGFP. The nuclei of the cells are stained with Hoechst.
Scale 50 µm.

4.1.2. Verification of *CSTB* knockdown in HeLa cells

Human cystatin B (*CSTB*) knockdown by using different siRNAs was verified by Western blot (WB) analysis (**Figure 13A**), and quantified by Image J software (**Figure 13B**). All four CSTB-siRNAs downregulated the CSTB protein expression, but some siRNA specific differences in efficiency were observed. The CSTB-siRNA4 was most efficient, reducing the protein expression level down to 1% of the control cells. CSTB-siRNA1-3 knocked down the expression level of CSTB to 7-15%. A decrease in CSTB expression was also observed in the positive control cells transfected with the MAPK1-siRNA. CSTB-knockdown did not, however, affect MAPK1-expression (**Figure 13A**). The obtained results are normalized to the values from the negative control siRNA (Neg-siRNA) transfected HeLa cells.

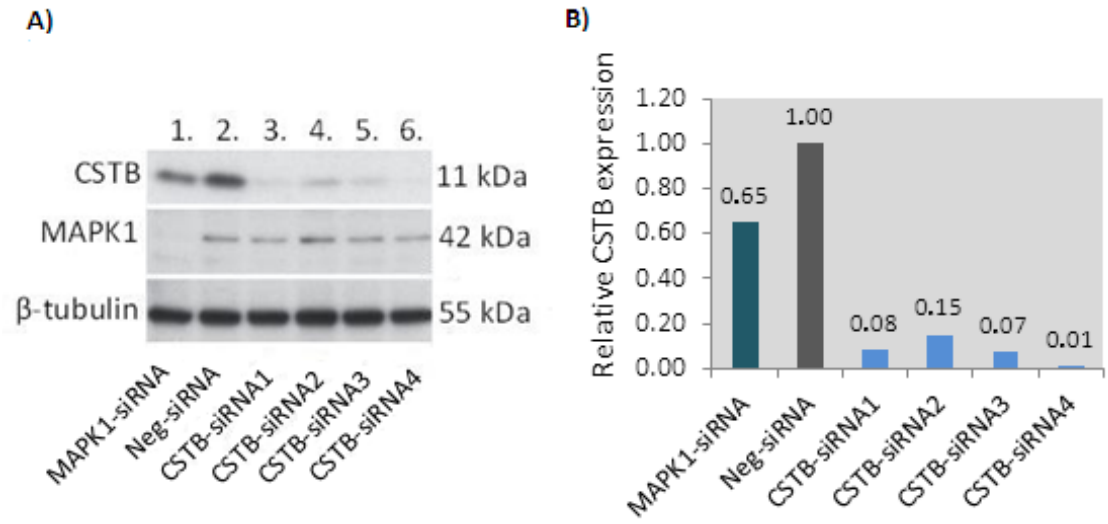

Figure 13. A. Western blot analysis of cystatin B (11 kDa) expression in HeLa cells. The siRNA mediated inhibition of *CSTB* (CSTB-siRNA1-4, lanes 3-6) was confirmed on protein level. Cells transfected with the positive control siRNA (MAPK1-siRNA, lane 1) and the negative control siRNA (Neg-siRNA, lane 2) express CSTB. MAPK1 (42 kDa) was downregulated in the positive control, but not in any other sample. β-tubulin (55 kDa) was used as loading control. The proteins are indicated on the left, and their molecular weights (kDa) on the right. **B. Quantification of the Western blot by the ImageJ software.** All CSTB-siRNAs (light blue) downregulated *CSTB*, but CSTB-siRNA4 was the most sensitive. A downregulation of CSTB was also observed in the MAPK1-knockdown cells (dark blue). All values are normalized to the values acquired from the Neg-siRNA (grey) transfected cells, and the obtained fold change is marked above the bars.

4.1.3. Effects of CSTB knockdown on STAT1, STAT2, and iNOS expression in HeLa cells

In order to verify whether CSTB downregulation had an effect on the members of the JAK/STAT signaling pathway, WB analysis was performed for the proteins STAT1, STAT2, and iNOS. Downregulation of CSTB in HeLa cells did not change the expression levels of STAT1 in a substantial manner (**Figure 14A and 14B**), however, STAT1 expression was increased by 2-fold in MAPK1-knockdown cells (**Figure 14B**). STAT2 and iNOS expression could not be detected by WB analysis (data not shown).

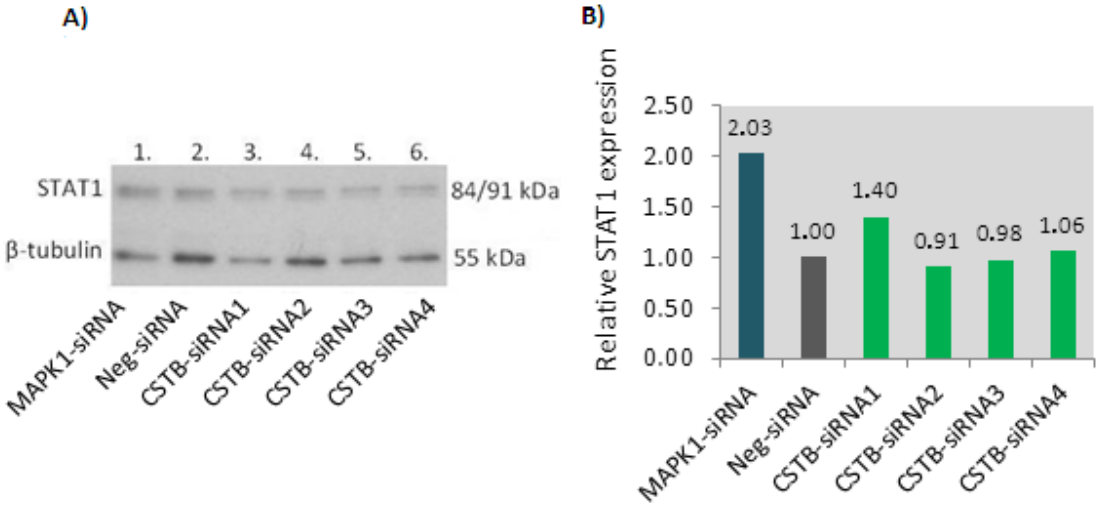

Figure 14. A. Western blot analysis of STAT1 (84/91 kDa) expression in CSTB knockdown HeLa cells. No clear difference in STAT1 expression was observed between the CSTB inhibited (lanes 3-6) and the MAPK1- and Neg-siRNA transfected control cells (lanes 1-2). β-tubulin (55 kDa) was used as a loading control. The proteins are indicated on the left, and their molecular weights (kDa) on the right. **B. Quantification of the Western blot with the ImageJ software.** Increased STAT1 expression was detected in the CSTB-siRNA1 transfected cells, but not in the other CSTB knockdown cells (green). MAPK1-downregulated cells (dark blue) had a 2-fold increase in STAT1 expression. All values are normalized to the values acquired from the Neg-siRNA transfected cells (grey), and the obtained fold change is marked above the bars.

4.2. Cystatin B knockdown in RAW264.7 cells

4.2.1. Transfection of siRNA to RAW264.7 cells

Cstb was knocked down in the murine macrophage cell line RAW264.7. Alexa Fluor-647 labeled siRNA molecules were used, which allowed the verification of successful transfection by IF microscopy. Nearly all cells were positive for the fluorochrome (**Figure 15a**), indicating a high transfection rate. Mock-transfected cells were used as control (**Figure 15b**).

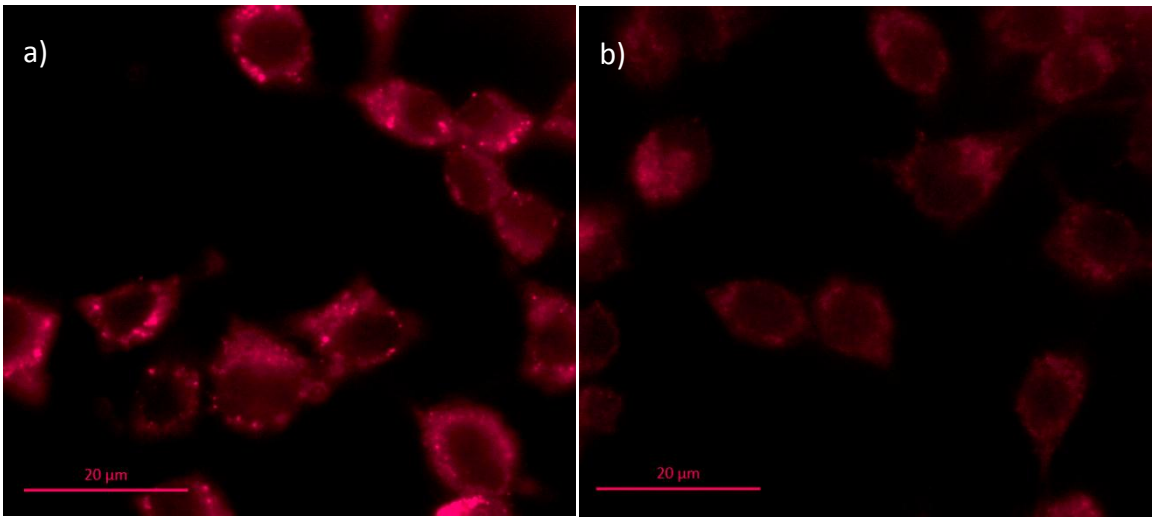

Figure 15. siRNA transfection in RAW264.7 cells was detected by immunofluorescence (IF) microscopy. The siRNA sequences were labeled with an Alexa Fluor-647 fluorochrome in their 3'-end, allowing their cellular location to be monitored by IF microscopy (a). Mock-transfected cells do not express the fluorescent signal (b).
Scale 20µm.

Transfected and control cells were monitored up to 96 hours post-transfection. With the exception of cells in two cell culturing flasks, no morphological changes were observed at any examined time point. The observed morphological changes in the two flasks were present in such cells (Neg-siRNA transfected and untreated control cells) which were aimed for protein extraction at the time point 60 hours. Protein lysates

and growth media were collected from these cells as planned, and the samples were used for Western blot analysis and to perform the Griess test.

4.2.2. Total RNA purity and reverse transcription of RNA to cDNA

After total RNA extraction, RNA purity and cDNA synthesis were confirmed by amplification of the ribosomal subunit S15 gene, and as a template were used both cDNA and RNA. The presence of the S15-fragment (361 bp) in samples with cDNA as template confirmed that reverse transcription was successful (**Figure 16**). The absence of the fragment in reactions with RNA as template confirmed that there was no genomic DNA contamination in the RNA.

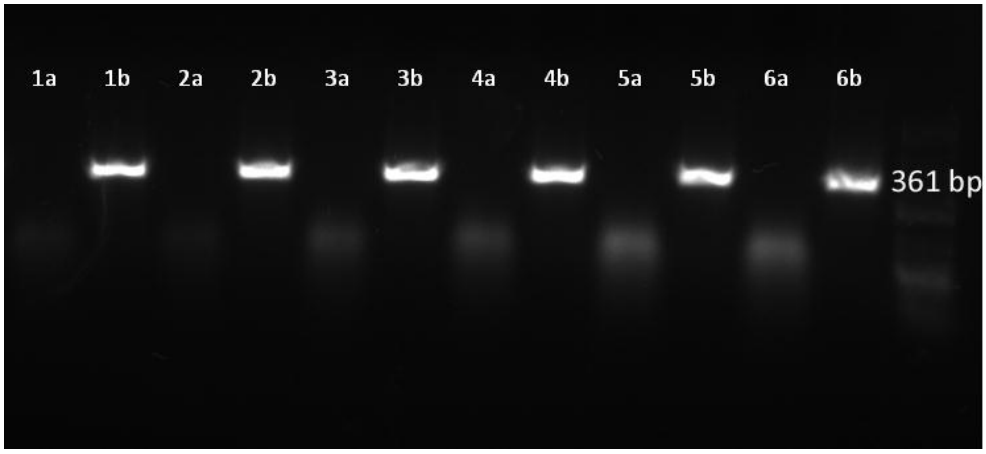

Figure 16. Representative S15-PCR-products electrophoresed in a 1.5% agarose/TBE gel. Sample "a" represents a PCR product with total RNA as template and sample "b" the corresponding sample with cDNA as template. Genomic contamination in the "a" sample would result in amplification of the S15 gene, which is not detected. The S15 gene was amplified in the "b" samples, confirming successful reverse transcription. The diffuse bands, seen in "a" samples, consist of primer-dimers.

4.2.3. Sensitivity of *Cstb* downregulation

Cstb downregulation was analyzed from Cstb-siRNA, Neg-siRNA, Gapdh-siRNA, and mock-transfected cells by qRT-PCR. The Cstb-siRNA sensitivity was high, seen as effective downregulation of *Cstb* mRNA (**Figure 17**). Downregulation of *Cstb* was not detected in the control cells, transfected with the Gapdh- or Neg-siRNA. The Gapdh-siRNA transfected cells did not change in *Cstb* expression during the time points (fold changes between 0.9 and 1.15), but some variation in *Cstb* expression was observed in the Neg-siRNA transfected cells, particularly between the time points 36 and 96 hours (fold changes between 0.95 and 1.4).

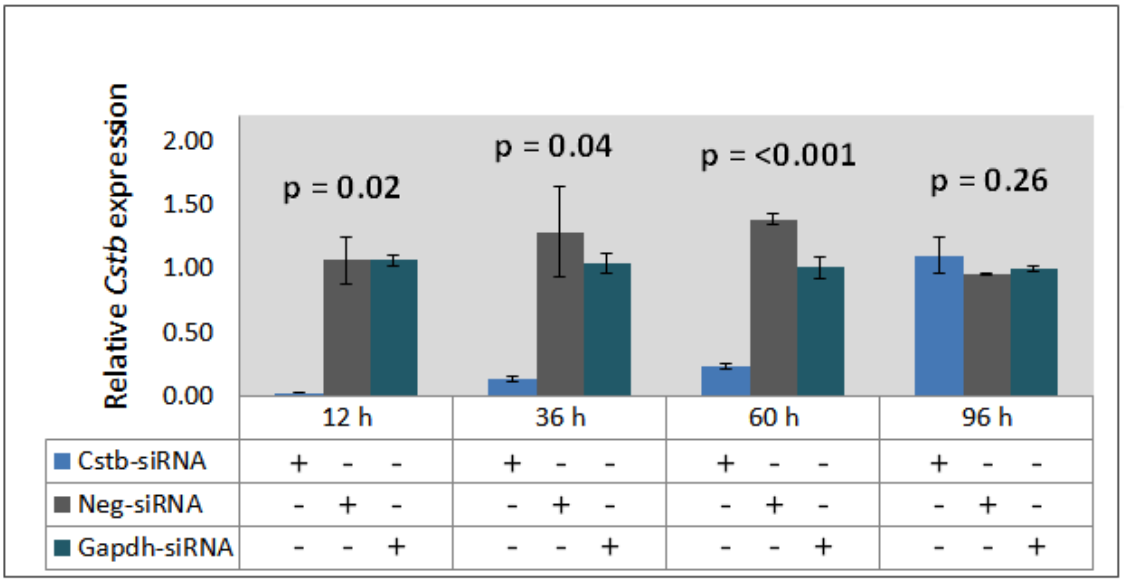

Figure 17. *Cstb* mRNA expression in siRNA transfected RAW264.7 cells at time points 12, 36, 60, and 96 hours. The *Cstb* mRNA inhibition was shown to be specific to the Cstb-siRNA sequence (light blue), and the obtained variation between Cstb- and Neg-siRNA (grey) transfected cells, indicated as p-values, remained significant until the 96-hour time point. Some variation in *Cstb* mRNA expression was detected in the Neg-siRNA, but not in the Gapdh-siRNA (dark blue) transfected control cells. The expression values were obtained from TaqMan using the Pflaffl –method, and the expression of *Cstb* mRNA was normalized to the expression levels of *Tbp*. The expression levels are shown in relation to mock-transfected cells. Measurements were performed three independent times, and the error bars represent the standard deviations (SD). P-values are marked above the bars. The + - and the – -signs at the lower panel indicate which siRNA the cells have, and have not been transfected with.

4.2.4. The kinetics of the *Cstb* mRNA expression

The *Cstb* mRNA levels were measured from siRNA and mock-transfected cells collected at time points 12, 24, 36, 48, 60, 72, and 96 hours post-transfection. The expression levels of *Cstb* mRNA from Cstb-siRNA transfected cells were normalized against the expression levels obtained from the mock-transfected cells, and a curve describing the kinetics of *Cstb* mRNA was plotted (**Figure 18**).

Cstb mRNA expression was at its minimum 12 hours post-transfection, being downregulated to 3% of mock-transfected cells. The expression levels of *Cstb* increased steadily after 12 hours, being 6% at 24 hours, 14% at 36 hours, 23% at 48 hours, and 24% at 60 hours. At the 72 hour time point, the expression levels of *Cstb* mRNA had increased to 50% of the control level. At 96 hours, the transient effect of the siRNA on *Cstb* expression could not anymore be detected.

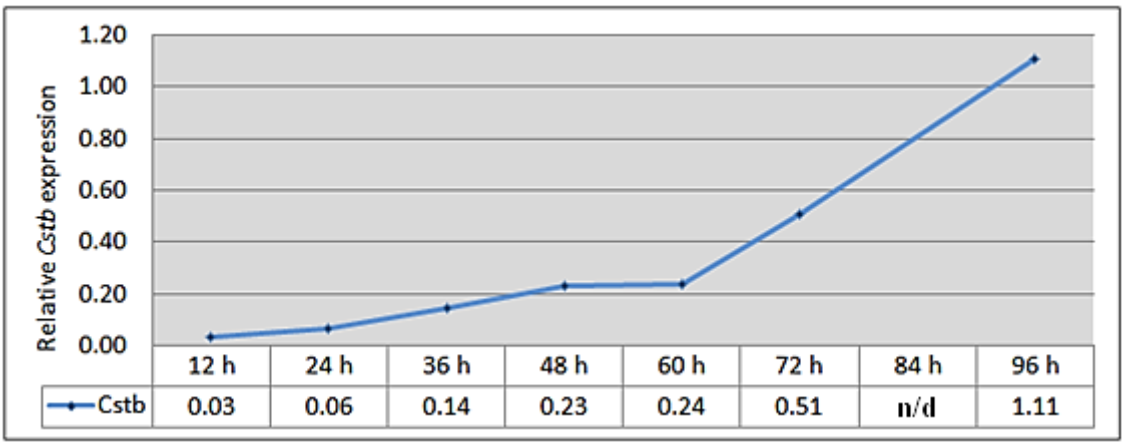

Figure 18. The kinetics of *Cstb* mRNA expression after Cstb-siRNA transfection in RAW264.7 cells. The *Cstb* mRNA expression levels were most downregulated at the first measured time point, 12 hours, being 3% of control values. The mRNA expression of *Cstb* increased steadily at the following time points, increasing steeply after 60 hours. At the final time point, 96 hours, the mRNA expression of *Cstb* was reverted. The *Cstb* expression level is not done (n/d) for the time point 84 hours. The expression values were obtained from TaqMan using the Pfaffl –method, and the expression of *Cstb* was normalized to the expression levels of *Tbp*. The expression levels are shown in relation to mock-transfected cells.

The positive control, Gapdh-siRNA, was used in order to verify the specific and to rule out the unspecific changes in *Cstb* knockdown cells. The kinetics of *Gapdh* mRNA (**Figure 19**) in the *Gapdh* knockdown cells resemble the kinetics observed with *Cstb* mRNA (**Figure 18**). The expression levels of *Gapdh* are, similarly to *Cstb* mRNA, most downregulated at the time point 12 hours, increasing after that. *Gapdh* mRNA stays, however, downregulated for a longer time period, estimated to reach 50% of the expression levels of mock-transfected cells around the time point 84 hours. Similarly to *Cstb* mRNA, *Gapdh* mRNA starts to increase linearly in expression after the time point 60 hours, but with a less steep slope.

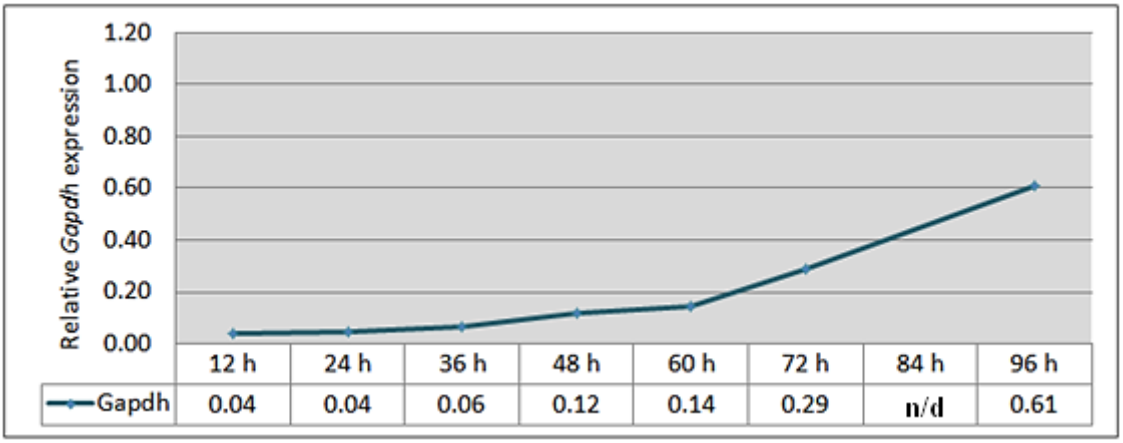

Figure 19. The kinetics of Gapdh mRNA expression at different time points. The kinetics of *Gapdh* mRNA expression levels resembles the kinetics of *Cstb* mRNA. *Gapdh* mRNA is, however, downregulated for a longer time. The *Gapdh* expression level is not done (n/d) for the time point 84 hours. The expression levels were obtained from TaqMan using the Pfaffl – method, and the expression of *Gapdh* mRNA was normalized to the expression levels of *Tbp*. The expression levels are shown in relation to mock-transfected cells.

4.2.5. The kinetics of the CSTB protein expression

The CSTB protein expression was detected by WB analysis (**Figure 20a**). The kinetics of the CSTB protein had similar progression as the *Cstb* mRNA expression, though CSTB was less downregulated on protein level (**Figure 20b**). At the time points 12 and 24 hours, CSTB was downregulated to 30% and 34%, respectively. The CSTB expression decreased at 36 and 48 hours to 23% and 22%, and it started to increase at 60 hours being 25%. At 72 hours, the expression level of CSTB was 46%. At the final time point, 96 hours, the protein was still downregulated to 53%, whereas on mRNA level, the expression was already reverted (**Figure 18**). The differential kinetics between the *Cstb* mRNA and the CSTB protein demonstrates i.a. the delay in translation to protein.

a)

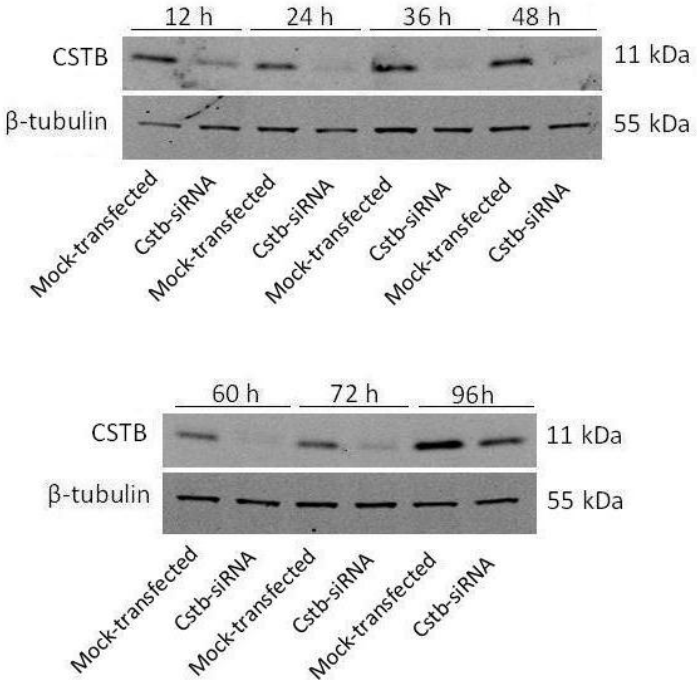

b)

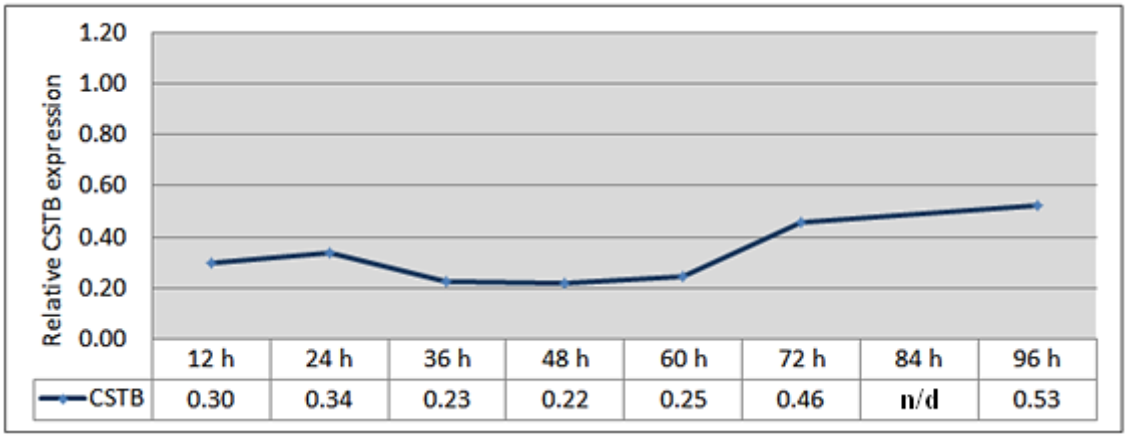

Figure 20. **A. Western blot analysis of CSTB (11 kDa) expression in RAW264.7 cells.** The siRNA mediated inhibition of *Cstb* was confirmed on protein level from samples collected at different time points. CSTB expression was downregulated throughout 12-96 hours, in particular between 36 and 60 hours. Mock-transfected cells express CSTB at all the time points. β-tubulin (55 kDa) was used as loading control. The proteins are indicated on the left, and their molecular weights (kDa) on the right. The time points are indicated above the lanes. **B. The kinetics of CSTB protein expression after Cstb-siRNA transfection in RAW264.7 cells.** Maximal downregulation of the CSTB protein is seen between the time points 36 and 48 hours. By the 96 hour time point CSTB is still downregulated by almost half. Expression of CSTB is shown in relation to mock-transfected cells, and the obtained fold change at each time point is shown at the panel below the figure. The CSTB expression level is not done (n/d) for the time point 84 hours. Quantification of the Western blot was done using the Odyssey software.

4.2.6. The effect of *Cstb* knockdown on the ISGF3-complex members

QRT-PCR, WB-, and IF microscopy analyses were performed in order to study the effects of *Cstb* knockdown on the expression levels of the ISFG3-complex members *Stat1*, *Stat2*, and *Irf9*.

4.2.6.1. Signal transducer and activator of transcription 1 (Stat1)

The *Stat1* mRNA expression, measured by qRT-PCR, increased initially after Cstb-siRNA transfection until the time point 36 hours (**Figure 21**). At the time point 48 hours the *Stat1* expression, however, decreased to the level of mock-transfected cells, and at the time point 60 hours, a downregulation to 65% of the control level was measured. After this downregulation, at the time point 72 hours, the *Stat1* mRNA expression level increased back to its base level, and stabilized in expression at 96 hours. Only minor changes in *Stat1* mRNA expression levels were observed in the positive control, *Gapdh* knockdown cells. In the Neg-siRNA transfected cells, the *Stat1* expression varied somewhat and presented with similar kinetics as with the *Cstb* knockdown cells. Variation in *Stat1* expression was, however, not detected in same degree as with the *Cstb* knockdown cells.

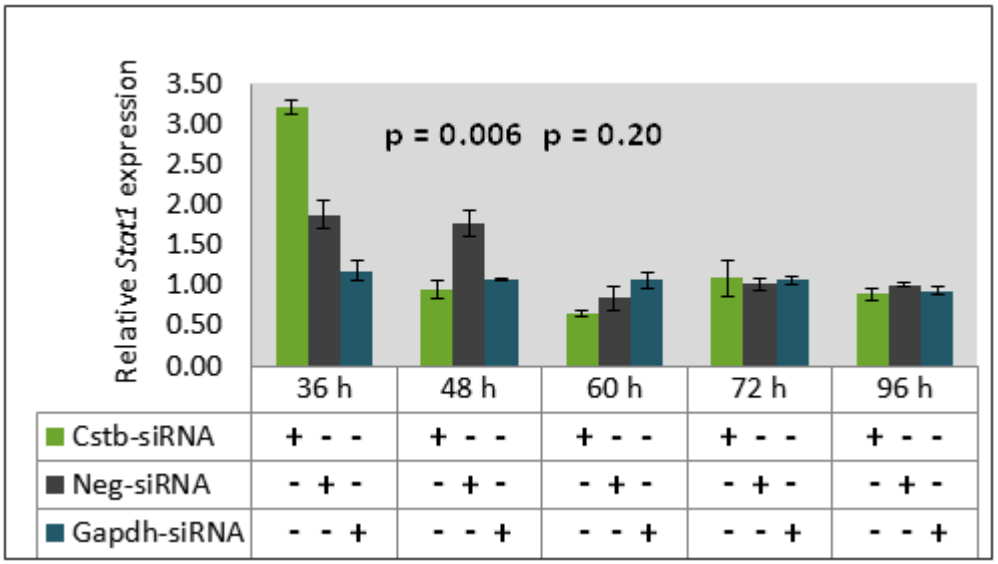

Figure 21. The mouse *Stat1* mRNA expression in differentially transfected RAW264.7 cells. *Stat1* mRNA expression levels were upregulated in Cstb-siRNA (green) transfected cells until the time point 36 hours. At the time point 48 hours, the *Cstb* knockdown cells had decreased *Stat1* expression and kept decreasing until the time point 60 hours (fold change 0.65). A brief increase in *Stat1* expression was detected at the last time points (72 and 96 h). Variation was observed in the Neg-siRNA (grey) transfected cells similarly as in the *Cstb* knockdown cells, however, the changes were not as intense. Changes in *Stat1* expression were not observed in the *Gapdh* knockdown (dark blue) cells at any time point. The expression values were obtained from TaqMan using the Pflaffl –method and the expression of *Stat1* was normalized to the expression levels of *Tbp.* The expression levels are shown in relation to mock-transfected cells. Measurements were performed three independent times, and the error bars represent the standard deviations (SD). P-values are marked above the bars. The + - and the – -signs at the lower panel indicate which siRNA the cells have, and have not been transfected with.

The changes in STAT1 expression in the *Cstb* knockdown cells were verified by WB analysis (**Figure 22**). The kinetics resemble those observed on mRNA level, however, a slight downregulation of STAT1 was not detected until the time point 96 hours (fold change 0.9).

An upregulation of STAT1 was detected at the 60 hour time point in the Neg-siRNA transfected cells (fold change 3.5)

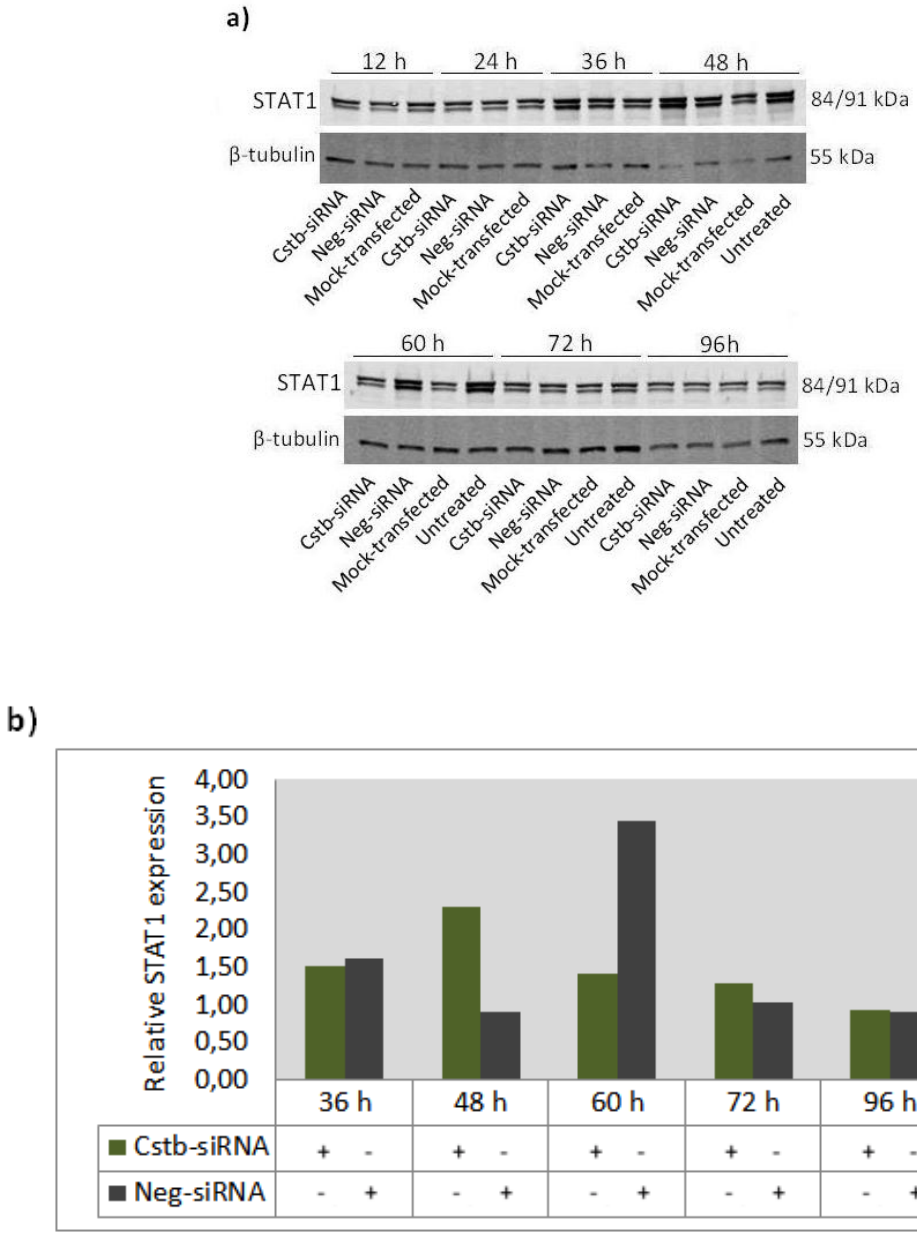

Figure 22. **A. Western blot analysis of the STAT1 protein expression in RAW264.7 cells.** STAT1 (84/91 kDa) upregulation was detected in *Cstb* knockdown cells (Cstb-siRNA) at the 36 and 48 hour time points. Neg-siRNA transfected and untreated cells presented with an upregulation of STAT1 at the 60 hour time point. β-tubulin (55 kDa) was used as loading control. The proteins are indicated on the left, and their molecular weights (kDa) on the right. The time points are indicated above the lanes. **B. Quantification of the Western blot by the Odyssey software.** As observed in Fig. 22a, the initial upregulation of STAT1 in *Cstb* knockdown cells (green) was reverted at the time point 60 hours, at which STAT1 decreased in expression. A slight downregulation in relative protein expression was detected at the time point 96 hours. STAT1 expression was also increased in the Neg-siRNA transfected cells (grey), but downregulated at 48 hours. With the exception of the time point 60 hours, the Neg-siRNA transfected cells express less STAT1 protein than the *Cstb* knockdown cells. Expression of STAT1 is shown in relation to mock-transfected cells. The + - and the – -signs at the lower panel indicate which siRNA the cells have, and have not been transfected with.

Downregulation of the STAT1 protein in the *Cstb* knockdown cells was also observed by IF microscopy at 96 hours (**Figure 23**). The cellular distribution of the STAT1 protein was mainly cytoplasmic in *Cstb*-knockdown cells, in comparison to the Neg-siRNA transfected cells, where it was located both in the cytoplasm and in the nucleus. The mock-transfected cells, used as reference, had a more even intracellular distribution of the STAT1 protein in comparison to the Cstb- and the Neg-siRNA transfected cells.

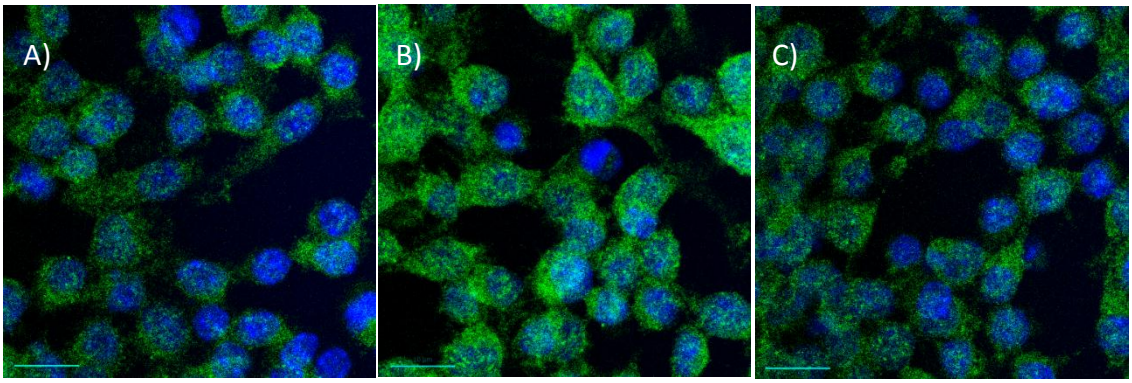

Figure 23. STAT1 (green) expression was downregulated at 96 hours in the *Cstb* knockdown cells (A) compared to the negative control (B), and the mock-transfected cells (C). An altered cellular distribution of the STAT1 protein was also observed in the *Cstb* knockdown cells. The nuclei of the cells are stained with Hoechst (blue).
Scale 10 µm.

4.2.6.2. Signal transducer and activator of transcription (Stat2)

In response to *Cstb* knockdown, the *Stat2* mRNA expression levels were increased in a similar way as *Stat1* (**Figure 24**). An upregulation in *Stat2* mRNA levels was detected in both Cstb-siRNA and Neg-siRNA transfected cells at the time point 36 hours (fold changes 3.1 and 1.5, respectively). At the time point 48 hours, both samples decreased in *Stat2* expression (fold changes 1.2 and 1.3, respectively), and continued decreasing until the time point 60 hours (fold changes for both 0.85). An increase in *Stat2* expression was detected for both samples at the time point 72 hours (fold changes 0.98 and 1.65), and at 96 hours there were only minor changes between the transfected samples (fold changes 1.0 and 1.1).

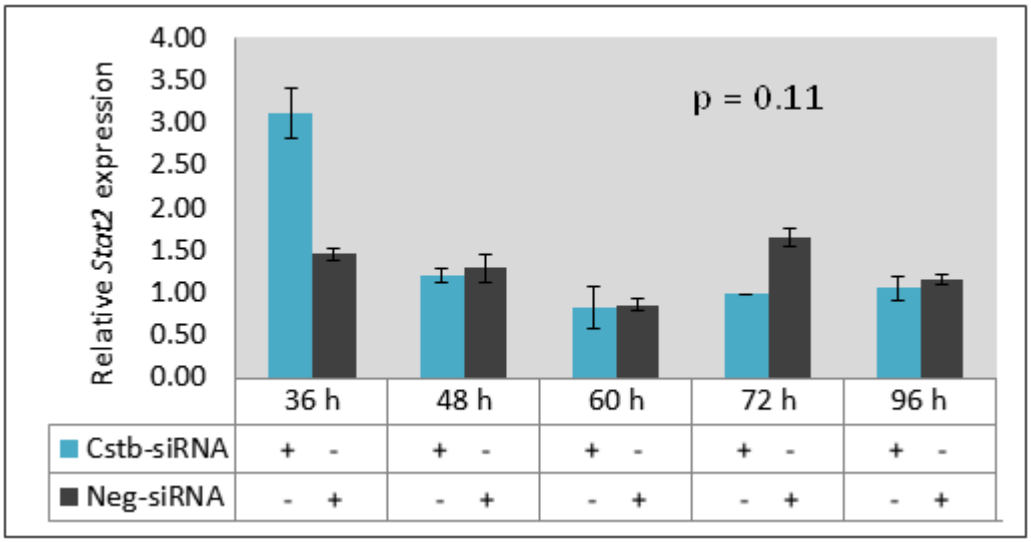

Figure 24. The mouse *Stat2* mRNA expression in differentially transfected RAW264.7 cells. A peak in upregulation of *Stat2* expression was observed in *Cstb* knockdown cells (blue) at the time point 36 hours (fold change 3.1), after which the *Stat2* expression levels started to decrease, reaching the lowest expression level at the time point 60 hours (fold change 0.8). At 72 and 96 hours the *Stat2* expression level had normalized to the control level. In the Neg-siRNA transfected cells (grey), the *Stat2* mRNA expression levels varied in the range from 0.85 to 1.65.The expression values were obtained from TaqMan using the Pflaffl –method and the expression of *Stat2* was normalized to the expression levels of *Tbp.* The expression levels are shown in relation to mock-transfected cells. Measurements were performed three independent times, and the error bars represent the standard deviations (SD). P-values are marked above the bars. The + - and the – -signs at the lower panel indicate which siRNA the cells have, and have not been transfected with.

The STAT2 expression was analyzed by WB, which presented similar results as seen on mRNA level (**Figure 25**). In *Cstb* knockdown cells, the STAT2 protein was upregulated at the time points 36, 48 and 60 hours. At the time point 72 hours a downregulation of STAT2 was detected (fold change 0.7). In Neg-siRNA transfected cells the STAT2 protein expression was similar as in the *Cstb* knockdown cells, but an upregulation of STAT2 was observed at the time point 60 hours (fold change 2.7).

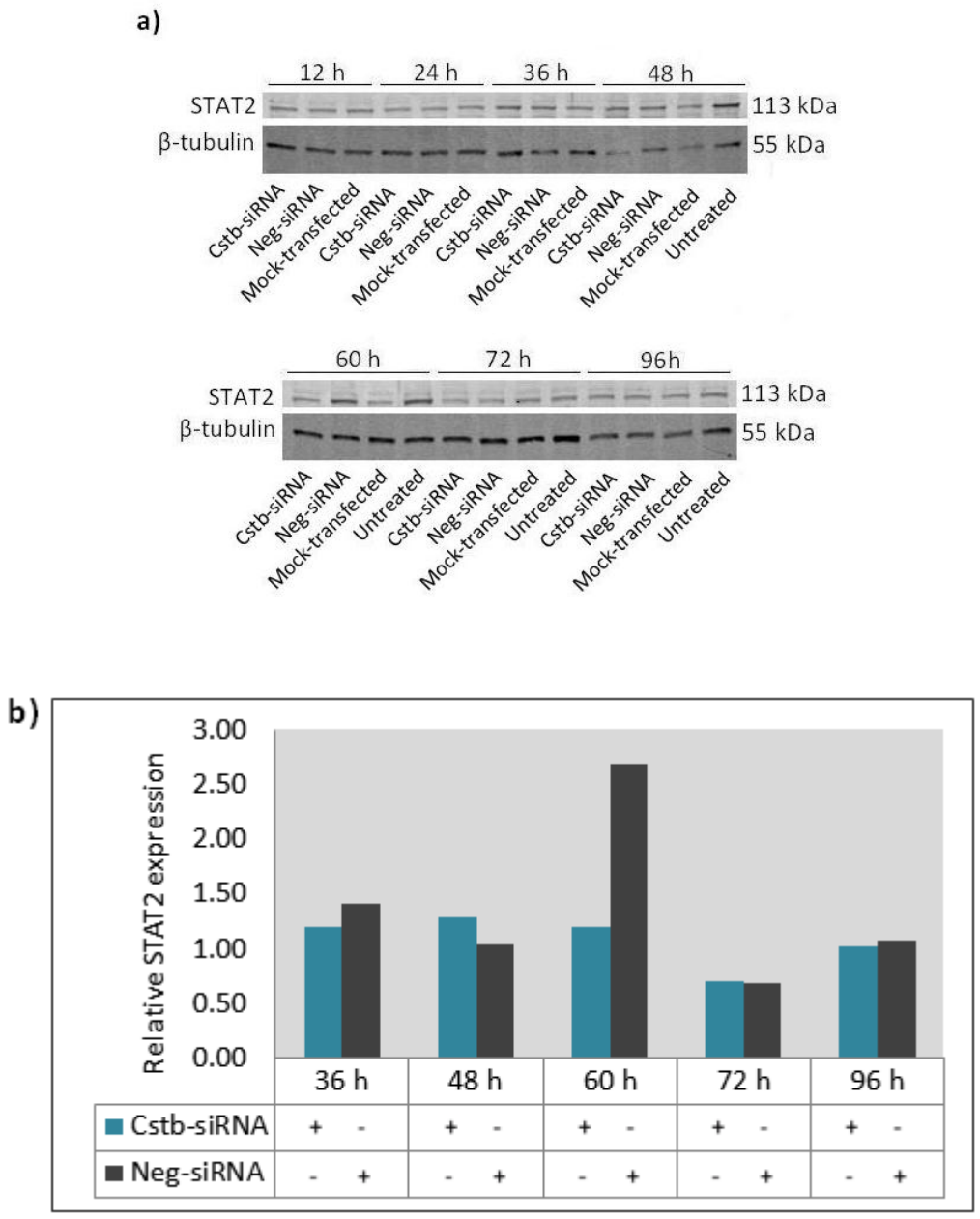

Figure 25. **A. Western blot analysis of the STAT2 expression in RAW264.7 cells.** STAT2 (113 kDa) upregulation was detected in *Cstb* knockdown cells (Cstb-siRNA) at the 36 and 48 hour time points. Neg-siRNA transfected and untreated cells presented with an upregulation of STAT1 at the 60 hour time point. β-tubulin (55 kDa) was used as loading control. The proteins are indicated on the left, and their molecular weights (kDa) on the right. The time points are indicated above the lanes. **B. Quantification of the Western blot by the Odyssey software.** As observed in Fig. 25a, STAT2 was slightly upregulated in *Cstb* knockdown cells (blue) at all but the 72 hour time point. The Neg-siRNA (grey) transfcted cells follow the kinetic profile of STAT2 expression, with the exception of the time point 60 hours, when STAT2 expression levels are increased. Expression of STAT2 is shown in relation to mock-transfected cells. The + - and the – -signs at the lower panel indicate which siRNA the cells have, and have not been transfected with.

4.2.6.3. Interferon regulatory factor 9 (Irf9)

Irf9 mRNA expression did not change in a substantial manner during the examined time points. The *Irf9* mRNA expression was slightly upregulated after transfection (**Figure 26**) in *Cstb* knockdown cells and remained upregulated (fold change 1.1) until the time point 60 hours. A downregulation of *Irf9* mRNA was detected at the time point 72 hours (fold change 0.9), and the expression levels stabilized to the level of mock-transfected cells by 96 hours. Neg-siRNA transfected cells expressed *Irf9* in a similar manner, however, with increased expression levels at 48 hours (fold change 1.65).

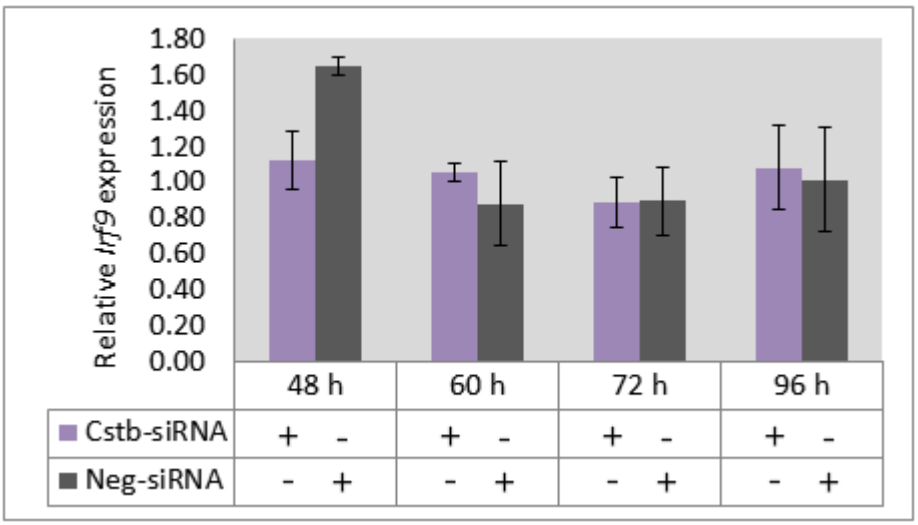

Figure 26. The mouse *Irf9* mRNA expression in differently transfected RAW264.7 cells. A slight increase of *Irf9* in the *Cstb* knockdown (purple) and in the Neg-siRNA (grey) transfected cells was detected, followed by a decrease in expression after 60 hours. The *Irf9* expression levels were downregulated at the 72 hour time point, increasing at 96 hours to the levels of the mock-transfected cells. The expression values were obtained from TaqMan using the Pflaffl –method and the expression of *Irf9* was normalized to the expression levels of *Tbp.* The expression levels are shown in relation to mock-transfected cells. Measurements were performed three independent times, and the error bars represent the standard deviations (SD). P-values are marked above the bars. The + - and the – -signs at the lower panel indicate which siRNA the cells have, and have not been transfected with.

The expression levels of IRF9 were detected by WB analysis (**Figure 27**). An initial increase in IRF9 expression was observed in all samples after the 12 hour time point, however, the time point specific changes in protein expression were small. The expression levels of IRF9 in *Cstb* knockdown cells remained downregulated (fold change 0.7) until the time point 60 hours, when an upregulation was detected (fold change 1.2). At the following time points, the expression levels of IRF9 were downregulated to 0.8. The negative control samples were equally downregulated, except at the time point 48 hours, being upregulated by 1.1 fold.

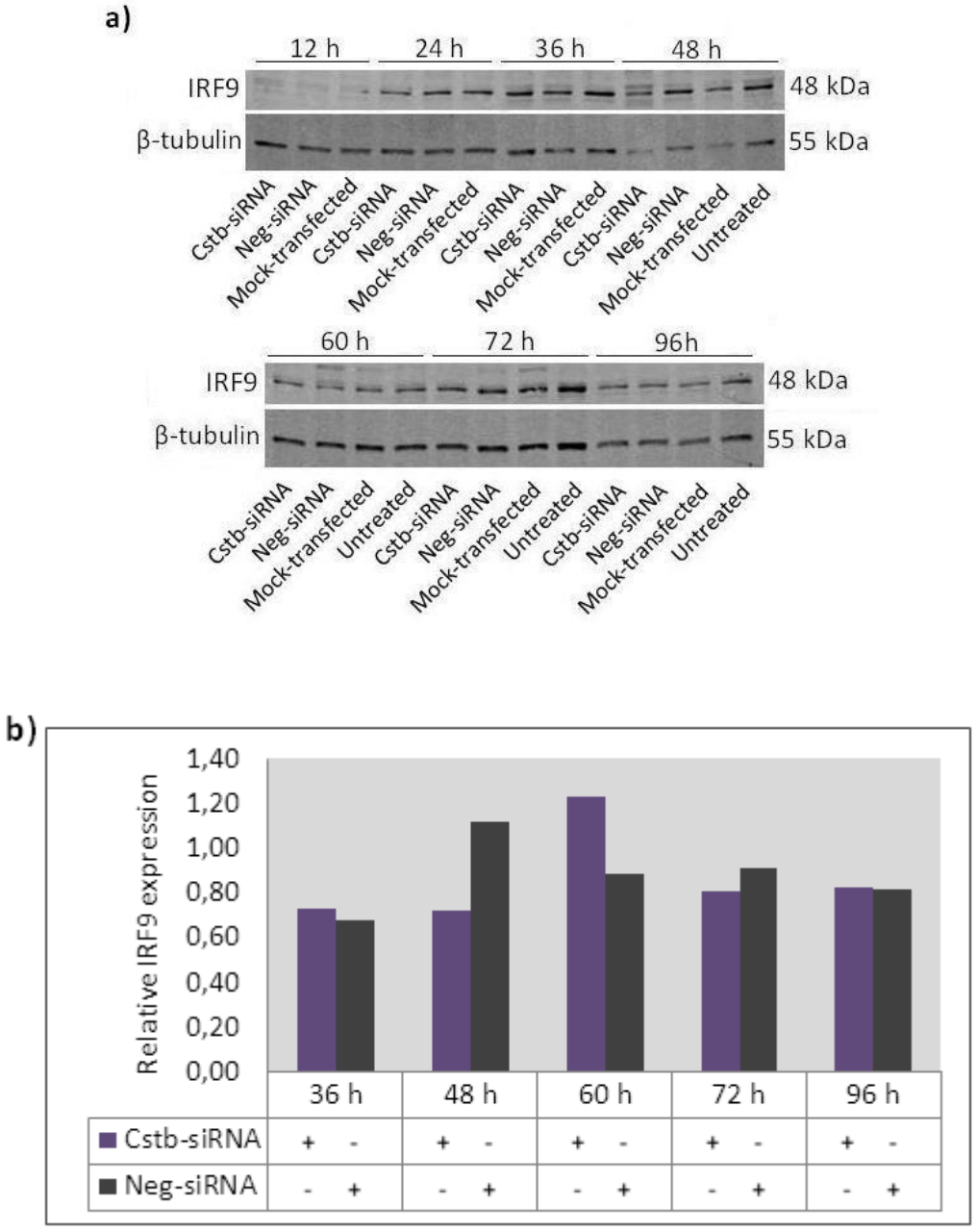

Figure 27. **A. Western blot analysis of the IRF9 expression in RAW264.7 cells.** IRF9 (48 kDa) expression remained rather vaguely expressed in *Cstb* knockdown cells throughout all time points. Neg-siRNA transfected cells presented with a similar expression pattern of IRF9 as the *Cstb* knockdown cells. β-tubulin (55 kDa) was used as loading control. The proteins are indicated on the left, and their molecular weights (kDa) on the right. The time points are indicated above the lanes. **B. Quantification of the Western blot by the Odyssey software.** The detected changes in IRF9 expression were small between *Cstb* knockdown (purple) and Neg-siRNA (grey) transfected cells. An increase in IRF9 expression was detected at the time points 60 hours for Cstb-siRNA (fold change 1.2), and 48 hours for the Neg-siRNA (fold change 1.1) transfected cells. The expression level decreased to 0.8 at the time point 72 hours for *Cstb* knockdown cells. Expression of IRF9 is shown in relation to mock-transfected cells. The + - and the – -signs at the lower panel indicate which siRNA the cells have, and have not been transfected with.

4.2.7. The effects of *Cstb* knockdown on markers for oxidative stress

In order to test whether markers for oxidative stress were increased in *Cstb* knockdown cells, WB analysis of the iNOS protein and subsequent nitric compound release measurements were performed.

4.2.7.1. Inducible nitric oxide synthase (iNOS)

The iNOS expression was detected by WB analysis (**Figure 28**) from the transfected and the control cells. The only iNOS positive signals were perceived from the untreated control and Neg-siRNA transfected cells, cellular samples which presented with morphological changes already previously, and collected at the time-point 60 hours post-transfection.

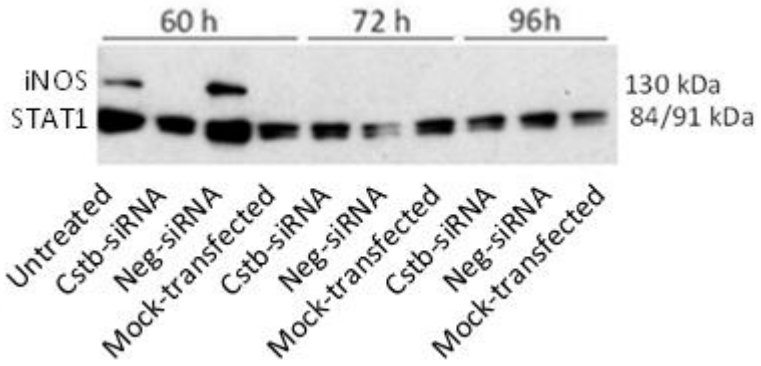

Figure 28. Western blot analysis of the iNOS protein. iNOS (130 kDa) was detected only in the untreated control cells and the Neg-siRNA transfected cells from the time point 60 hours. No other sample was positive for iNOS expression. STAT1 (84/91 kDa) expression is shown as marker for the other samples.

The iNOS expression was evaluated also by IF microscopy (**Figure 29**). In *Cstb* knockdown cells, the iNOS positive cells increased in amount over time and at the final time point, 96 hours, a maximal amount of iNOS positive cells, about 20 per coverslip, was detected. A difference in the amount of iNOS positive cells between the Cstb-siRNA and Neg-siRNA transfected cells was, however, not observed. No iNOS positive

cells were detected in the mock-transfected cells at any time point. LPS activated RAW264.7 macrophages (kind gift from I. Körber, group A-E. Lehesjoki, Helsinki, Finland) were used as positive control for iNOS detection, and those cells expressed iNOS up to 85%. The activated macrophages are bigger in size and they possess different morphological features, such as a round, outspread phenotype, which is not seen in naïve RAW264.7 cells.

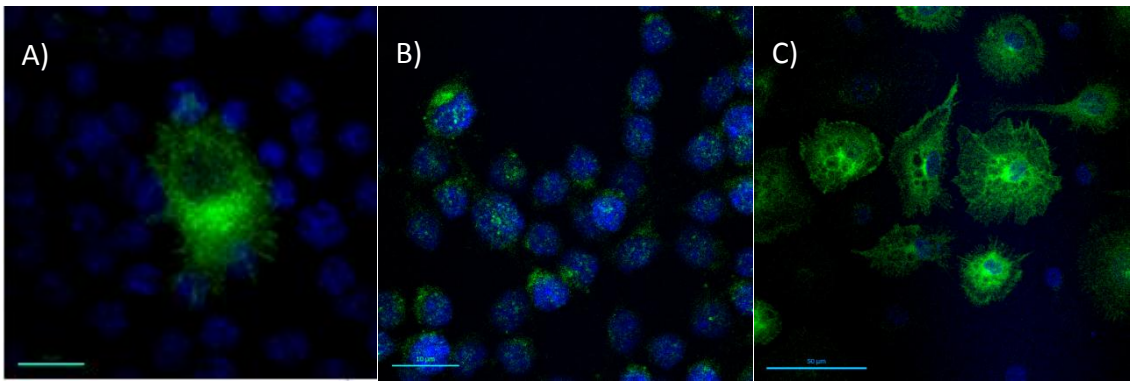

Figure 29. The iNOS (green) protein expression was altered at 96 hours in the *Cstb* knockdown cells. Cstb knockdown cells (A) presented with an unpregulation in iNOS expression, when compared to mock-transfected cells (B). A similar amount of iNOS positive cells was, however, observed in the Neg-siRNA transfected cells (not shown). LPS-activated RAW264.7 macrophages (C) were used as a positive control for iNOS detection. Besides increased iNOS expression, a clear morphological phenotype was observed in the LPS activated control cells. The nuclei of the cells are stained with Hoechst (blue).
Scale 10 µm for A and B, 50 µm for C.

4.2.7.2. The Griess test

Release of nitric compounds from the transfected and control RAW264.7 cells was measured from the growth media by the Griess test. All test results, apart from the untreated control and Neg-siRNA transfected cells at the 60 hour time-point, were negative for nitrite release. The growth media from the untreated control and Neg-siRNA transfected cells was collected from the same cell culture flasks as the corresponding protein lysates were taken from.

4.2.8. Summary of the most important findings

Knockdown of *Cstb* in RAW264.7 cells resulted in an initial upregulation of all examined genes (**Figure 30**), before a downregulation of *Stat1* and *Stat2* became prominent. Transfection with the Cstb-siRNA was both sensitive and specific, and the kinetics of the *Cstb* mRNA and CSTB protein showed at what time points the downregulation was maximal. At the same time point when CSTB protein expression was at its lowest, a decrease in *Stat1* and *Stat2* mRNA expression became detectable by qRT-PCR. This downregulation was later observed also on protein level.

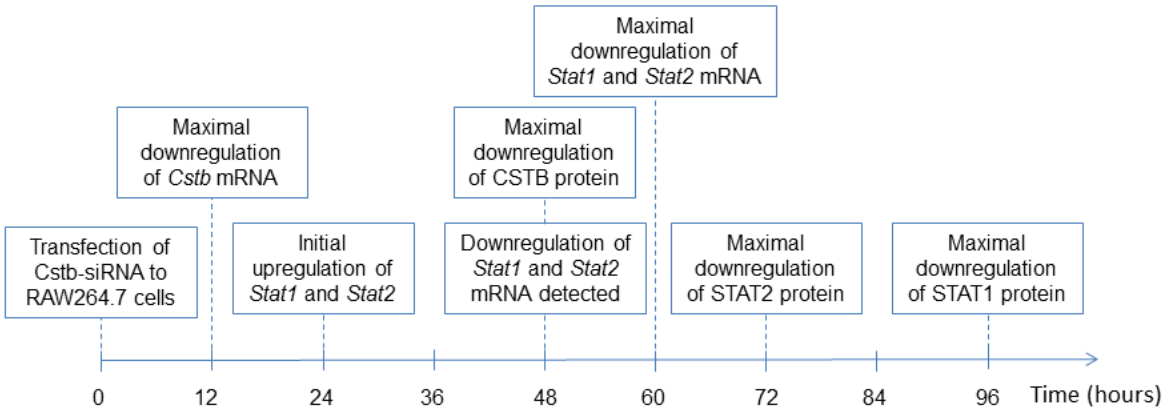

Figure 30. Timeline of findings at different time points in the *Cstb* knockdown RAW264.7 cells. The timeline describes the findings between Cstb-siRNA transfection until 96 hours. The timeline contains changes both on mRNA and protein level, and links the changes together. A transition from *Cstb* to *Stat1* and *Stat2* happened at the time point 48 hours, when the CSTB protein and the *Stat1* and *Stat2* mRNA were downregulated to their minimum.

5. DISCUSSION

The chronic changes of EPM1 have so far been studied in patient cells and tissues and in the *Cstb*$^{-/-}$ mouse. Patient samples are, however, hard to obtain, and the existing mouse model breeds poorly. Therefore, there has been a need for an *in vitro* model, in which the acute pathogenesis of the disease could be further investigated on molecular level.

In the present work, we employed RNA interference (RNAi) to create a cystatin B (*Cstb*) -knockdown model in the human HeLa and the murine macrophage RAW264.7 cell lines. We also utilized these cell models to study the members of the JAK/STAT signaling pathway, which had previously been shown to be affected in the primary microglia of *Cstb*$^{-/-}$ mice (Körber et al, unpublished).

We used siRNA transfection to transiently downregulate the *Cstb* mRNA, and based on the kinetics of CSTB knockdown, we hypothesized the timeframe when changes in the expression of the members of the JAK/STAT signaling pathway could be detected. For further validation of the method in EPM1 pathophysiology, we also looked for markers of oxidative stress, which has previously been reported to co-occur in *Cstb*$^{-/-}$ mice (Lehtinen et al, 2009).

5.1. Transfection in HeLa and RAW264.7 cells

Knockdown of *CSTB* was first conducted in the cell line HeLa. The cell line was chosen as part of this experiment in order to optimize the method in an easily manipulated cell line, but also to compare the cell line specific effects of *CSTB* knockdown. The manufacturer of the electroporation kit provided us with a readily optimized protocol for HeLa transfection. We chose to transfect a GFP encoding plasmid (pEGFP) together with the CSTB-siRNA in order to determine a percentual transfection efficiency by IF microscopy of the GFP protein. Transfection was easy, cell mortality was low, and IF stainings showed that the transfection efficiency was over 50%. By performing WB

analysis of protein lysates from the HeLa cells, we also observed that CSTB was effectively downregulated by the siRNAs.

The cell line RAW264.7 was chosen for this study due to its monocytic origin. The cell line is used in several immunological studies, and it is relatively easy to maintain. The manufacturer of the electroporation kit had an optimized protocol for transfection of this cell line, but the obtained transfection efficiency was not as high as reported in the protocol. Further re-optimization had been published by another research group (Yunus et al, 2010), but despite replicating the experiment with the reported parameters, we did not obtain similar results. We had to optimize the protocol by adjusting cell and siRNA amounts, which finally lead to transfection efficiency of over 80%. The siRNA molecules we used for transfecting RAW264.7 cells were labelled with an Alexa Fluor-647 fluorochrome, which enabled us to monitor the transfection efficiency without conducting laborious and time-consuming IF-stainings. Since there is unfortunately no proper antibody against the mouse CSTB protein, we were not able to study the downregulation of CSTB on cell-specific level. QRT-PCR and WB analysis, however, showed that the siRNA sequence that we used was sensitive for *Cstb* mRNA, and downregulated it almost completely.

5.2. *CSTB* knockdown in HeLa cells did not result in changes in the JAK/STAT signaling pathway

Downregulation of *CSTB* mRNA by siRNA transfection was shown to be efficient in HeLa cells. However, effects of *CSTB* knockdown in the expression levels of members of the JAK/STAT signaling pathway, such as STAT1 and STAT2 were not detectable on protein level. These results may be explained by the tissue specific consequences of *CSTB* knockdown. In EPM1 patients, histopathological changes have been described only in the brain and the bones (Cohen et al, 2011; Eldridge et al, 1983; Haltia et al, 1969; Korja et al, 2007; Koskenkorva et al, 2009; Koskenkorva et al, 2012; Koskiniemi et al, 1974; Suoranta et al, 2012), even if the CSTB protein is ubiquitously expressed (Alakurtti et al, 2005; Brännvall et al, 2003; Laitala-Leinonen et al, 2006). Changes in STAT1 and STAT2 expression in HeLa cells require interferon stimulation in order to

become detectable by WB, as observed from previous literature (Nishio et al, 2001). Based on these observations, we concluded that the cell line HeLa was not a good tool in our study for investigating gene specific changes of monocytic origin. However, the cell line HeLa was used to optimize the RNAi method, which we applied when continuing the study in RAW264.7 cells.

5.3. *Cstb* knockdown in RAW264.7 cells

5.3.1. The specificity of the Cstb-siRNA and the kinetics of *Cstb*

In the RAW264.7 cell line, siRNA transfection and *Cstb* knockdown were successful, which could be visualized by IF microscopy, and monitored by qRT-PCR and WB analysis. The *Cstb* mRNA was downregulated to its minimum at 12 hours post transfection, thereafter the expression level rapidly increased. The optimal siRNA incubation time is generally considered to be 24-72 hours depending on cell type and gene to be silenced (Mirus Bio,
http://www.mirusbio.com/tech_resources/tips/optimize_sirna_transfection).
However, in our case the *Cstb* expression levels had exceeded 10% already at the time point 36 hours and showed an increased expression (50%) at 72 hours. Therefore, the time frame when *Cstb* expression levels were comparable to those measured from the cultured primary microglia of the $Cstb^{-/-}$ mouse (Körber et al, unpublished), which this work is based on, was rather narrow.

The mRNA of *Gapdh* was knocked down as positive control and to rule out unspecific effects of *Cstb* inhibition. *Gapdh* expression levels remained downregulated for a longer time period, demonstrating the gene-specific differences of RNAi. The kinetics was, however, similar between the mRNAs, both being most downregulated at 12 hours and increasing in expression after that. The similar kinetics between the *Cstb* and *Gapdh* mRNA implied that *Gapdh* was a good positive control for our study.

We did not observe significant variation in *Cstb* expression levels in the Gapdh-siRNA transfected cells. Some changes in *Cstb* expression were, however, detected in the

Neg-siRNA transfected cells. This raised a question whether the Neg-siRNA sequence could somehow affect *Cstb* mRNA expression. This could unfortunately not be further investigated due to the proprietary sequence of the Neg-siRNA.

The duration for translation of mRNA to protein is both gene and tissue specific (Wilusz & Wilusz, 2004). There is no published data about the life span of the CSTB protein in macrophages, but, based on our kinetic profiles of the *Cstb* mRNA and the CSTB protein, it is around 30 hours in the cell line RAW264.7.

Downregulation of CSTB was not as effective on protein as on mRNA level, which endogenous siRNA inhibitors and dilution of siRNA concentration in the cells due to cell proliferation contributes to in a high degree (Rao et al, 2009a; Sandy et al, 2005). Moreover, the extrapolation from mRNA levels to protein abundance involves several cellular processes, and is not as straight forward as it appears (Brewer, 2002).

Due to our hypothesized CSTB life span, we expected to detect changes in expression of members of the JAK/STAT signaling pathway at the later time points, first on mRNA level and later, depending on the half-life of the target protein, on protein level.

5.3.2. *Cstb* downregulation had an effect on *Stat1*, *Stat2*, and *Irf9*

Downregulation of *Cstb* affected the expression levels of *Stat1*, *Stat2*, and *Irf9* in RAW264.7 cells, as previous results had shown in *Cstb*$^{-/-}$ microglia (Körber et al, unpublished). After detection of *Cstb* knockdown, there was an initial increase in the expression levels of *Stat1*, *Stat2*, and also somewhat on *Irf9*. These changes were also detected in the Neg-siRNA, but not in the Gapdh-siRNA transfected cells. We had previously observed that the Neg-siRNA sequence affects the expression levels of *Cstb*, proposing that the response pathway after Neg-siRNA transfection involves at least to some extent *Cstb*. Without the Gapdh-siRNA control, these changes would have been considered unspecific and due to transfection.

A decrease in the mRNA expression levels of *Stat1* and *Stat2* was detected by qRT-PCR at the time point 48 hours, at the same time point when CSTB protein expression was downregulated to its minimum, further suggesting interplay between CSTB and the

Stats. Downregulation of *Gapdh*, which we assumed would not affect the JAK/STAT signaling pathway, did not change expression levels of either *Cstb* or *Stat1* at any of the measured time points. The Neg-siRNA transfected cells showed, however, similar kinetics of *Stat1* and *Stat2* mRNA expression as the *Cstb* knockdown cells, suggesting that the response of the *Stats* was unspecific. Due to fluctuations in the *Cstb* mRNA expression levels in the Neg-siRNA transfected cells, this remains, however, unresolved.

The rather late time point (60 hours) when the *Stats* were downregulated on mRNA level implied that we would perhaps not be able to detect any changes on protein level. Literature revealed that the life span of the STATs is >24 hours i.e. in the lymphoblastic cell line Daudi (Lee et al, 1997; Lee et al, 2011), delaying the time point for detecting downregulation on protein level to >70 hours. Downregulation was, however, observed at the time points 72 and 96 hours for STAT2 and STAT1, respectively. Within this time frame, siRNA dilution is evident, and most of the cultured cells are untransfected daughter cells, resulting in less prominent downregulation on protein level when compared to the previously obtained mRNA expression levels.

Changes in *Irf9* expression were not as evident as with the *Stats*. Similarly as with the *Stats*, an increase in *Irf9* mRNA expression was observed, but it was apparently transfection dependent, as has been previously reported (Li et al, 2005). After CSTB downregulation, a minor decrease was, however, observed in *Irf9* expression levels, further supporting the involvement of *Cstb* in the members of the JAK/STAT signaling pathway.

The statistical analyses were performed with expression values from the Neg-siRNA transfected cells as control dataset. Considering that there was similar variation in mRNA expression levels obtained from the Neg-siRNA transfected cells as in *Cstb* knockdown cells, the control set-up was not optimal. This fact does, however, not affect the results as such, only the obtained P-values. Due to unchanged expression values of *Cstb* and *Stat1* in the Gapdh-siRNA transfected cells, this dataset would have been a better choice for control. Unfortunately, qRT-PCR analyses beyond *Cstb* and

Stat1 in *Gapdh* knockdown cells were not performed, which would have limited our results to these genes.

5.3.3. Morphologically active cells had increased CSTB, STAT1, STAT2, and iNOS expression

While performing the time point experiments, two sets of samples, Neg-siRNA transfected cells and untreated control cells, aimed for protein extraction, presented with morphological changes at the 60 hour time point, indicating an activated phenotype. Activated macrophages grow in size and start proliferating, but they also secrete cyto- and chemokines, NO, and growth factors (Brown & Neher, 2010; Czeh et al, 2011), which are known to activate other macrophages (Liu et al, 1998b). Transfection of bacterial and mammalian DNA to RAW264.7 cells has been reported to activate the cells (Jiang et al, 2004; McCoy et al, 2004), but synthetic siRNA sequences below 30 nucleotides should overcome this problem (Elbashir et al, 2001). We did not observe activation of cells in any of the other samples, indicating a sporadic event due to external stimuli.

In these morphologically active samples, an upregulation of the proteins CSTB, STAT1, and STAT2 was detected by WB analysis. This was contrary to the findings on mRNA level, which we used naïve samples for, but in concordance with literature about the first line defense against pathogens (Darnell et al, 1994; Liu et al, 1998b; Liu et al, 1998b), and the observation that CSTB is upregulated in RAW264.7 cells as response to LPS activation (24h) (Körber et al, unpublished).

The immunoeffector molecules, which the activated macrophages secrete, include NO, indirectly implying increased iNOS expression. iNOS catalyzes the production of NO, which gets secreted from the cell and activates other macrophages. Nitric compounds were measured from the growth media by the Griess test, and iNOS expression was analyzed by WB. Only the morphologically active samples (Neg-siRNA transfected and untreated control cells, 60h) were positive for the Griess test and iNOS expression. The signaling event for activating other macrophages includes the JAK/STAT signaling pathway, which induces iNOS expression. The increased sensitivity for oxidative stress

in *Cstb* deficient cells might, however, not be directly dependent on the JAK/STAT signaling pathway, but rather on an imbalance in the redox homeostasis (Lehtinen et al, 2009), which is necessary not an instant effect of *Cstb* knockdown, but require chronic *Cstb* downregulation to be detected.

5.3.4. Conclusions and future work

The conducted study consisted of two parts, firstly to set up a siRNA based method to knock down the *Cstb* mRNA in two different cell lines, and secondly to compare its effects on the interferon regulated genes of the JAK/STAT signaling pathway. Knockdown of *Cstb* was successful in both cell lines HeLa and RAW264.7. Because changes in *Stat1*, *Stat2*, *Irf9*, and iNOS could only be seen in the murine macrophage cell line RAW264.7, these cells were mainly used for conducting the second part of the study.

Our working hypothesis was based on microarray results from primary microglia of *Cstb*$^{-/-}$ mice (Körber et al, unpublished). The cell line RAW264.7 is despite its monocytic origin not directly comparable with microglia, which possibly contributed to the results. The kinetics of *Cstb* downregulation revealed that the actual timeframe of *Cstb* knockdown by siRNA inhibition is narrow, and one of the future plans based on these results is the creation of a stable knockdown of *Cstb* in RAW264.7 cells.

Downregulation of the members of the JAK/STAT signaling pathway in the *Cstb* knockdown cells seem to verify our working hypothesis. However, in order to confirm the specificity of the downregulation to *Cstb* knockdown cells, a *Cstb*-rescue experiment, outside the frame of this thesis, is being conducted. In the future, siRNA mediated *Cstb* knockdown will be extended to study the direct consequences of CSTB downregulation also in neurons.

ACKNOWLEDGEMENTS

Firstly, I would like to thank Professor Anna-Elina Lehesjoki for giving me the opportunity to work within the EPM1 project, and thereby introducing me to the fascinating world of PMEs and the research groups of Folkhälsan. I admire your constant enthusiasm, kind words, and your positive attitude, features that cannot be taken for granted in the business world of today.

My thesis supervisors Inken and Tarja, you have been a tremendous help during this project, both in the lab and outside of it. Inken, your knowledge about things amazes me, likewise your systematic and organized way of operating. However, I guess that is something German... ☺ Tarja, your enthusiasm, helpfulness, and a shared (bad) sense of humor have been a great support during this project.

Outi, my unofficial supervisor, I value your knowledge, practical skills, and candidness, qualities that have made your help truly irreplaceable.

pH, you know I would have tossed my computer in the garbage can several times without you. Takk for hjelpen, Norge ☺

Ann-Liz, you are truly the person of this lab, thanks for keeping up my spirit!

Paula, Olesya, Saara, Mervi, Jaakko… there are many times when my work would not have proceeded without you. Thanks!

I also want to thank the rest of the Folkhälsan personnel, especially people in my office who have been nice and quiet.

Brenkku, Uwe, Paula, Marde, Riikka, all my friends at MolNeuro: thank you for all the joyful coffee moments, for all the advice I've gotten, and mostly, for keeping me sane.

Jomppa, your friendship means more to me than words can describe. Either work or personal business, I have always been able to count on you and your help. You have probably read my thesis more often than I have, and I hope I can return the favour in one year or so ☺

My friends who I met during my studies in biology, Carina, Eme, Michelle, Miika, and especially Karen, thank you for your endless support. My best wishes to fellow TransMeders as well.

My civil friends, especially Malin, Sari, Laura A., and Laura H., those small but so important moments together have probably kept me from sinking too deep into the world of science.

Last but not least, I would like to thank my family, who has shown their support during the past years.

Helsinki

12.06.2013

Katarin Sandell

REFERENCES

Alakurtti K, Weber E, Rinne R, Theil G, de Haan GJ, Lindhout D, Salmikangas P, Saukko P, Lahtinen U, & Lehesjoki AE (2005) Loss of lysosomal association of cystatin B proteins representing progressive myoclonus epilepsy, EPM1, mutations. *Eur J Hum Genet* **13**: 208-215

Aquilano K, Baldelli S, Cardaci S, Rotilio G, & Ciriolo MR (2011) Nitric oxide is the primary mediator of cytotoxicity induced by GSH depletion in neuronal cells. *Journal of Cell Science* **124**: 1043-1054

Avignone E, Ulmann L, Levavasseur F, Rassendren F, & Audinat E (2008) Status Epilepticus Induces a Particular Microglial Activation State Characterized by Enhanced Purinergic Signaling. *The Journal of Neuroscience* **28**: 9133-9144

Baran-Marszak F, Feuillard J, Najjar I, Le Clorennec C, Béchet J, Dusanter-Fourt I, Bornkamm GW, Raphaël M, & Fagard R (2004) Differential roles of STAT1α and STAT1β in fludarabine-induced cell cycle arrest and apoptosis in human B cells. *Blood* **104**: 2475-2483

Beach TG, Woodhurst WB, MacDonald DB, & Jones MW (1995) Reactive microglia in hippocampal sclerosis associated with human temporal lobe epilepsy. *Neurosci Lett* **191**: 27-30

Berkovic SF, Andermann F, Carpenter S, & Wolfe LS (1986) Progressive myoclonus epilepsies: specific causes and diagnosis. *N Engl J Med* **315**: 296-305

Bespalova IN, Pranzatelli M, & Burmeister M (1997a) G to C transversion at a splice acceptor site causes exon skipping in the cystatin B gene. *Mutation reseach* **382**: 67-74

Bespalova IN, Adkins S, Pranzatelli M, & Burmeister M (1997b) Novel cystatin B mutation and diagnostic PCR assay in an Unverricht-Lundborg progressive myoclonus epilepsy patient. *Am J Med Genet* **74**: 467-471

Black J (1976) Dead or alive: the problem of in vitro tissue mechanics. *J Biomed Mater Res* **10**: 377-389

Brännvall K, Hjelm H, Korhonen L, Lahtinen U, Lehesjoki AE, & Lindholm D (2003) Cystatin-B is expressed by neural stem cells and by differentiated neurons and astrocytes. *Biochem Biophys Res Commun* **308**: 369-374

Brewer G (2002) Messenger RNA decay during aging and development. *Ageing Research Reviews* **1**: 607-625

Brömme D, Rinne R, & Kirschke H (1991) Tight-binding inhibition of cathepsin S by cystatins. *Biomedica biochimica acta* **50**: 631-635

Brosnan C, Lee S, & Liu J (1997) Regulation of inducible nitric oxide synthase expression in human glia: implications for inflammatory central nervous system diseases. *Biochemical society transactions* **25**: 679-683

Brown G & Neher J (2010) Inflammatory Neurodegeneration and Mechanisms of Microglial Killing of Neurons. *Mol Neurobiol* **41**: 242-247

Burnett J & Rossi J (2012) RNA-Based Therapeutics: Current Progress and Future Prospects. *Chem Biol* **19**: 60-71

Buzzi A, Chikhladze M, Falcicchia C, Paradiso B, Lanza G, Soukupova M, Marti M, Morari M, Franceschetti S, & Simonato M (2012) Loss of cortical GABA terminals in Unverricht–Lundborg disease. *Neurobiol Dis* **47**: 216-224

Canafoglia L, Gennaro E, Capovilla G, Gobbi G, Boni A, Beccaria F, Viri M, Michelucci R, Agazzi P, Assereto S, Coviello DA, Di Stefano M, Rossi Sebastiano D, Franceschetti S, & Zara F (2012) Electroclinical presentation and genotype-phenotype relationships in patients with Unverricht-Lundborg disease carrying compound heterozygous CSTB point and indel mutations. *Epilepsia* **53**: 2120-2127

Carralot J, Kim T, Lenseigne B, Boese AS, Sommer P, Genovesio A, & Brodin P (2009) Automated High-Throughput siRNA Transfection in Raw 264.7 Macrophages: A Case Study for Optimization Procedure. *Journal of Biomolecular Screening* **14**: 151-160

Čeru S, Konjar Š, Maher K, Repnik U, Križaj I, Benčina M, Renko M, Nepveu A, Žerovnik E, Turk B, & Kopitar-Jerala N (2010a) Stefin B Interacts with Histones and Cathepsin L in the Nucleus. *Journal of Biological Chemistry* **285**: 10078-10086

Čeru S, Layfield R, Zavasnik-Bergant T, Repnik U, Kopitar-Jerala N, Turk V, & Zerovnik E (2010b) Intracellular aggregation of human stefin B: confocal and electron microscopy study. *Biology of the Cell* **102**: 319-334

Chan CY, Carmack CS, Long DD, Maliyekkel A, Shao Y, Roninson IB, & Ding Y (2009) A structural interpretation of the effect of GC-content on efficiency of RNA interference. *BMC Bioinformatics* **10 Suppl 1**: S33

Chan ED & Riches DWH (2001) IFN-γ + LPS induction of iNOS is modulated by ERK, JNK/SAPK, and p38 mapk in a mouse macrophage cell line. *American Journal of Physiology - Cell Physiology* **280**: C441-C450

Cohen N, Hammans S, Macpherson J, & Nicoll J (2011) New neuropathological findings in Unverricht-Lundborg disease: neuronal intranuclear and cytoplasmic inclusions. *Acta Neuropathol* **121**: 421-427

Czeh M, Gressens P, & Kaindl AM (2011) The Yin and Yang of Microglia. *Developmental neuroscience* **33**: 199-209

Darnell JE,Jr, Kerr IM, & Stark GR (1994) Jak-STAT pathways and transcriptional activation in response to IFNs and other extracellular signaling proteins. *Science* **264**: 1415-1421

De Haan G, Halley DJ, Doelman JC, Geesink HH, Augustijn PB, Jager-Jongkind AD, Majoie M, Bader AJ, Leliefeld-ten Doeschate LA, Deelen WH, Bertram E, Lehesjoki AE, & Lindhout D (2004) Univerricht-Lundborg Disease: Underdiagnosed in the Netherlands. *Epilepsia* **45**: 1061-1063

de Siqueira L (2010) Progressive myoclonic epilepsies: review of clinical, molecular and therapeutic aspects. *J Neurol* **257**: 1612-1619

de Weerd NA, Samarajiwa SA, & Hertzog PJ (2007) Type I Interferon Receptors: Biochemistry and Biological Functions. *Journal of Biological Chemistry* **282**: 20053-20057

Delgado-Escueta AV, Ganesh S, & Yamakawa K (2001) Advances in the genetics of progressive myoclonus epilepsy. *Am J Med Genet* **106**: 129-138

Dropulic LK & Cohen JI (2011) Severe Viral Infections and Primary Immunodeficiencies. *Clinical Infectious Diseases* **53**: 897-909

Eberle F, Gießler K, Deck C, Heeg K, Peter M, Richert C, & Dalpke AH (2008) Modifications in Small Interfering RNA That Separate Immunostimulation from RNA Interference. *The Journal of Immunology* **180**: 3229-3237

Elbashir SM, Harborth J, Lendeckel W, Yalcin A, Weber K, & Tuschl T (2001) Duplexes of 21-nucleotide RNAs mediate RNA interference in cultured mammalian cells. *Nature* **411**: 494-498

Eldridge R, Iivanainen M, Stern R, Koerber T, & Wilder B (1983) "Baltic" myoclonus epilepsy: hereditary disorder of childhood made worse by phenytoin. *Lancet* **2**: 838-842

Erdinc O, Joensuu T, İlgen-Ulsu F, Bebek N, Özkara Ç, Tutkavul,K., Gündü,A., Lehesjoki AE, & Baykan B (2010) Unverricht-Lundborg Disease in Turkey: Delineating The Phenotype Between Cystatin B Mutation Positive and Negative Cases. *Journal of Neurological Sciences (Turkish)* **27**: 1-11

Fagerlund R, Melén K, Kinnunen L, & Julkunen I (2002) Arginine/Lysine-rich Nuclear Localization Signals Mediate Interactions between Dimeric STATs and Importin α5. *Journal of Biological Chemistry* **277**: 30072-30078

Fire A, Xu S, Montgomery MK, Kostas SA, Driver SE, & Mello CC (1998) Potent and specific genetic interference by double-stranded RNA in Caenorhabditis elegans. *Nature* **391**: 806-811

Frahm T, Hauser H, & Köster M (2006) IFN-type-I-mediated signaling is regulated by modulation of STAT2 nuclear export. *Journal of Cell Science* **119**: 1092-1104

Fu XY, Kessler DS, Veals SA, Levy DE, & Darnell JE (1990) ISGF3, the transcriptional activator induced by interferon alpha, consists of multiple interacting polypeptide chains. *Proceedings of the National Academy of Sciences* **87**: 8555-8559

Fu XY, Schindler C, Improta T, Aebersold R, & Darnell JE (1992) The proteins of ISGF-3, the interferon alpha-induced transcriptional activator, define a gene family involved in signal transduction. *Proceedings of the National Academy of Sciences* **89**: 7840-7843

Gao J, Morrison DC, Parmely TJ, Russell SW, & Murphy WJ (1997) An Interferon-γ-activated Site (GAS) Is Necessary for Full Expression of the Mouse iNOS Gene in Response to Interferon-γ and Lipopolysaccharide. *Journal of Biological Chemistry* **272**: 1226-1230

Gartler SM, Gandini E, & Ceppellini R (1962) Glucose-6-Phosphate Dehydrogenase Deficient Mutant in Human Cell Culture. *Nature* **193**: 602-603

Genton P (2010) Unverricht-Lundborg disease (EPM1). *Epilepsia* **51**: 37-39

Green G, Kembhavi A, Davies M, & Barrett A (1984) Cystatin-like cysteine proteinase inhibitors from human liver. *The Biochemical Journal* **218**: 939-946

Guo L, Guo H, Gao C, Mi Z, Russell WB, & Kuo PC (2007) Stat1 acetylation inhibits inducible nitric oxide synthase expression in interferon-γ–treated RAW264.7 murine macrophages. *Surgery* **142**: 156-162

Gutch MJ, Daly C, & Reich NC (1992) Tyrosine phosphorylation is required for activation of an alpha interferon-stimulated transcription factor. *Proceedings of the National Academy of Sciences* **89**: 11411-11415

Haltia M, Kristensson K, & Sourander P (1969) Neuropathological studies in three Scandinavian cases of progressive myoclonus epilepsy. *Acta Neurol Scand* **45**: 63-77

Heid CA, Stevens J, Livak KJ, & Williams PM (1996) Real time quantitative PCR. *Genome Res* **6**: 986-994

Heneka MT & Feinstein DL (2001) Expression and function of inducible nitric oxide synthase in neurons. *J Neuroimmunol* **114**: 8-18

Holland PM, Abramson RD, Watson R, & Gelfand DH (1991) Detection of specific polymerase chain reaction product by utilizing the 5'----3' exonuclease activity of Thermus aquaticus DNA polymerase. *Proceedings of the National Academy of Sciences* **88**: 7276-7280

Hoorfar J, Malorny B, Abdulmawjood A, Cook N, Wagner M, & Fach P (2004) Practical considerations in design of internal amplification controls for diagnostic PCR assays. *J Clin Microbiol* **42**: 1863-1868

Houseweart MK, Pennacchio LA, Vilaythong A, Peters C, Noebels JL, & Myers RM (2003) Cathepsin B but not cathepsins L or S contributes to the pathogenesis of Unverricht-Lundborg progressive myoclonus epilepsy (EPM1). *J Neurobiol* **56**: 315-327

Ilmarinen T, Kangas H, Kytömaa T, Eskelin P, Saharinen J, Seeler J, Tanhuanpää K, Chan FY, Slattery RM, Alakurtti K, Palvimo JJ, & Ulmanen I (2008) Functional interaction of AIRE with PIAS1 in transcriptional regulation. *Mol Immunol* **45**: 1847-1862

Jack C, Ruffini F, Bar-Or A, & Antel JP (2005) Microglia and multiple sclerosis. *J Neurosci Res* **81**: 363-373

Järvinen M & Rinne A (1982) Human spleen cysteine proteinase inhibitor. Purification, fractionation into isoelectric variants and some properties of the variants. *Biochimica et Biophysica Acta* **708**: 210-217

Jiang W, Reich III CF, & Pisetsky DS (2004) Mechanisms of activation of the RAW264.7 macrophage cell line by transfected mammalian DNA. *Cell Immunol* **229**: 31-40

Joensuu T, Kuronen M, Alakurtti K, Tegelberg S, Hakala P, Aalto A, Huopaniemi L, Aula N, Michellucci R, Eriksson K, & Lehesjoki AE (2007) Cystatin B: mutation detection, alternative splicing and expression in progressive myclonus epilepsy of Unverricht-Lundborg type (EPM1) patients. *European Journal of Human Genetics* **15**: 185-193

Joensuu T, Lehesjoki AE, & Kopra O (2008) Molecular background of EPM1-Unverricht-Lundborg disease. *Epilepsia* **49**: 557-563

Kagitani-Shimono K, Imai K, Okamoto N, Ono J, & Okada S (2002) Unverricht-Lundborg disease with cystatin B gene abnormalities. *Pediatr neurol* **26**: 55-60

Kälviäinen R, Khyuppenen J, Koskenkorva P, Eriksson K, Vanninen R, & Mervaala E (2008) Clinical picture of EPM1-Unverricht-Lundborg disease. *Epilepsia* **49**: 549-556

Kim JA, Cho K, Shin MS, Lee WG, Jung N, Chung C, & Chang JK (2008) A novel electroporation method using a capillary and wire-type electrode. *Biosensors and Bioelectronics* **23**: 1353-1360

Koprowski H, Zheng YM, Heber-Katz E, Fraser N, Rorke L, Fu ZF, Hanlon C, & Dietzschold B (1993) In vivo expression of inducible nitric oxide synthase in experimentally induced neurologic diseases. *Proceedings of the National Academy of Sciences* **90**: 3024-3027

Korja M, Kaasinen V, Lamusuo S, Marttila RJ, & Parkkola R (2007) Hyperostosis frontalis interna as a novel finding in Unverricht-Lundborg disease. *Neurology* **68**: 1077-1078

Koskenkorva P, Hyppönen J, Äikiä M, Mervaala E, Kiviranta T, Eriksson K, Lehesjoki AE, Vanninen R, & Kälviäinen R (2011) Severer Phenotype in Unverricht-Lundborg Disease (EPM1) Patients Compound Heterozygous for the Dodecamer Repeat Expansion and the c.202C>T Mutation in the*CSTB*Gene. *Neuro-degenerative disease* **8**: 515-522

Koskenkorva P, Khyuppenen J, Niskanen E, Kononen M, Bendel P, Mervaala E, Lehesjoki AE, Kalviainen R, & Vanninen R (2009) Motor cortex and thalamic atrophy in Unverricht-Lundborg disease: Voxel-based morphometric study. *Neurology* **73**: 606-611

Koskenkorva P, Niskanen E, Hyppönen J, Könönen M, Mervaala E, Soininen H, Kälviäinen R, & Vanninen R (2012) Sensorimotor, Visual, and Auditory Cortical Atrophy in Unverricht-Lundborg Disease Mapped with Cortical Thickness Analysis. *American Journal of Neuroradiology* **33**: 878-883

Koskiniemi M, Donner M, Majuri H, Haltia M, & Norio R (1974) Progressive myoclonus epilepsy. A clinical and histopathological study. *Acta Neurol Scand* **50**: 307-332

Koskiniemi M (1987) Baltic myoclonus. *Annals of clinical research* **19**: 311-312

Koskiniemi M (1986) Baltic myoclonus. *Advances in neurology* **43**: 57-64

Krebs DL & Hilton DJ (2001) SOCS Proteins: Negative Regulators of Cytokine Signaling. *Stem Cells* **19**: 378-387

Kreutzberg GW (1996) Microglia: a sensor for pathological events in the CNS. *Trends Neurosci* **19**: 312-318

Kröncke K, Fehsel K, & Kolb-Bachofen V (1998) Inducible nitric oxide synthase in human diseases. *Clinical & Experimental Immunology* **113**: 147-156

Kröncke K, Fehsel K, & Kolb-Bachofen V (1997) Nitric Oxide: Cytotoxicity versus Cytoprotection— How, Why, When, and Where? *Nitric Oxide* **1**: 107-120

Lafreniere RG, Rochefort DL, Chretien N, Rommens JM, Cochius JI, Kalviainen R, Nousiainen U, Patry G, Farrell K, Soderfeldt B, Federico A, Hale BR, Cossio OH, Sorensen T, Pouliot MA, Kmiec T, Uldall P, Janszky J, Pranzatelli MR, Andermann F et al

(1997) Unstable insertion in the 5' flanking region of the cystatin B gene is the most common mutation in progressive myoclonus epilepsy type 1, EPM1. *Nature Genetics* **15**: 298-302

Laitala-Leinonen T, Rinne R, Saukko P, Väänänen HK, & Rinne A (2006) Cystatin B as an intracellular modulator of bone resorption. *Matrix Biology* **25**: 149-157

Lalioti MD, Mirotsou M, Buresi C, Peitsch MC, Rossier C, Ouazzani R, Baldy-Moulinier M, Bottani A, Malafosse A, & Antonarakis SE (1997a) Identification of mutations in cystatin B, the gene responsible for the Unverricht-Lundborg type of progressive myoclonus epilepsy (EPM1). *American journal of Human genetics* **60**: 342-351

Lalioti MD, Scott HS, Buresi C, Rossier C, Bottani A, Morris MA, Malafosse A, & Antonarakis SE (1997b) Dodecamer repeat expansion in cystatin B gene in progressive myoclonus epilepsy. *Nature* **386**: 847-851

Lalioti MD, Scott HS, Genton P, Grid D, Ouazzani R, M'Rabet A, Ibrahim S, Gouider R, Dravet C, Chkili T, Bottani A, Buresi C, Malafosse A, & Antonarakis SE (1998) A PCR amplification method reveals instability of the dodecamer repeat in progressive myoclonus epilepsy (EPM1) and no correlation between the size of the repeat and age at onset. *American journal of Human genetics* **62**: 842-847

Lee CK, Bluyssen HAR, & Levy DE (1997) Regulation of Interferon-α Responsiveness by the Duration of Janus Kinase Activity. *Journal of Biological Chemistry* **272**: 21872-21877

Lee J, Hahn H, Kim Y, Nguyen H, Yang J, Kang J, & Hahn M (2011) Adaptor protein containing PH domain, PTB domain and leucine zipper (APPL1) regulates the protein level of EGFR by modulating its trafficking. *Biochem Biophys Res Commun* **415**: 206-211

Lehesjoki AE (2003) Molecular background of progressive myoclonus epilepsy. *EMBO Journal* **22**: 3473-3478

Lehesjoki AE (2002) Clinical features and genetics of Unverricht-Lundborg disease. *Advances in neurology* **89**: 193-197

Lehesjoki AE, Koskiniemi M, Sistonen P, Miao J, Hästbacka J, Norio R, & de la Chapelle A (1991) Localization of a gene for progressive myoclonus epilepsy to chromosome 21q22. *Proceedings of the National Academy of Sciences* **88**: 3696-3699

Lehtinen MK, Tegelberg S, Schipper H, Su H, Zukor H, Manninen O, Kopra O, Joensuu T, Hakala P, Bonni A, & Lehesjoki AE (2009) Cystatin B Deficiency Sensitizes Neurons to Oxidative Stress in Progressive Myoclonus Epilepsy, EPM1. *The Journal of Neuroscience* **29**: 5910-5915

Li S, Wilkinson M, Xia X, David M, Xu L, Purkel-Sutton A, & Bhardwaj A (2005) Induction of IFN-regulated factors and antitumoral surveillance by transfected placebo plasmid DNA. *Mol Ther* **11**: 112-119

Lim CP & Cao X (2006) Structure, function, and regulation of STAT proteins. *Molecular Biosystems* **2**: 536-550

Liu B & Hong J (2003) Role of Microglia in Inflammation-Mediated Neurodegenerative Diseases: Mechanisms and Strategies for Therapeutic Intervention. *Journal of Pharmacology and Experimental Therapeutics* **304**: 1-7

Liu B, Liao J, Rao X, Kushner SA, Chung CD, Chang DD, & Shuai K (1998a) Inhibition of Stat1-mediated gene activation by PIAS1. *Proceedings of the National Academy of Sciences* **95**: 10626-10631

Liu KD, Gaffen SL, & Goldsmith MA (1998b) JAK/STAT signaling by cytokine receptors. *Curr Opin Immunol* **10**: 271-278

Livak KJ & Schmittgen TD (2001) Analysis of relative gene expression data using real-time quantitative PCR and the 2(-Delta Delta C(T)) Method. *Methods* **25**: 402-408

Llave C, Kasschau KD, Rector MA, & Carrington JC (2002) Endogenous and Silencing-Associated Small RNAs in Plants. *The Plant Cell Online* **14**: 1605-1619

Lundborg H (ed) (1903) *Die progressive myoclonus-epilepsie (Unverrichts myoclonie).* Almqvist&Wiksell: Uppsala

Magaudda A, Ferlazzo E, Nguyen V, & Genton P (2006) Unverricht-Lundborg Disease, a Condition with Self-limited Progression: Long-term Follow-up of 20 Patients. *Epilepsia* **47**: 860-866

Marseille Consensus Group (1990) Classification of progressive myoclonus epilepsies and related disorders. *Ann Neurol* **28**: 113-116

Martin E, Nathan C, & Xie Q (1994) Role of interferon regulatory factor 1 in induction of nitric oxide synthase. *The Journal of experimental medicine* **180**: 977-984

McCoy SL, Kurtz SE, Hausman FA, Trune DR, Bennett RM, & Hefeneider SH (2004) Activation of RAW264.7 Macrophages by Bacterial DNA and Lipopolysaccharide Increases Cell Surface DNA Binding and Internalization. *Journal of Biological Chemistry* **279**: 17217-17223

McGeer P, Itagaki S, Boyes B, & McGeer E (1988) Reactive microglia are positive for HLA-DR in the substantia nigra of Parkinson's and Alzheimer's disease brains. *Neurology* **38**: 1285-1291

Nakajima K & Kohsaka S (2001) Microglia: Activation and Their Significance in the Central Nervous System. *Journal of Biochemistry* **130**: 169-175

Nimmerjahn A, Kirchhoff F, & Helmchen F (2005) Resting Microglial Cells Are Highly Dynamic Surveillants of Brain Parenchyma in Vivo. *Science* **308**: 1314-1318

Nishio M, Tsurudome M, Ito M, Kawano M, Komada H, & Ito Y (2001) High resistance of human parainfluenza type 2 virus protein-expressing cells to the antiviral and anti-cell proliferative activities of alpha/beta interferons: cysteine-rich V-specific domain is required for high resistance to the interferons. *J Virol* **75**: 9165-9176

Norio R & Koskiniemi M (1979) Progressive myoclonus epilepsy: genetic and nosological aspects with special reference to 107 Finnish patients. *Clinical genetics* **15**: 382-398

Orr CF, Rowe DB, & Halliday GM (2002) An inflammatory review of Parkinson's disease. *Prog Neurobiol* **68**: 325-340

Ousman SS, Wang J, & Campbell IL (2005) Differential Regulation of Interferon Regulatory Factor (IRF)-7 and IRF-9 Gene Expression in the Central Nervous System during Viral Infection. *Journal of Virology* **79**: 7514-7527

Pagano JS & Vaheri A (1965) Enhancement of infectivity of poliovirus RNA with diethylaminoethyl-dextran (DEAE-D). *Archiv für die gesamte Virusforschung* **17**: 456-464

Pecot CV, Calin GA, Coleman RL, Lopez-Berestein G, & Sood AK (2011) RNA interference in the clinic: challenges and future directions. *Nat Rev Cancer* **11**: 59-67

Pennacchio LA, Bouley DM, Higgins KM, Scott MP, Noebels JL, & Myers RM (1998) Progressive ataxia, myoclonic epilepsy and cerebellar apoptosis in cystatin B-deficient mice. *Nature Genetics* **20**: 251-258

Pennacchio LA, Lehesjoki AE, Stone NE, Willour VL, Virtaneva K, Miao J, D'Amato E, Ramirez L, Faham M, Koskiniemi M, Warrington JA, Norio R, de la Chapelle A, Cox DR, & Myers RM (1996) Mutations in the Gene Encoding Cystatin B in Progressive Myoclonus Epilepsy (EPM1). *Science* **271**: 1731-1734

Pfaffl MW (2001) A new mathematical model for relative quantification in real-time RT–PCR. *Nucleic Acids Research* **29**: e45-e45

Pinto E, Freitas J, Duarte A,Joana, Ribeiro I, Ribeiro D, Lima J,Lopes, Chaves J, & Amaral O (2012) Unverricht-Lundborg disease: homozygosity for a new splicing mutation in the cystatin B gene. *Epilepsy research* **99**: 187-190

Proudnikov D, Yuferov V, Zhou Y, LaForge KS, Ho A, & Kreek MJ (2003) Optimizing primer–probe design for fluorescent PCR. *J Neurosci Methods* **123**: 31-45

Rao DD, Senzer N, Cleary MA, & Nemunaitis J (2009a) Comparative assessment of siRNA and shRNA off target effects: what is slowing clinical development. *Cancer Gene Ther* **16**: 807-809

Rao DD, Vorhies JS, Senzer N, & Nemunaitis J (2009b) siRNA vs. shRNA: Similarities and differences. *Adv Drug Deliv Rev* **61**: 746-759

Rawlings N & Barrett A (1990) Evolution of proteins of the cystatin superfamily. *Journal of Molecular Evolution* **30**: 60-71

Reich NC (2002) Nuclear/cytoplasmic localization of IRFs in response to viral infection or interferon stimulation. *Journal of interferon and cytokine research* **22**: 103-109

Reich NC (2007) STAT dynamics. *Cytokine & growth factor reviews* **18**: 511-518

Riccio M, Santi S, Dembic M, Di Giaimo R, Cipollini E, Costantino-Ceccarini E, Ambrosetti D, Maraldi NM, & Melli M (2005) Cell-specific expression of the epm1 (cystatin B) gene in developing rat cerebellum. *Neurobiol Dis* **20**: 104-114

Rinne R, Saukko P, Järvinen M, & Lehesjoki AE (2002) Reduced cystatin B activity correlates with enhanced cathepsin activity in progressive myoclonus epilepsy. *Annals of medicine* **34**: 380-385

Ritonja A, Machleidt W, & Barrett AJ (1985) Amino acid sequence of the intracellular cysteine proteinase inhibitor cystatin B from human liver. *Biochem Biophys Res Commun* **131**: 1187-1192

Robbins M, Judge A, & MacLachlan I (2009) siRNA and innate immunity. *Oligonucleotides* **19**: 89-102

Sandy P, Ventura A, & Jacks T (2005) Mammalian RNAi: a practical guide. *BioTechniques* **39**: 215-224

Savitsky D, Tamura T, Yanai H, & Taniguchi T (2010) Regulation of immunity and oncogenesis by the IRF transcription factor family. *Cancer Immunology Immunotherapy* **59**: 489-510

Schindler C, Shuai K, Prezioso V, & Darnell J (1992) Interferon-dependent tyrosine phosphorylation of a latent cytoplasmic transcription factor. *Science* **257**: 809-813

Sekimoto T, Nakajima K, Tachibana T, Hirano T, & Yoneda Y (1996) Interferon-γ-dependent Nuclear Import of Stat1 Is Mediated by the GTPase Activity of Ran/TC4. *Journal of Biological Chemistry* **271**: 31017-31020

Shahwan A, Farrell M, & Delanty N (2005) Progressive myoclonic epilepsies: a review of genetic and therapeutic aspects. *The Lancet Neurology* **4**: 239-248

Shannon P, Pennacchio L, Houseweart M, Minassian B, & Myers R (2002) Neuropathological changes in a mouse model of progressive myoclonus epilepsy: cystatin B deficiency and Unverricht-Lundborg disease. *Journal of Neuropathology and experimental neurology* **61**: 1085-1091

Sledz CA, Holko M, de Veer MJ, Silverman RH, & Williams BR (2003) Activation of the interferon system by short-interfering RNAs. *Nat Cell Biol* **5**: 834-839

Stark A, Bushati N, Jan CH, Kheradpour P, Hodges E, Brennecke J, Bartel DP, Cohen SM, & Kellis M (2008) A single Hox locus in Drosophila produces functional microRNAs from opposite DNA strands. *Genes & Development* **22**: 8-13

Stubbs MT, Laber B, Bode W, Huber R, Jerala R, Lenarcic B, & Turk V (1990) The refined 2.4 A X-ray crystal structure of recombinant human stefin B in complex with the cysteine proteinase papain: a novel type of proteinase inhibitor interaction. *The EMBO Journal* **9**: 1939-1947

Suoranta S, Manninen H, Koskenkorva P, Könönen M, Laitinen R, Lehesjoki AE, Kälviäinen R, & Vanninen R (2012) Thickened skull, scoliosis and other skeletal findings in Unverricht–Lundborg disease link cystatin B function to bone metabolism. *Bone* **51**: 1016-1024

Takasaki S (2010) Efficient prediction methods for selecting effective siRNA sequences. *Comput Biol Med* **40**: 149-158

Taniwaki Y, Kato M, Araki T, & Kobayashi T (1996) Microglial activation by epileptic activities through the propagation pathway of kainic acid-induced hippocampal seizures in the rat. *Neurosci Lett* **217**: 29-32

Tegelberg S, Kopra O, Joensuu T, Cooper J, & Lehesjoki AE (2012) Early microglial activation precedes neuronal loss in the brain of the Cstb-/- mouse model of progressive myoclonus epilepsy, EPM1. *Journal of Neuropathology and experimental neurology* **71**: 40-53

Unverricht H (ed) (1891) *Die Myoclonie.* Franz Deuticke: Leipzig

Virtaneva K, D'Amato E, Miao J, Koskiniemi M, Norio R, Avanzini G, Franceschetti S, Michelucci R, Tassinari CA, Omer S, Pennacchio LA, Myers RM, Dieguez-Lucena JL, Krahe R, de la Chapelle A, & Lehesjoki AE (1997) Unstable minisatellite expansion causing recessively inherited myoclonus epilepsy, EPM1. *Nature Genetics* **15**: 393-396

Watson DE & Li B (2005) TaqMan applications in genetic and molecular toxicology. *International journal of toxicology* **24**: 139-145

Wilusz CJ & Wilusz J (2004) Bringing the role of mRNA decay in the control of gene expression into focus. *Trends in Genetics* **20**: 491-497

Xu W, Charles IG, Liu L, Moncada S, & Emson P (1996) Molecular Cloning and Structural Organization of the Human Inducible Nitric Oxide Synthase Gene (NOS2). *Biochem Biophys Res Commun* **219**: 784-788

Yunus MA, Chung LMW, Chaudhry Y, Bailey D, & Goodfellow I (2010) Development of an optimized RNA-based murine norovirus reverse genetics system. *J Virol Methods* **169**: 112-118

Zhang X, Edwards JP, & Mosser DM (2009) The expression of exogenous genes in macrophages: obstacles and opportunities. *Methods Mol Biol* **531**: 123-143

ELECTRONIC REFERENCES

Online Mendelian Inheritance in Man: http://www.omim.org

Ingenuity Systems: www.ingenuity.com

BLAST: http://blast.ncbi.nlm.nih.gov

Mirus: http://www.mirusbio.com/tech_resources/tips/optimize_sirna_transfection

APPENDICES

Reagents used in cell culture:

Phosphate buffered saline (PBS), 0.01 M (1x) (Liuoslaboratorio, Biomedicum, Helsinki, Finland)

NaCl, 137 mM
KCl, 2.7 mM
Na_2HPO_4, 10 mM
KH_2PO_4, 1.8 mM
H_2O, up to desired volume

Reagents used in transfection:

Transfection media, 500 ml

DMEM with 4.5 mg/l D-glucose (Lonza, Stockholm, Sweden)
L-glutamine, 1x
Sodium pyruvate, 110 mg/l (Lonza, Stockholm, Sweden)
FBS, 10%

Reagents used in reverse transcription of RNA to cDNA and the S15 gene polymerase chain reaction:

Primer sequences for S15-PCR

S15 F 5'-TTCCGCAAGTTCACCTACC-3' (Sigma-Aldrich, Helsinki, Finland)
S15 F 5'-CGGGCCGGCCATGCTTTACG-3' (Sigma-Aldrich, Helsinki, Finland)

Reagents used in protein extraction:

1x Cell lysis buffer

NaCl, 250 mM (Sigma, Steinheim, Germany)
Na_3VO_4, 100 mM (Sigma, Steinheim, Germany)
NaF, 50 mM (Sigma, Steinheim, Germany)
DTT, 1 mM (Fisher-Scientific, Loughborough, UK)
Protease inhibitor, diluted to 1x (Roche Diagnostics, Espoo, Finland)
2x NP-40 lysis buffer, diluted to 1x
H_2O, up to desired volume

2x NP-40 lysis buffer

NP-40, 1% (Merck, Darmstadt, Germany)
Tris, pH 8.0, 100 mM (Sigma, Steinheim, Germany)
Glycerol, 20% (Sigma, Steinheim, Germany)
EDTA, 200 µM (Riedel-de-Haen, Seelze, Germany)

Reagents used in SDS-polyacrylamide gel electrophoresis (SDS-PAGE):

5x Laemmli buffer, 100 ml

Glycerol, 15 ml (Sigma, Steinheim, Germany)
Tris-HCl, 0.5M, pH 6.8, 15 ml (Sigma, Steinheim, Germany)
SDS, 20% (w/v), 10 ml (Sigma, Steinheim, Germany)
Bromophenol Blue, 15 mg (Merck, Espoo, Finland)
H_2O, up to 100 ml

1x SDS-PAGE electrophoresis running buffer (Liuoslaboratorio, Biomedicum, Helsinki, Finland)

Tris, 25 mM
Glycine, 192 mM
SDS, 0.1%
H2O, up to desired volume

Reagents used in Western blot:

Ponceau S, 2%, 100 ml

Ponceau S, 2g (Sigma, Steinheim, Germany)
Trichloracetic acid, 30g (Merck, Darmstadt, Germany)
Sulfosalicylic acid, 30g (Riedel-de-Haen, Seelze, Germany)
H_2O, up to 100ml

1x Tris-glycine transfer buffer (Liuoslaboratorio, Biomedicum, Helsinki, Finland)

Tris, 25 mM
Glycine, 192 mM
H_2O, up to desired volume

+20% MeOH